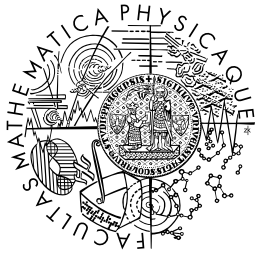

FACULTY
OF MATHEMATICS
AND PHYSICS
Charles University

DOCTORAL THESIS

Marek Čapek

Mathematical modelling of blood coagulation process

Mathematical Institute of Charles University

Supervisor of the doctoral thesis:	RNDr. Jaroslav Hron, Ph.D.
Study programme:	Physics
Study branch:	Mathematical and Computer Modelling

Prague 2019

I declare that I carried out this doctoral thesis independently, and only with the cited sources, literature and other professional sources.

I understand that my work relates to the rights and obligations under the Act No. 121/2000 Sb., the Copyright Act, as amended, in particular the fact that the Charles University has the right to conclude a license agreement on the use of this work as a school work pursuant to Section 60 subsection 1 of the Copyright Act.

In Prague June 20, 2019

I would say thanks to my supervisor Dr. Jaroslav Hron to guide me well throughout the research works. He provided me with invaluable help during whole course of my studies. His pieces of advice, hints and incentives ranged from mathematical ideas to useful programming tips and tricks.
I would like to thank Prof. Jan Evangelista Dyr from Institute of Hematology and Blood Transfusion, who introduced me into the field of blood coagulation from the side of clinical biochemistry.
My research would have been impossible without the aid and support of Mathematical institute of Charles university. The teachers and researchers of the institute were an immense source of inpiration for my work.
This study might have never happened without the possibility to use computing resources of IT4ICZ. The computational part of this work was supported by The Ministry of Education, Youth and Sports from the Large Infrastructures for Research, Experimental Development and Innovations project „IT4Innovations National Supercomputing Center – LM2015070“
Speaking of computation I must mention the priceless help of deal.ii community with programming issues I encountered. Many thanks go to all developers taking part in development of the deal.ii library.
Last but not least, I am grateful to my parents, siblings, and other members of my family, especially my aunt and uncle. I consider myself nothing without them. They gave me enough moral support, encouragement and motivation to accomplish the personal goals.
My two lifelines (parents) have always supported me financially so that I only pay attention to the studies and achieving my objective without any obstacle on the way.

Title: Mathematical modelling of blood coagulation process

Author: Marek Čapek

Institute: Mathematical Institute of Charles University

Supervisor: RNDr. Jaroslav Hron, Ph.D., Mathematical Institute of Charles University

Abstract:

On vessel wall injury the complex process of blood coagulation is set off. It is composed of vasoconstriction, primary hemostasis, secondary hemostasis and fibrinolysis. This work enriches current model of primary hemostasis of [1]. The previous model used ALE formalism for tracing of development of platelet plug. The phase field method is used for tracing of the development of interface blood-thrombus. The primary hemostasis model [1] was extended to capture the fact, that the platelets can be activated in the blood flow in the area of reactive surface not only by influence of chemical agents like thromboxane, ADP and thrombin but also by their exposure to elevated values of shear stress. In our first approach we deal the emerging thrombus as a fluid with very high viscosity. In the second approach it was assumed, that platelet plug develops as a viscoelastic material according to constitutive equations of clot introduced in [2]. In this manner platelet clot matures into blood clot. In both approaches the blood is represented as a non-Newtonian fluid. The framework of the phase field method was applied also to the model of high shear rate thrombosis of [3]. The original model of Weller [3] took advantage of the cylindrical symmetry of computational domains for its computations, hence the computations were actually two dimensional. Computations in three dimensions were performed using the finite element library deal.ii [4]. It was used its ability to distribute computations across large number of cores/nodes using the MPI interface. A scalability study was done for the model [3]. The results of the final model, where the clot was taken as a viscoelastic material, are compared with the in vivo experiment of Falati [5].

Keywords: Blood coagulation, finite element method, biofluid mechanics, blood flow, thrombus developement modelling, phase-field formulation.

Název práce: Matematické modelování procesu koagulace krve

Autor: Marek Čapek

Ústav: Matematický ústav Univerzity Karlovy

Vedoucí disertační práce: RNDr. Jaroslav Hron, Ph.D., Matematický ústav Univerzity Karlovy

Abstrakt:

V předložené práci se věnujeme studiu procesu koagulace krve z hlediska matematického modelování. Koagulace krve sestává z vazoskonstrikce, primární a sekundární hemostáze a fibrinolýzy. V práci je modifikován model primární hemostáze [1] nahrazením ALE formulace phase-field metodou pro sledování rozhraní mezi sraženinou a tekoucí krví. Model [1] je obohacen přidáním možnosti aktivace krevních destiček vyššími hodnotami smykového napětí kromě aktivace krevních destiček chemickými sloučeninami - tromboxanem, ADP nebo trombinem. Na rozdíl od [1] je použit také nenewtonovský model krve. Používáme dva přístupy pro modelování sraženiny. V prvním přístupu je sraženina modelována jako newtonovská tekutina s vysokou viskozitou. V druhém přístupu se předpokládá, že sraženina je viskoelastický material, jehož reologické vlastnosti procházejí vývojem dle modelu vyvinutého v [2]. Phase-field metoda byla také aplikována na model hemostáze vyvolané vysokými hodnotami smykového napětí [3]. Weller využil cylindrické symetrie výpočetních oblastí, čímž výpočty redukoval na dvourozměrné problémy. V této práci byly provedeny výpočty na trojrozměrných výpočetních oblastech za použití knihovny deal.ii [4]. Je plně využita její schopnost distribuovat výpočty na větší počty výpočetních jednotek (jádra/nody). Práce obsahuje studii škálovatelnosti kódu pro modifikaci Wellerova modelu. Výsledky výpočtů na základě modelu, kdy je sraženina popsána jako viskoelastický materiál, jsou porovnány s experimentem [5].

Klíčová slova: Koagulace krve, metoda konečných prvků, mechanika biotekutin, tok krve, phase-field formulace.

Contents

1. Introduction

Blood coagulation is a natural process, whose purpose is to seal an injury to the blood vessel. During this process it is important both the rheology and the biochemistry.
The rheology of the coagulation process is affected by non-Newtonian features of both the blood and the emerging clot. Namely the blood posesses such features like viscoelasticity, shear-thinning and thixotropy.
The biochemistry of the blood coagulation process is quite complicated, as it can be said, that tens of chemical species take part in the blood coagulation process. Last but no least, we should not forget the influence of the vessel walls on the blood coagulation. On the one hand the walls constrict on injury to prevent loss of blood, the process is called *vasoconstriction*. On the other hand the damage to the wall causes unveiling of some species present in the vessel wall. They then interact with the species flowing in the blood flow. Therefore it can be said, that the wall species trigger the whole coagulation process.
As the whole process is rather complicated it is hard to be approached from the side of mathematical modelling and computer simulation. The situation of latter is however improving, as we are witnessing for quite a long time significant increase of performance of high performance computers. Hence we can nowadays solve much bigger system of equations originating from even more computationally demanding mathematical models than it was several years ago.
One must however note, that the area of modelling of blood coagulation process is vast, as we have different types of clots, different flow conditions at which the clot arises. Therefore it is not possible to formulate all embracing model of blood coagulation. Rather we must decide in advance, which type of blood coagulation we want to take into account. Only after such a choice, we should formulate a mathematical model of blood coagulation.
The proces of blood coagulation has one goal - to stop leakage of blood on the blood vessel injury. It is also called *hemostasis* or *haemostasis*. The process is roughly composed of four mechanisms

- Vasoconstriction
- Platelet plug formation -*Primary hemostasis*
- Blood lot formation -*Secondary hemostasis*
- Fybrinolysis

It must be however stressed, that the first three mechanisms happen more or less concurrently. We can only be quite sure, that the process of decomposition of clot, i.e. *fybrinolysis*, happens as the last one.

1.1 Motivation

It can be generally said, that disorders of the blood coagulation process have negative impact on human life.

We will firstly review the case, when the blood coagulation is not strong enough to seal the vessel wall injuries. The most known patologies of this kind are the hemophilias. We know three types of hemophilias - hemophilia A, hemophilia B and hemophilia C. The ilness are caused by deficiencies of one of the clotting factors - factor VII, factor IX and factor XI, respectively.
In order to prevent hemmorhage of patients suffering from the hemophilias it is necessary to supply the missing factors to the body of the patients. It is also possible to treat the hemophilias by other medicines - so called coagulants.
We review shortly the opposite case, when the inreased rate of coagulation causes problems in human body. The process can be started even in the absence of the vessel wall injury. Stasis of the flow downstream of a stenosis or in aneurysms can lead to emergence of thrombi, which are then released into blood flow. The emboli can then cause the stroke or the heart attack.
Another cause of occurence of thrombi is the artificial surface of implants, one of the big achievements of modern medicine.
The above mentioned processes are quite well qualitatively described. However what is lacking is a feasible quantitative mathematical model, which could help the physicians or engineers in the field of medicine with the design of the implants and prosthetic devices. The newly designed artificial parts of human body would then initiate the coagulation process with lower probability. We are also highly motivated to develop the model also by the possibility of delivering new insights into the proper design of drugs curing coagulation disorders. Such drugs can not only be more effective in treatment of the coagulation related diseases, but they could reduce the number of their side effects.
We mention yet another field of application for mathematical modelling of blood coagulation process. Current medicine can detect aneurysms, which can lead on rupture to severe life complications for patients or even to their death. However on finding the aneurysm it is not always necessary to operate on the patient as the operation itself can represent non-negligible risk for the patient. Some criterion would be welcome, which could help with making the decision, whether it should be operated on patient or not. We are able to see the aneurysm using modern imaging methods. What would be interesting for us is the distribution of stress on the walls of aneurytic vessel. The stress is incurred either by the flowing blood in the aneurysm or the clot, which appeared in the aneurysm.
Hence the ideal solution for the neurosurgeons would be to get the image of the aneurysm. The image would be then given as input to the mathematician, which would adjust the model of blood flow in the aneurysm and the model of creation and development of the clot in the aneurysm. The models would be patient specific, i.e. they would reflect each patient individually. The output of simulations using the models would then be the stress distribution in aneurysm, which would help the neurosurgeons in the final decision, whether to operate or not.

1.2 Objectives

The thesis has the following main objectives

- Use of the phase-field method for modelling of the blood coagulation process - application on:

(A) simpler model already capturing shear rate dependent platelet activation, the blood is taken as a Newtonian fluid

(B) model of platelet clot growth, wherein platelet clot is taken as a fluid with high viscosity, blood is taken as a non-Newtonian fluid

(C) model of platelet clot growth, followed by the platelet clot development into blood clot, blood is taken as a non-Newtonian fluid

- Implementation of all three submodels in (C) - in one codebase, i.e. the viscoelastic blood model, the model of *primary hemostasis*, the model of *secondary hemostasis*.
- Study of scaling of our code, for the simpler model of blood coagulation (A).
- Identification of the key features of the new model (C) in the results of simulation. Comparison with the in-vivo experiment [5].

1.3 Research results

When we model simultaneous development of the flowing blood and developing clot, we combine equations describing fluid with the equations capturing development of clot. We need to discern two areas in the (injured) vessel - the area of flowing blood and the area of the developing thrombus. For that purpose we use as a tracing function the phase-field function, which obeys Cahn-Hilliard equation. We must stress, that the phase-field does not have any thermodynamic significance for us, i.e. it is only a marker function.
The main novelty of our approach, from the modelling point of view, is twofold. Firstly we introduce into our model rheological activation of unactivated, i.e. resting, platelets by exposure of platelets to high values of shear stresses. Secondly we extend model of *primary hemostasis* so, that the formed platelet plug starts to mature into blood clot during the process of *secondary hemostasis*.
The main result from the point of the development of efficient numerical solvers lies in our implementation of solution procedure of large system of equations, which are intrinsically coupled. We solve the systems as decoupled, splitted. Therefore recoupling is necessary. The formulated equations describe physical processes with different characteristic scales. Hence adaptive-time stepping scheme is employed for equations corresponding to the specific processes. The scheme supplies a timestep for each equation, which is solved. The resulting timestep is then chosen as a minimum of proposed timesteps.

The following list summarizes the major contributions of this work:

- Extension of existing models of blood coagulation into a model, which encompasses both *primary hemostasis* and *secondary hemostasis*.
- Codebase was developed, which enables to run the proposed models on arbitrary 3D domain and which can be distributed to large number of computing units.
- Numerical study as well as scaling study of our implementation of modified model of Weller, [6, 3].

- The relevance of our proposed model is shown by comparison with the in-vivo experiment of Falati, [5].

- The codebase is written in modular way using all advanced object oriented features of C++ language, therefore further development of the model and the code is possible, e.g. change of constitutive equations for the clot, adding new populations of platelets and/or new chemical species.

1.4 Outline

In Chapter 2 we decribe the relevant blood biology for the blood coagulation process. We introduce the main components of blood, which are most relevant for our modelling. Further we provide a short list of most important actors in the blood coagulation process. Afterwards we show the original model of blood coagulation, so called Virchow's triad, and compare it with more recent, alternative, description of coagulation, so called high shear rate thrombosis.

In Chapter 3 we review relevant fluid rheology for blood flow and possible models of blood coagulation process. We concentrate on the model of blood as a Newtonian fluid, which is valid in larger vessels, and on viscoelastic model of Owens [7]. We propose a new model of the blood coagulation process, where the clot is either represented as a fluid with large viscosity or as a viscoelastic material undergoing change of rheological properties. The change captures the development of clot from platelet clot, which developed according to model of Storti [8] to blood clot. The aging of the platelet clot according to model of [2] reflects creation of fibrin strands in the platelet clot.

Chapter 4 presents the numerical treatment of the equations of proposed models. We split Navier-Stokes system using IPCS method. We perform adaptive timestepping. As the systems of equations are solved as splitted, recoupling is needed. For the computation of Kempen relevant numerics a rather specific numerical treatment is necessary.

Finally Chapter 5 shows the results of simulations. We show results of computations of the modified Weller's model, where we used phase field as the marker interface. We used two geometries for the computations - cylinder and perfusion chamber geometry. We performed numerical study of our implementation of the modified Weller's model. We checked numerical properties of recoupling scheme. We studied also scaling properties of our code, both from the point of view of weak and strong scaling.
In Section 5.3 we present results originating from Storti's modified model, where the clot is taken as a high viscosity Newtonian fluid.
In Section 5.4 we show results of computations of our complete model merging all three models, i.e. viscoelastic model of blood, Storti's model of *primary hemostasis* and Kempen's model of *secondary hemostasis*. We compare the results with the results from Section 5.3. In Section 5.4.3 we perform visual comparison of the complete model with an in-vivo experiment of Falati [5].

2. Biology of the blood

Blood is a fluid in the body, which serves several vitally important purposes. First of all, it is responsible for transport of substances like gases, i.e. oxygen and carbon dioxide, between lungs and the rest of the body. It transports heat to the skin, which has thermoregulatory function. It delivers nutrients from the digestive tract and places of storage to the rest of the body. It also transports waste products from the body to kidneys or to the liver, where they are detoxified or removed. Blood has also protective function, as the leukocytes defend the body against malicious microorganisms and cancer cells. It also contains antibodies and other proteins, that eliminate pathogenic substances in the body. Blood can also stop blood loss by the process of blood coagulation, about which we will speak in the following sections.

2.1 Main blood components

Blood is composed of an extracellular fluid - blood plasma and formed elements. Formed elements are elements contained in a cell membrane and they have a definite shape and structure. Except platelets formed elements are cells. Platelets are small fragments of bone marrow cells.
We will now describe erythrocytes (red blood cells - RBCs), leukocytes (white blood cells - WBCs) and blood plasma. Platelets will be treated in Section 2.2.1, as they are one of the components of the blood coagulation process.

Red blood cells A red blood cell has a biconcave discoid shape with surface area approximately 130 μm^2, diameter 6-8 μm and volume 98 μm^3. As erythrocytes are highly flexible, the sizes of them can change very easily.
Red blood cells are functioning as carriers of oxygen from lungs to the rest of body. They transport carbon dioxide from the body to lungs as well. They accomplish this using the protein hemoglobin (or haemoglobin). Their membrane is filled with a solution of hemoglobin in water, which lends erythrocytes their red color [9].
Red blood cells are the most numerous of the formed elements in blood (about 98%), so they have the largest impact on the mechanical properties of blood [10], as will be discussed in chapter 3.2.

White blood cells Leukocytes are blood cells with a spherical shape, with diameters between 7 and 22 μm. As they are not so numerous in blood as red blood cells (about 1%), they influence the rheological properties of blood only a little.
They are further divided into granulocytes (neutrophile, eosinophils, basophils) and agranulocytes (lymphocytes, monocytes). Their primary function is to fight against infection originating from bacteria or viruses by their destruction or by the creation of antibodies [9].

Plasma Plasma is an aqueous solution of water (90-92% by weight), plasma proteins and organic substances. Among plasma proteins are albumins, globulins

and fibrinogen. Fibrinogen is a vital part of the blood coagulation process, so we will focus on it in Section 2.2.1. Globulins include high density lipoproteins (HDL) and low density lipoproteins (LDL). These two proteins are key elements of fat transport to cells. Their imbalance is the cause of arteriosclerosis or atherosclerosis, one of the lifestyle diseases [9], [11], [12].

2.2 Blood coagulation

Blood coagulation is a natural process, whose aim is to stop blood loss in the case of the vessel injury. It is so potent, that it saves life not only in the case of the minor vessel injury but also during serious injuries in the larger arteries.
However this process can be triggered because of other circumstances in the human body as well. The most well known condition of blood coagulation is the stasis of blood in the vessel. It is one of the key elements of Virchow's triad, which is known since 19th century. This state is mostly present in the smaller vessels [9] . For a long time the Virchow's triad was accepted as the only possible way of creation of thrombi in the blood flow [13].
Nevertheless the current research shows, that thrombosis can happen even under conditions, where the stasis is by far not present. To be precise, the thrombosis may appear under conditions of high shear rate in the blood flow in the rather larger arteries [13], [14].
We will try to explain this seeming discrepancy in the comprehension of the process of blood clotting in Section 2.2.3. First of all we will introduce the key components of the blood coagulation process.

2.2.1 The protagonists of hemostasis

Platelets (thrombocytes) Platelets are bone marrow born cells without nucleus. They are discoids with a diameter 2-4 μm. They exhibit such a shape only under normal conditions, whereas during the clotting process they undergo substantial morphological changes. They develop into sticky spheres with so called pseuodopodia, which enables them to adhere to other elements forming the clot. The process is called platelet activation [15], [9].
In their membrane there are receptors, which have an important role in clotting. Platelets contain also corpuscles, which are called α granules and dense (or δ) granules. The former are responsible for production of important species for blood coagulation, namely fibrinogen and von Willebrand Factor (vWF). The latter possess ADP (adenosinediphosphate), serotonin and calcium. They also produce thromboxane A2 and other platelet activators [9], [16].

The numbered factor pairs We can see in well-known schemes of blood coagulation components which are described by Roman numbers (see e.g. Figure 2.1).
The order of the numbering corresponds to the chronological order of their discovery. We observe, that the factors are present in pairs, i.e. they have an inactive and an active form. The former is called zymogen. The zymogen becomes an enzyme

(protease).
It can be generally said, that only zymogens are present in a blood vessel under normal conditions. There is an exception - we can encounter both factor FVII and FVIIa in the blood flow. However we must concede that the concentration of FVIIa is minimal, under normal flow conditions, and that its activity is mostly visible in the presence of the tissue factor [9].
Some factors have its own name, for instance FII - prothrombin, FIIa - thrombin, FI - fibrinogen, FIa - fibrin. The key role of thrombin is to initiate the polymerization of fibrinogen into fibrin, which then creates a network forming the initial clot [9].

von Willebrand Factor(vWF) vWF is a multimer present in variable lengths both in a blood vessel and in subendothelium of blood vessels wall. The former is associated in a complex with FVIII in which it is not active. Its reactivity depends on shear stress - the stretched molecules are more active [14], [13].
Its main role is during the *primary hemostasis* and during the main phase of clotting. The high activity in these phases occurs under conditions of a sufficiently high shear stress.
The majority of vWF is expressed in the endothelial cells, a smaller part is hidden in cytoplasmic granules of many cells. It is for instance released after the activation of platelets. The circulating FVIII-vWF complex breaks into the factors during the fastest phase of the coagulation process [9], [16].
vWF is also very important during the high shear rate thrombus formation, as will be explained in Section 2.2.3.

Tissue factor Tissue factor is also called thromboplastin or FIII. It is produced by cells, which do not have contact with blood. It is also released by monocytes as an effect of inflammatory processes [9].
It is a widely acknowledged fact that the exposure of TF on the injury site triggers off clot formation [16].

Complexes in the blood coagulation process The pure factors are not the only participants in blood clotting. The crucial role is also played by so called complexes, which are composed of factors. Besides FVIII-vWF, let us mention important complexes for clotting

- FVIIa-TF
- FVa-FXa (prothrombinase)
- FVIIIa-FIXa-Ca^{++}(tenase)

Inhibitors of blood coagulation There is a specific group of chemical species which terminate (or prevent from) coagulation [15]

- TFPI - tissue factor pathway inhibitor
- AT-III - antithrombin III
- PC - Protein C

2.2.2 Short overview of hemostasis

As was said in Introduction,i.e. Section 1, blood coagulation consists of four phases - vasoconstriction, platelet plug formation (*primary hemostasis*), blood clot formation (*secondary hemostasis*) and fybrinolysis. The first three phases do not have to proceed consecutively. On the contrary, they can happen more or less concurrently.
In the following three sections we will describe shortly each of the three phases.

Vasoconstriction

When the blood vessel wall is injured, vascular smooth muscle cells contract. Hence the damaged vessel constrict, which leads to lower loss of blood. The activated platelets release cytoplasmic granules containing thromboxane A2, ADP and serotonin. Vasoconstriction becomes more pronounced by effect of these chemicals.

Primary hemostasis - platelet plug formation

In blood flow platelets are circulating. In case of the blood vessel wall injury the platelets come in contact with injured endothelium. This contact causes change of shape of platelets, release of granules from platelets, increase of stickiness of platelets. In the granules there is serotonin, thromboxane A2 and ADP. Serotonin is a vasoconstrictor, thromboxane takes part in platelet aggregation, vasoconstriction and degranulation, ADP draws other platelets to the site of the platelet clot [9].

Secondary hemostasis - clot formation

The following model of blood coagulation is the mostly acknowledged model in recent literature. It is known since 1964. We will sketch the model for completeness. The main feature of the model is, that two branches of the coagulation convene in a final stage. The two branches are called an intrinsic and extrinsic pathway. The final stage is called a common pathway, see Fig. 2.1
If a vessel is injured the hemostatic system is triggered. It happens because the subendothelial cells, which are unveiled during the injury, release specific procoagulant species. The chemical reagents then set off the whole system of reactions. This system results in coagulation, platelet aggregation and fybrinolysis. We have to emphasize that the reactions are not to be taken in isolation from blood flow conditions. The flow is actually transporting incessantly the chemical species taking part in blood clotting. It not only delivers new reagents to the place of the injury, but it also regulates the removal of activated species from the region of the vessel wall injury.
The proper setting of the blood coagulation system can suffer from deviations to either persistent bleeding and hemorrhage, or thrombosis. The both conditions could be lethal for the human body.
The healthy vessel walls have upper part composed of single layer of endothelial cells. Under normal physiological conditions the layer does not react with the flowing blood.
Situation changes on the vessel wall disruption, when the specific membrane protein - tissue factor (TF) - is exposed. This event sparks off the above mentioned extrinsic pathway. The protein plays an important role in the activation of clotting

factor VII (FVII). The activated complex TF:FVIIa is crucial for activation of other two coagulation factors FIX and FX, [15].
During the injury blood platelets may bind, become activated, to collagen in subendothelium. Platelets are small discoid cell fragments approximately 6 μm^3 in volume under normal physiological conditions. However they undergo a series of chemical and morphological changes during the binding. An activated platelet is a sticky spiny sphere. This is not the only one way of activation of platelets, they can be actually activated via interaction with adhesive glycoproteins in the vessel wall, or due to interaction with thrombin or adenosine diphosphate (ADP) flowing in blood, [9].
The activated platelets have an important role in the clotting system, as they secrete chemical reagents which partially activate neighbouring platelets. They expose receptors bound to their surface as well. The receptors are then the place of reactions of reagents.
Up to now we talked only about activation of the protein VII (FVII) into the active complex TF:FVIIa. This form of reactions is typical for the blood coagulation system, namely conversion of unactivated form of a species into activated with use of species from previous steps of the coagulation cascade. The activated form plays then the role of a catalyst of conversion of another unactivated species into activated species, see Fig. 2.1.
The system of reactions is about to end with the conversion of prothrombin to thrombin. Thrombin is then necessary not only for the conversion of fibrinogen to fibrin but also for the conversion of unactivated platelets into activated. This positive feedback has an immense influence on activation of platelets. To be more precise - the rate of activation of blood platelet due to thrombin related system is much larger than that due to the contact with TF and adhesive glycoproteins in the vessel wall and that due to the contact with ADP from already activated platelets.
Till now we have talked about so called extrinsic pathway followed by so called common pathway. There could be another entrance into the common pathway - so called intrinsic coagulation pathway, which begins with activation of factor XII (FXII) to factor XIIa (FXIIa) during a contact with a negatively charged surface. Cofactors of the reaction are kininogen and kallikrein. This initial reaction fires a whole system of reactions of already mentioned type, which ends in the end in the common pathway, [16], [9].

2.2.3 High shear rate thrombus formation

We have seen in the previous section, that one type of startup of coagulation process requires flow stasis, one of the components of the famous Virchow's triad. We can however observe from experiments, that thrombi in the larger arteries are platelet-rich, in contrast with the thrombi in the smaller vessels [13], [18].
Recent studies have provided an explanation for this fact [13], [14]. The main precondition of both types of clotting is the same - reactive surface. This thrombogenic surface can be subendothelial collagen exposed by the injury or artificial material of prosthetic devices like polyester or stainless steel. On the surface are caught platelets and adhesive proteins like fibrinogen and von Willebrand factor

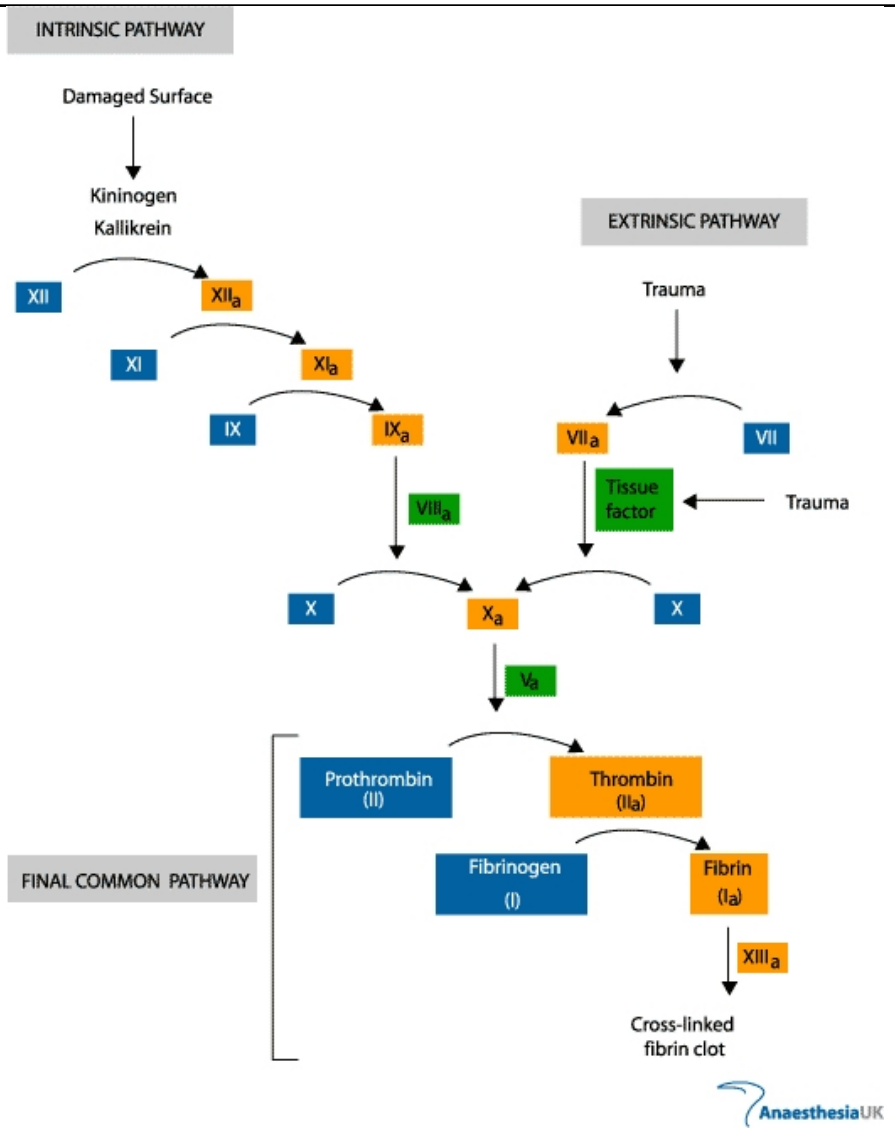

Figure 2.1: Coagulation cascade, [17]

(vWF). It is obvious, that the coverage of the surface by these is determined by the concentration of platelets and proteins in the vicinity of the thrombogenic surface.
Concentration of platelets and proteins in the blood under static conditions is minute. However, once the blood is under shear, red blood cells are pushing the other blood species outside of the center of the vessel. The increased diffusivity causes margination of platelets and proteins. Therefore they are at reactive surface disposal in increased concentration [19].
Although vWF is in the blood present in low concentration, its chemical composition makes it the key actor in the high shear type of blood coagulation. It is contained in blood plasma, platelet α-granules and the extracellular matrix of blood vessels. It creates chemical bonds mainly with itself, fibrillar collagen, platelet receptor glycoprotein (GP) Ib, and platelet integrin $\alpha_{IIb}\beta_3$ (GPIIb/IIIa). The molecule of vWF has vWF-A1 binding sites on its surface. The availability of the sites depends on the conformation of the molecule of vWF. Namely, in the globular form some part of these sites is hidden from the surrounding environment.

On the other hand, on the transition of vWF into stretched conformation the binding sites are more exposed. The changeover from the globular to the elongated form is caused by the increase of shear rate in the blood flow and it is reversible, [20], [13] . The stretched molecules of vWF form a network, in which majority of platelets in the vicinity of the vessel wall get caught. What is more, even the fast moving platelets are captured by the net.

It is important to note that the platelets do not need to be activated to be captured. Namely, vWF-A1 binding sites associate with GPIb receptors on the surface of platelets, which are always prepared to bind, [13].

We can prove the prevalence of this process in the high shear rate thrombogenesis by the fact that the time of passing of platelets through stenosis is too short for platelets to activate. So, as the platelets actually bind, we can conclude, that the overwhelming factor of the capture of platelets into the thrombus is the affinity of the A1 binding sites of vWF and the GPIb receptors of platelets in the blood flow.

Followingly captured mural platelets activate due to the exposition to high shear rates for longer time. The time necessary for adsorption and activation of platelet is called the lagtime. It depends on the shear rate - it decreases with higher shear rate. This dependence could have two reasons. Firstly, proteins and platelets are marginated in elevated measure due to high shear rate, as noted above. Secondly, high shear rate reduces the time of mural platelet activation.

The newly activated platelets set free platelet granule stores of vWF and other procoagulant species, which either stabilize the thrombus (such as platelet integrin $\alpha_{IIb}\beta_3$) or are carried away by the flow. The newly released vWF is captured into already existing nets and enhances further platelet capture. This positive feedback leads to tremendous growth of thrombus, [21] .

The growing thrombus changes rheological conditions in the blood vessel, as its diameter is narrowing. This causes increase of shear rate, which again stimulates the growth of the thrombus, [14].

The initially captured platelets do not need to be stable, which can lead to occurence of rotating platelet aggregates at high shear rates, which do not have to be activated. Either platelet integrin $\alpha_{IIb}\beta_3$ irreversibly bounded to vWF or fibrinogen converted to fibrin can stabilize the high shear rate thrombus. If the bound between platelet integrin $\alpha_{IIb}\beta_3$ and vWF is too weak, the high shear stress can tear off parts of thrombus and form emboli, [21].

The high shear rate thrombus (white clot) can be seen as a precursor of red clot, under certain circumstances. Namely, the stasis condition created by the white clot is necessary for the set up of red clot (one of conditions of the Virchow's triad), [14]. This situation is depicted in Figure 2.3.

The process of high shear thrombus formation is summed up in Table 2.1. In Figure 2.2 there is graphical representation of catching of platelets (red ones) into the vWF nets (green ones). See [22] for details.

Table 2.1: Process of high shear rate thrombus formation

1. In the stenosed region high values of wall shear rate appear.
2. To walls composed of collagen or artificial surface molecules of vWF bind, due to the high values of wall shear rate they uncoil.
3. Blood platelets are marginated to the walls due to the shear enhanced diffusivity caused by pushing red blood cells in the center of the vessel.
4. Unactivated platelets near the wall are caught by the vWF, which is already bound to the vessel wall.
5. Already bound platelets release in large amounts vWF, which activate $\alpha_{IIb}\beta_3$ on the platelets. This causes firm adhesion.
6. Due to the capture of platelets nets created from vWF are created on the surface of the emerging thrombus.
7. The networks of vWF catch quickly lot of platelets, which create a large thrombus. The clot can either occlude the vessel or embolize.

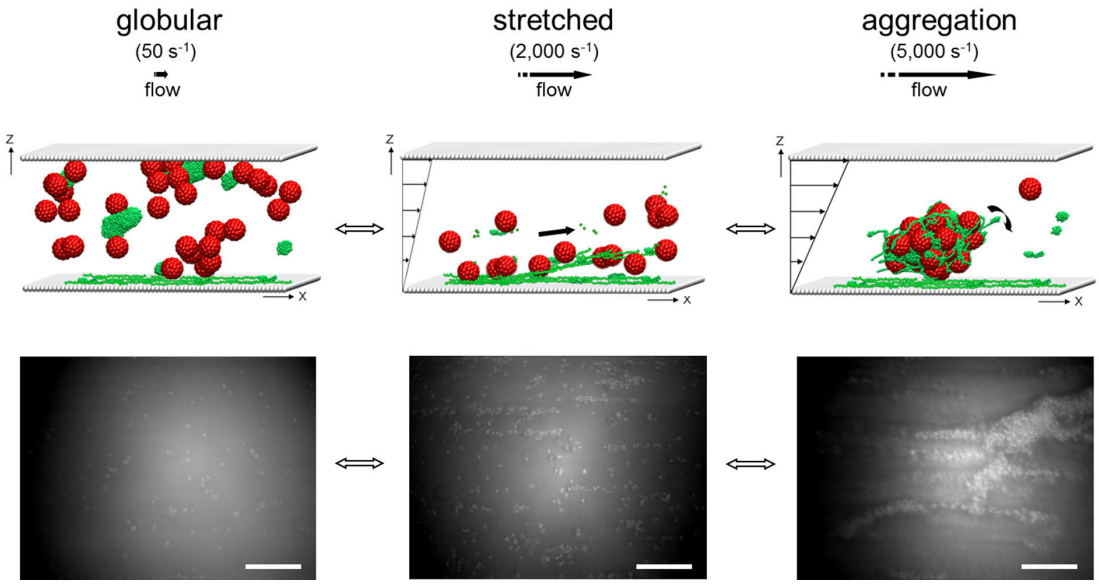

Figure 2.2: vWF collective networks interactions from globular to stretched to aggregation transition, [22]

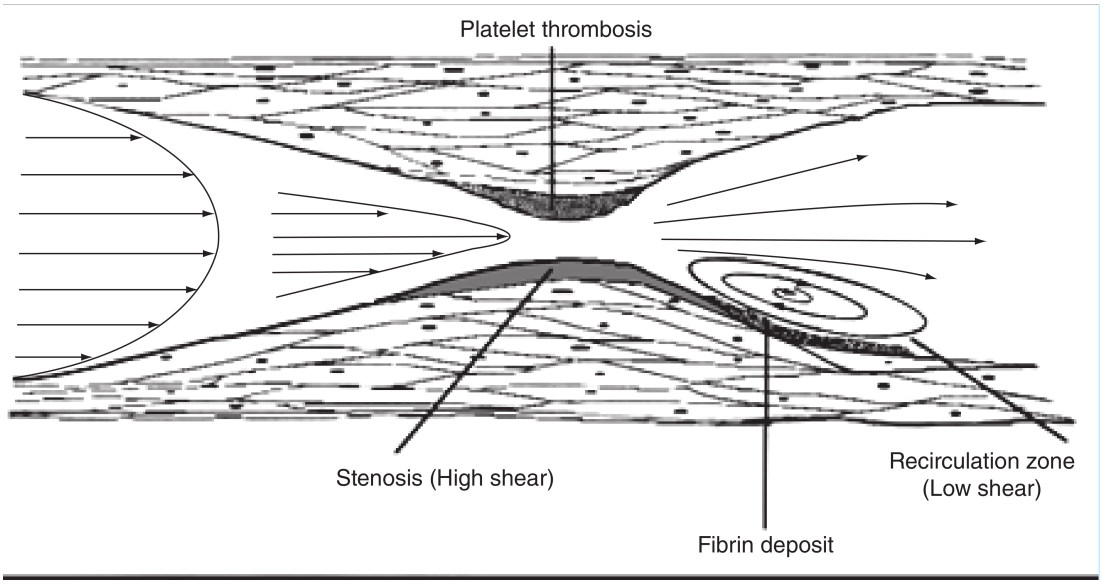

Figure 2.3: Two kinds of thrombus generated at stenotic lesion, [14]

3. Mathematical modelling

3.1 Overview of rheology

We will now outline basics of the fluid rheology, namely the conservation laws and the short note on the Newtonian fluids, similarly to [23]. Afterwards we delve into the topic of non-Newtonian fluids. We review the properties of non-Newtonian fluids, which blood exhibits under certain conditions.

3.1.1 Conservation laws

Conservation of mass

The mass conservation dictates, that for any volume $V(t)$ closed to all transfers of matter and energy the mass of the volume must remain constant over time:

$$\frac{d}{dt}\int_{V(t)} \rho dV = 0, \tag{3.1}$$

where ρ is density. From the previous equation it could be derived using Reynolds transport theorem the continuity equation:

$$\frac{D\rho}{Dt} + \operatorname{div} \mathbf{u} = 0, \tag{3.2}$$

where $\frac{D}{Dt} = \frac{\partial}{\partial t} + \mathbf{u} \cdot \nabla$ is the material derivative and $\mathbf{u}$ is the fluid velocity. On assumption of incompressibility $\frac{D\rho}{Dt} = 0$ we obtain the condition of soledoinality for the velocity field:

$$\operatorname{div} \mathbf{u} = 0. \tag{3.3}$$

Conservation of linear momentum

The momentum of fluid in the material volume $V(t)$ is given as

$$\int_{V(t)} \rho \mathbf{u} dV. \tag{3.4}$$

From the principle of linear momentum, i.e. statement that the rate of change of momentum is equal to the applied force for any closed system,

$$\frac{d}{dt}\int_{V(t)} \rho \mathbf{u} dV = \int_{\partial V(t)} \boldsymbol{s}_{\bar{\boldsymbol{n}}}(\mathbf{x}, t) dS + \int_{V(t)} \rho \mathbf{b} dV, \tag{3.5}$$

it can be derived using Reynolds transport theorem and the continuity equation (3.2) the equation of balance of linear momentum:

$$\int_{V(t)} \rho \frac{D\mathbf{u}}{Dt} dV = \int_{\partial V(t)} \boldsymbol{s}_{\bar{\boldsymbol{n}}}(\mathbf{x}, t) dS + \int_{V(t)} \rho \mathbf{b} dV, \tag{3.6}$$

where $\boldsymbol{s}_{\bar{\boldsymbol{n}}}$ is the stress vector, $\mathbf{b}$ is the body force per unit mass and ∂V is the surface of volume of fluid V.

Conservation of angular momentum

This principle states, that the change of angular momentum of control volume $V(t)$ is only due to the stress $\boldsymbol{s}_{\bar{\boldsymbol{n}}}$ and the body force $\mathbf{b}$:

$$\frac{D}{Dt}\int_{V(t)}(\mathbf{x}\times\rho\mathbf{u})\,dV=\int_{\partial V(t)}(\mathbf{x}\times\boldsymbol{s}_{\bar{\boldsymbol{n}}})\,dS+\int_{V(t)}(\mathbf{x}\times\rho\mathbf{b})\,dV. \tag{3.7}$$

We can again employ Reynolds transport theorem and the continuity equation (3.2) to derive the following equation:

$$\int_{V(t)}\left(\mathbf{x}\times\rho\frac{D\mathbf{u}}{Dt}\right)dV=\int_{\partial V(t)}(\mathbf{x}\times\boldsymbol{s}_{\bar{\boldsymbol{n}}})\,dS+\int_{V(t)}(\mathbf{x}\times\rho\mathbf{b})\,dV. \tag{3.8}$$

We can prove using (3.5) and (3.8) existency and symmetry of the stress tensor $\boldsymbol{T}$ fullfilling the relation

$$\boldsymbol{s}_{\bar{\boldsymbol{n}}}(\mathbf{x},t)=\bar{\mathbf{n}}\cdot\mathbf{T}, \tag{3.9}$$

where $\bar{\mathbf{n}}$ outward unit normal vector to the surface of volume $V(t)$.

(3.5) can then be reformulated in the differential form

$$\rho\frac{D\mathbf{u}}{Dt}=\operatorname{div}\boldsymbol{T}+\rho\mathbf{b}. \tag{3.10}$$

3.1.2 Newtonian fluids

We set the components of $\boldsymbol{T}$ as

$$T_{ij}=-p\delta_{ij}+S_{ij}, \tag{3.11}$$

where the pressure p is defined as:

$$p=-\frac{1}{3}T_{ii}. \tag{3.12}$$

The extra-stress tensor $\boldsymbol{S}$ is taken here as a linear function of the velocity gradient $\nabla\mathbf{u}$. In the following we will use the rate-of-strain (or rate-of-deformation) tensor $\boldsymbol{D}$ given as

$$\mathbf{D}=\frac{1}{2}\left(\nabla\mathbf{u}+(\nabla\mathbf{u})^T\right). \tag{3.13}$$

We assume further, that the fluid is isotropic and incompressible. We then get the following relation

$$T_{ij}=-p\delta_{ij}+\eta D_{ij}, \tag{3.14}$$

where η is the dynamic viscosity. On substitution of (3.14) into (3.10) we obtain Navier-Stokes equations for an incompressible fluid:

$$\rho\frac{D\mathbf{u}}{Dt}=-\nabla p+\eta\Delta\mathbf{u}+\rho\mathbf{b}. \tag{3.15}$$

3.1.3 Non-Newtonian fluids

Nonlinear viscous fluids

We assume the following constitutive equation for an incompressible viscous fluid

$$\mathbf{T} = -p\mathbf{I} + \boldsymbol{S}(\mathbf{L}), \tag{3.16}$$

where $\boldsymbol{S}$ is now generally nonlinear tensor function of the velocity gradient $\mathbf{L} = \nabla\mathbf{u}$. On application of the material frame indifference principle and the representation theorem for symmetric isotropic tensor functions (3.16) can be written as

$$\boldsymbol{S} = \phi_0(II_D, III_D)\mathbf{I} + \phi_1(II_D, III_D)\mathbf{D} + \phi_2(II_D, III_D)\mathbf{D}^2, \tag{3.17}$$

where

$$II_D = \frac{1}{2}((\operatorname{tr}\mathbf{D})^2 - \operatorname{tr}\mathbf{D}^2) \qquad \text{and} \qquad III_D = \det\mathbf{D} \tag{3.18}$$

are the second and third principal invariant of the tensor $\mathbf{D}$, respectively.
Reiner-Rivlin fluids are all incompressible fluids, whose constitutive equation can be formulated as

$$\mathbf{T} = -p\mathbf{I} + \phi_1(II_D, III_D)\mathbf{D} + \phi_2(II_D, III_D)\mathbf{D}^2. \tag{3.19}$$

If we compute the viscometric functions for the Reiner-Rivlin fluids in simple shear flow and compare them with behaviour of real fluids we arrive at the following incompressible constitutive equation

$$\mathbf{T} = -p\mathbf{I} + 2\eta(II_D, III_D)\mathbf{D}, \tag{3.20}$$

where $\eta(II_D, III_D)$ is a function of II_D and III_D. In the literature it is common to neglect the functional dependence of η on III_D. II_D is not a positive quantity in isochoric motions, therefore a positive measure of the rate of deformation, the shear rate $\dot{\gamma}$, is introduced:

$$\dot{\gamma} \equiv \sqrt{2\operatorname{tr}(\mathbf{D^2})} = \sqrt{-4II_D}. \tag{3.21}$$

Hence (3.20) can be rewritten as

$$\mathbf{T} = -p\mathbf{I} + 2\eta(\dot{\gamma})\mathbf{D}. \tag{3.22}$$

This fluid, i.e. the fluid with shear rate dependent viscosity, is called incompressible generalized Newtonian fluid.
One of the simpler examples of shear rate dependent viscosity functions is the power-law model:

$$\eta(\dot{\gamma}) = K\dot{\gamma}^{n-1}, \tag{3.23}$$

which for $n = 1$ gives Newtonian fluid, whereas for $n > 1$ and $n < 1$ shear thinning viscosity and shear thickening viscosity, respectively. The shear thinning model, which is often used for the blood, has the disadvantage, that it predicts infinite viscosity for zero shear rate and it goes to zero as shear rate approaches infinity.

Yield stress fluids

Some fluids have the specific behaviour that they start to flow only after a critical stress level is achieved. Some researchers assume existence of a material property - *yield value* or *yield stress*, S_Y. This topic is however still controversial in the specialist community [24], [25].
We have to select a metric of the stress tensor. In simple shear flow we have only two nonzero components of the extra stress tensor and they are equal - $S_{12} = S_{21}$. The metric is then simply $|S_{12}|$ and the yield criterion becomes $|S_{12}| = S_Y$. If $|S_{12}| < S_Y$ the material behaves rigidly(without deformation) or it exhibits non-rigid behaviour(e.g. deforms elastically). For $|S_{12}| > S_Y$ the materials starts to flow.
The previous criterion is however well grounded only for simple shear flow. In general flow it is necessary to take a general function of the extra stress tensor $f(\boldsymbol{S})$. The most general yield criterion of this form fulfilling the principle of material invariance gets the following shape

$$f(I_S, II_S, III_S) = S_Y, \tag{3.24}$$

where

$$I_S = \mathrm{tr}\boldsymbol{S}, \qquad II_S = \frac{1}{2}((\mathrm{tr}\,\boldsymbol{S})^2 - \mathrm{tr}\,\boldsymbol{S}^2). \qquad III_S = \mathrm{det}\boldsymbol{S}. \tag{3.25}$$

If we want to retain consistency of the yield function with simple shear flow criterion from above, we take

$$f(I_S, II_S, III_S) = \sqrt{|II_S|}, \tag{3.26}$$

hence the yield criterion gets the following form

$$\sqrt{|II_S|} = S_Y. \tag{3.27}$$

Bingham model This material behaves rigidly until certain value of extra stress, the yield criterion, is reached. After this criterion is reached it behaves like an incompressible Newtonian fluid. The material behaves according the following equations

$$\begin{aligned} &|S_{12}| < S_Y \Longrightarrow \dot{\gamma} = 0, \\ &|S_{12}| \geq S_Y \Longrightarrow S_{12} = S_Y + \mu\dot{\gamma}, \end{aligned} \tag{3.28}$$

where μ is the constant viscosity. The generalization to three dimensions of 3.28 has the following form

$$\begin{aligned} &\sqrt{|II_\tau|} < S_Y \Longrightarrow D_{ij} = 0, \\ &\sqrt{|II_\tau|} \geq S_Y \Longrightarrow S_{ij} = 2\left(\mu + \frac{S_Y}{2\sqrt{|II_D|}}\right) D_{ij}. \end{aligned} \tag{3.29}$$

Herschel–Bulkley model Like in the Bingham model the material behaves rigidly, until a critical value is reached. The previous model however assumed linear dependence of viscosity on shear rate. The current model introduces a power-law viscosity after the startup of flow:

$$\begin{aligned} |S_{12}| < S_Y &\Longrightarrow \dot{\gamma} = 0, \\ |S_{12}| \geq S_Y &\Longrightarrow S_{12} = S_Y + K\dot{\gamma}^n. \end{aligned} \tag{3.30}$$

The generalization to three dimensions of 3.30 has the following form

$$\begin{aligned} \sqrt{|II_\tau|} < S_Y &\Longrightarrow D_{ij} = 0, \\ \sqrt{|II_\tau|} \geq S_Y &\Longrightarrow S_{ij} = 2\left(K\dot{\gamma}^{n-1} + \frac{S_Y}{2\sqrt{|II_D|}}\right) D_{ij}. \end{aligned} \tag{3.31}$$

Casson model In this model the material behaves after reaching the critical yield stress like shear thinning fluid [26]:

$$\begin{aligned} |S_{12}| < S_Y &\Longrightarrow \dot{\gamma} = 0, \\ |S_{12}| \geq S_Y &\Longrightarrow S_{12}^{\frac{1}{2}} = S_Y^{\frac{1}{2}} + (\mu\dot{\gamma}^{\frac{1}{2}}). \end{aligned} \tag{3.32}$$

The generalization to three dimensions of 3.32 has the following form:

$$\begin{aligned} \sqrt{|II_\tau|} < S_Y &\Longrightarrow D_{ij} = 0, \\ \sqrt{|II_\tau|} \geq S_Y &\Longrightarrow S_{ij} = 2\left(\sqrt{\mu} + \frac{\sqrt{S_Y}}{\sqrt[4]{4|II_D|}}\right)^2 D_{ij}. \end{aligned} \tag{3.33}$$

Viscoelastic fluids

Truesdell and Noll [27] introduced the following categorization of viscoelastic models:

- differential type - the extra stress tensor can be expressed as an explicit function of finite number of temporal derivatives of suitable strain measures at the current time
- integral type - simple fluids whose history integral is composed of one or more integrals
- rate type- these models contain on or more time derivatives of the extra stress tensor

Some model can be expressed both as a rate type and as an integral type model, e.g. Maxwell B model.

In [28], [27], [29] and [30] constitutive equations are developed from general principles. Yet another approach provides the thermodynamic framework outlined and used in [31],[32].
In the following Section we show an elementary way, how to develop viscoelastic constitutive equations. Afterwards we compare one of the results of this elementary modelling with the microstructure-based derivation of the same constitutive equations, namely Oldroyd-B constitutive equations.

Viscoelastic models obtained by generalization from 1D analogs to 3D
Viscoelastic models originate in this approach from combination of two basic materials: a Newtonian viscous fluid and a linear elastic material. The corresponding mechanical analogs are a linear dashpot and a Hookean spring, respectively.
From the analogs a more complex elements are composed. Serial connection of the spring and dashpot analog is called Maxwell element, whereas their parallel connection is called Kelvin-Voigt element.
So called Oldroyd element is a connection of linear dashpot and a Maxwell element in parallel. Because of the geometric setting the strain of the dashpot is equal to the strain of the Maxwell element, whereas the stress of the whole element equals to the sum of stresses in the dashpot and in the Maxwell element.
After some manipulation a 1D constitutive equation of Oldroyd material can be written:

$$T(t) = \eta_N \dot{\gamma} + \tau, \tag{3.34}$$

$$\tau + \lambda \dot{\tau} = \eta_P \dot{\gamma}, \tag{3.35}$$

where $\dot{\gamma}$ is the rate of deformation, T is the stress, λ is the relaxation time of the spring, η_P is the viscosity of dashpot in the Maxwell element, whereas η_N is the viscosity of linear dashpot connected in parallel with the Maxwell element.
The model is generalized to three dimensions by substituting tensor $\mathbf{S}$ for τ and strain rate tensor $\mathbf{D}$ for $\dot{\gamma}$. In the equation (3.35) a time derivative of stress appears, which can not be uniquelly generalized to three dimensions.
A lot of nonlinear viscoelastic constitutive equations can be taken as special cases of **quasi-linear rate-type viscoelastic model**, Maxwell model see [33]. This general model shows a structural similarity with the 1-D constitutive equation (3.35). They have the following form:

$$\boldsymbol{S} + \lambda \frac{\mathcal{D}\boldsymbol{S}}{\mathcal{D}t} = 2\eta \mathbf{D}. \tag{3.36}$$

There are several definitions of the operator $\frac{\mathcal{D}}{\mathcal{D}t}$, which are not introduced arbitrarily, but they have to take into account the requirement of objectivity and symmetry of the resulting second-order tensor. Some of them are:
Upper convective derivative

$$\overset{\triangledown}{\boldsymbol{S}} = \frac{D\boldsymbol{S}}{Dt} - \mathbf{L} \cdot \boldsymbol{S} - \boldsymbol{S} \cdot \mathbf{L}^T, \tag{3.37}$$

Lower convective derivative

$$\overset{\triangle}{\boldsymbol{S}} = \frac{D\boldsymbol{S}}{Dt} + \boldsymbol{S} \cdot \mathbf{L} + \mathbf{L}^T \cdot \boldsymbol{S}, \tag{3.38}$$

Co-rotational derivative

$$\mathring{\boldsymbol{S}} = \frac{1}{2}(\overset{\triangledown}{\boldsymbol{S}} + \overset{\triangle}{\boldsymbol{S}}). \tag{3.39}$$

Johnson-Segalman model We can superpose objective operators as we get again an objective operator. One frequently chosen operator is

$$\overset{\square}{\boldsymbol{S}} = (1 - \frac{\iota}{2}) \overset{\triangledown}{\boldsymbol{S}} + \frac{\iota}{2} \overset{\triangle}{\boldsymbol{S}} . \tag{3.40}$$

After substitution into (3.36), adding a constant viscosity η_2 of inelastic contribution (solvent contribution), defining η_1 as a constant viscosity of the viscoelastic element, we obtain the four constant Johnson-Segalman model [34]:

$$\boldsymbol{S} = \boldsymbol{S}^{(1)} + \boldsymbol{S}^{(2)}, \tag{3.41}$$

where

$$\boldsymbol{S}^{(1)} + \lambda \overset{\square}{\boldsymbol{S}}^{(1)} = 2\eta_1 \mathbf{D} \tag{3.42}$$

and

$$\boldsymbol{S}^{(2)} = 2\eta_2 \mathbf{D}. \tag{3.43}$$

Convected Maxwell models Taking $\eta_2 = 0$ in (3.43), $\iota = 2$ or $\iota = 0$ in (3.41) we obtain lower convected (LCM) Maxwell or upper convected Maxwell (UCM) models, respectively:

LCM

$$\boldsymbol{S} + \lambda \overset{\triangle}{\boldsymbol{S}} = 2\eta \mathbf{D} \tag{3.44}$$

UCM

$$\boldsymbol{S} + \lambda \overset{\triangledown}{\boldsymbol{S}} = 2\eta \mathbf{D} \tag{3.45}$$

Oldroyd-A and Oldroyd-B models Taking $\iota = 2$ or $\iota = 0$ we obtain Oldroyd-A and Oldroyd-B models, respectively. We concentrate on Oldroyd-B model, as no real fluid has been shown till now to exhibit Oldroyd-A behaviour. Oldroyd-B model reads as

$$\boldsymbol{S} = \boldsymbol{S}^{(1)} + \boldsymbol{S}^{(2)}, \tag{3.46}$$

where

$$\boldsymbol{S}^{(1)} + \lambda \overset{\triangledown}{\boldsymbol{S}}^{(1)} = 2\eta_1 \mathbf{D} \tag{3.47}$$

and

$$\boldsymbol{S}^{(2)} = 2\eta_2 \mathbf{D} \tag{3.48}$$

Alternative derivation of Oldroyd-B model Above we arrived at Oldroyd-B model by a phenomenological approach. In this part we derive the Oldroyd-B model using microstructure based modelling in order to show the relevance of this type of modelling. In the Section 3.2.3 we will derive microstructure based model of blood using the similar reasoning as here.
Microstructure based modelling has one great advantage over phenomenological modelling - the parameters that we discover in constitutive equations have clear physical interpretation. These parameters are namely related to the microstructure properties of fluid, which are measurable.
The Oldroyd-B model derivation is based on a simplification of basic microstructure

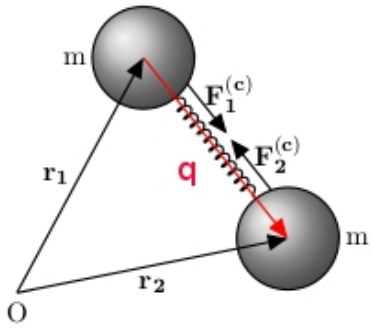

Figure 3.1: Elastic dumbbell, [35]

in fluid flow - the elastic dumbbell model, see Fig. 3.1. The elastic dumbbell is an idealization consisting of two identical beads connected by a massless spring. The derivation of the constitutive model begins with postulation of the force balance for each of the beads:

$$\mathbf{F_i^{(f)}} + \mathbf{F_i^{(c)}} + \mathbf{F_i^{(b)}} = \mathbf{0} \qquad \mathbf{i} = 1, 2, \tag{3.49}$$

where $\mathbf{F_i^{(f)}}$ is a friction force, $\mathbf{F_i^{(c)}}$ a spring force, $\mathbf{F_i^{(b)}}$ a Brownian force. As we are dealing with the Brownian force, which is a stochastic process, we have to solve the following stochastic differential equations for $\mathbf{q}$ - the end to end-vector-of a dumbbell.

$$\frac{d\mathbf{q}}{dt} = \nabla\mathbf{u}\cdot\mathbf{q} - \frac{2K}{\zeta}\mathbf{q} - \sqrt{\frac{4k_BT}{\zeta}}d\mathbf{W}(t), \tag{3.50}$$

where ζ is so-called friction coefficient, $\boldsymbol{W}(t)$ is a multidimensional Wiener process, K is a spring constant, k_B is Boltzmann constant, T is the temperature. A viable possibility how to solve the equation is to transform it to Fokker-Planck or diffusion equation

$$\frac{\partial}{\partial t}\psi(\mathbf{q},t) = -\frac{\partial}{\partial\mathbf{q}}\cdot\left[\left(\nabla\mathbf{u}\cdot\mathbf{q} - \frac{2K}{\zeta}\mathbf{q}\right)\psi(\mathbf{q},t) + \frac{2k_BT}{\zeta}\frac{\partial}{\partial\mathbf{q}}\psi(\mathbf{q},t)\right], \tag{3.51}$$

where $\psi(\mathbf{q},t)$ is the probability density function for the end-to-end vector $\mathbf{q}$ at time t. Having the probability density function $\psi(\mathbf{q},t)$ we can define the expectation of a function of $\mathbf{q}$, $g(\mathbf{q})$, as

$$\langle\langle g(\mathbf{q})\rangle\rangle = \int g(\mathbf{q})\psi(\mathbf{q},t)d\mathbf{q}. \tag{3.52}$$

From equation (3.51) we can derive the equation of change of $<< g(\mathbf{q}) >>$

$$\begin{aligned}\frac{d}{dt} << g(\mathbf{q}) >> = &\left\langle\left\langle(\nabla\mathbf{u}\cdot\mathbf{q})\frac{\partial}{\partial\mathbf{q}}g(\mathbf{q})\right\rangle\right\rangle + \frac{2k_BT}{\zeta}\left\langle\left\langle\frac{\partial}{\partial\mathbf{q}}\cdot\frac{\partial}{\partial\mathbf{q}}g(\mathbf{q})\right\rangle\right\rangle \\ &- \frac{2K}{\zeta}\left\langle\left\langle\mathbf{q}\cdot\frac{\partial}{\partial\mathbf{q}}g(\mathbf{q})\right\rangle\right\rangle.\end{aligned} \tag{3.53}$$

The equation for $g(\mathbf{q}) = \langle\langle\mathbf{qq}\rangle\rangle$ takes the following form:

$$\frac{\partial}{\partial t}\langle\langle\mathbf{qq}\rangle\rangle - \nabla\mathbf{u}\,\langle\langle\mathbf{qq}\rangle\rangle - \langle\langle\mathbf{qq}\rangle\rangle\,\nabla\mathbf{u}^T = \frac{4k_BT}{\zeta}\mathbf{I} - \frac{4K}{\zeta}\langle\langle\mathbf{qq}\rangle\rangle. \tag{3.54}$$

Let us suppose the following decomposition of the total stress tensor $\boldsymbol{T}$ into the part corresponding to the solvent $\mathbf{T}_S$ and to the polymer $\mathbf{T}_P$:

$$\boldsymbol{T} = \boldsymbol{T}_S + \boldsymbol{T}_P = (-p_S\mathbf{I} + \mathbf{S}_S) + (-p_P\mathbf{I} + \boldsymbol{S_P}) = -p\mathbf{I} + \boldsymbol{S}, \tag{3.55}$$

where $p = p_S + p_P$ and $\boldsymbol{S} = \boldsymbol{S}_S + \boldsymbol{S}_P = 2\eta_N\mathbf{D} + \boldsymbol{S}_P$. Kramers performed elementary physical derivation of $\boldsymbol{S}_P$. He got in the end so called Kramers expression for the extra-stress tensor

$$\boldsymbol{S} = \boldsymbol{S}_S + \boldsymbol{S_P} = 2\eta_N\mathbf{D} + n_c H << \mathbf{qq} >> -n_c k_B T\mathbf{I}, \tag{3.56}$$

where n_c is the number density of dumbbells. On substitution of (3.54) in the previous equation we arrive at Giesekus expression

$$\boldsymbol{S} = 2\eta_N\mathbf{D} - \frac{n_c\zeta}{4} << \overset{\triangledown}{\mathbf{qq}} >> . \tag{3.57}$$

We define the relaxation time

$$\lambda = \frac{\zeta}{4K}, \tag{3.58}$$

the polymeric viscosity

$$\eta_P = \frac{n_c k_B T\zeta}{4K} = n_c k_B T\lambda, \tag{3.59}$$

the total viscosity $\eta_0 = \eta_N + \eta_P$, the characteristic relaxation time

$$\lambda_r = \frac{\eta_N}{\eta_0}\lambda. \tag{3.60}$$

Then we can write the equation for the total extra stress tensor

$$\boldsymbol{S} + \lambda \overset{\triangledown}{\boldsymbol{S}} = 2\eta_0(\mathbf{D} + \lambda_r \overset{\triangledown}{\mathbf{D}}), \tag{3.61}$$

which is the Oldroyd-B model. We can write it in the split form of the Oldroyd-B model:

$$\boldsymbol{S} = 2\eta_N\mathbf{D} + \boldsymbol{S}_P, \tag{3.62}$$

$$\boldsymbol{S}_P + \lambda \overset{\triangledown}{\boldsymbol{S}}_P = 2\eta_P\mathbf{D}, \tag{3.63}$$

in which the model originating from 1-D analogs, i.e. (3.47) and (3.48), can be identified.

Thixotropic fluids

There is a lot of definitions of thixotropy, one of them is:

"When a reduction in magnitude of rheological properties of a system, such as elastic modulus, yield stress, and viscosity, for example, occurs reversibly and isothermally with a distinct time dependence on application of shear strain, the system is described as thixotropic [36]."

If a liquid has some kind of microstructure it is a candidate for

thixotropic behavior. In our specific case, blood, the microstructure is the rouleaux, i.e. stack of red blood cells, which form under specific flow conditions. Usually it takes some time for microstructure to form and break, which causes time dependence of the material properties mentioned in the citation above. There are many theories, which capture thixotropy. Barnes [37] divided them into three categories:

- indirect microstructural theories, where a scalar parameter is introduced to capture the level of microstructure. An evolution equation is then introduced to trace the rate of change of this parameter due to aggregation and disaggregation of microstructures.
- direct structural theories, where an approximate physical model is introduced.
- more phenomenological theories

3.2 Modelling blood flow

3.2.1 Blood as a non-Newtonian fluid

It is widely acknowledged, that the blood plasma is a Newtonian fluid. What makes blood a non-Newtonian fluid is the presence of red blood cells, erythrocytes. It must be however noted, that in order to treat blood as a non-Newtonian fluid, the continuum hypothesis must be valid. In medium size vessels, where the erythrocytes are much smaller than the size of the vessel blood is flowing in, the hypothesis holds. Should we describe behaviour of blood in yet smaller vessels, in so called microcirculation, we have to use an another approach.

Viscosity of blood Erythrocytes tend to form columnar aggregates, so called rouleaux, under low shear rate conditions, [38]. If the rouleuax are exposed to high shear rate, they disaggregate. If the shear rate achieves certain critical value, the rouleaux break up completely. In such a flow only individual red blood cells are present.

It was observed, that the aggregates are not created, if the plasma proteins, fibrinogen and globulins, are missing. Hence blood behaves as Newtonian fluid in the absence of fibrinogen and globulins, see [39], [40].

Non-Newtonian behaviour of red blood cells in plasma was observed. Namely the buildup of rouleaux in low shear rate flow leads to increased viscosity, whereas as rouleuax split up down to individual cells under high shear rate conditions, viscosity decreases,[41]. Therefore blood exhibits the shear-thinning viscosity. A possibility how to capture shear-thinning viscosity of a fluid using a power-law model was introduced in Section 3.1.3.
It must be however noted that such conditions of low shear rate are mostly apparent in the venous system and in some places, where a recirculation is present, like in aneurysms or downstream stenoses, [42], [43], [44], [45].
In the majority of arterial system blood behaves as a Newtonian fluid, because of the higher shear rates or because of the speed of the flow, which do not allow the buildup of rouleaux.

Size of the aggregates does not depend only on shear rate, it is dependent also on cell shape, plasma composition and haematocrit, see [40] and [46]. Therefore viscosity of blood depends also on cell shape, plasma composition and haematocrit. Viscosity is also a function of temperature, see [47], [46], [48].

Viscoelasticity of blood Blood as a viscoelastic fluid has the ability to store and release energy [49]. The viscoelasticity of blood originates from the reversible deformation of red blood cells. They are elastic because of the elastic properties of the membrane of red blood cells. The buildup of rouleuax increases the viscoelastic properties of blood [50], [51]. It was observed, that viscoelasticity of blood is most apparent at low shear rate (up to $10s^{-1}$). Some approaches, how to model viscoelastic fluids were shown or referenced in Section 3.1.3.

Thixotropy of bloood Thixotropy of blood is mostly attributed to the finite time, which is required for the aggregation-disaggregation process of rouleaux. Thixotropic fluids were shortly reviewed in Section 3.1.3.

Yield stress of blood There is a discussion on the existence of yield stress of blood, see [24], [52]. Its value ranges from 0.002 to 0.40 $dynes/cm^2$, [53]. Different studies come with a wide range of possible values for yield stress, see [54]. We have mentioned several approaches to modelling yield stress of fluids in Section 3.1.3.

3.2.2 Review of models of blood flow

The simplest solution for capturing the shear thinning viscosity of blood in a model is using of a power-law model for viscosity. It suffers however from the drawback of power-law models - zero shear rate viscosity is unbounded, whereas large shear rate viscosity tends to zero. Because of this the power law model for blood is applicable only to limited range of shear rates.
There are however other models of shear thinning viscosity of blood like Cross, Carreau [55], which cope with the mentioned disadvantages of the power-law model.
The generalised Newtonian models outlined in Section 3.1.3 do not capture the viscoelasticity of blood. The model [56] captures the shear-thinning of blood over a wide interval of shear rates. However its relaxation times do not depend on shear rate, which is not in agreement with experiments.
We will now shortly review models capturing viscoelasticity of blood. In [57] was developed a viscoelastic model in the thermodynamic framework of [58].
Yet another approach to blood constitutive modelling present works of Quemada [59], [60], [61], Williams [62] and De Kee [63], [64]. They all end in a generalised Maxwell-like equation, see Section 3.1.3. In their models there is a structure variable, number fraction of red blood cells (aggregated particles) ([59], [60], [61] and [63], [64]) or of aggregated cell faces [62]. The viscosity and the relaxation time then depend on this structure variable.
In this paper we will use the model of Owens, [65], [66], which also traces the number density of red blood cells. The model is the microstructure based one, as will be apparent. So the derivation is philosophically similar to the microstructure

based derivation of Oldroyd-B model in Section 3.1.3. We will advocate this model, because it seems to us, that such a kind of model is most appropriate for the proposed aim of realistic blood coagulation process modelling. The used model is based on an assumption of nonhomogeneous flow, whereas a simplification of the model presented in [67] assumes homogeneous flow. The latter model is however not able to capture the spatially and temporally nonconstant distribution of red blood cells, i.e. hematocrit as a function of time and space, across the blood vessel.

3.2.3 A non-homogeneous model of blood

Model derivation

Owens [65], [66] uses for the derivation of his model results from polymer kinetic theory, see [68] for details. We have shown the microstructure based derivation of Oldroyd-B fluid model in Section 3.1.3. Suppose we have a solution of non-interacting dumbbells in a viscous solvent. If we assume, that the characteristic size of dumbbell in equilibrium l_0 is tiny in comparison with the tube radius, we can arrive at the following equation for the density of dumbbells N

$$\frac{DN}{Dt} = D_{tr}\Delta N - \frac{1}{2\zeta}\nabla\nabla : \boldsymbol{\tau}, \tag{3.64}$$

where $D_{tr} = \frac{k_B T}{2\zeta}$ is the translational diffusivity, k_B is the Boltzmann constant, T the temperature, ζ is a friction factor, $\boldsymbol{\tau}$ the elastic part of extra stress tensor. We need to clarify the symbol $\nabla\nabla$, it is the Hessian matrix, i.e. outer product of two nabla operators.
Tensor quantity $\mathbf{qq}$, where $\mathbf{q}$ is end-to-end dumbbell vector, develops under assumption $||\nabla\mathbf{v}|| << \lambda_H^{-1}$ according to the following equation

$$< \overset{\nabla}{\mathbf{qq}} >= D_{tr}\Delta < \mathbf{qq} > + \frac{4Nk_BT}{\zeta}\boldsymbol{I} - \frac{4K}{\zeta} < \mathbf{qq} >, \tag{3.65}$$

where $\boldsymbol{I}$ is the identity tensor. λ_H is the relaxation time of an isolated dumbbell and it is interrelated with the friction factor ζ and the spring constant K by the following equation

$$\lambda_H = \frac{\zeta}{4K}. \tag{3.66}$$

General quantity in our framework related to a dumbbell is a function of the position vector of the center of mass $\mathbf{r}_c$, the end-to-end vector $\mathbf{q}$, the momentum vector related to the center of mass $\mathbf{p}$ and the momentum vector related to the internal degrees of freedom $\mathbf{P}$, $B = B(\mathbf{r}_c, \mathbf{q}, \mathbf{p}, \mathbf{P})$. In the equation (3.65) an ensemble average is used, which is defined as

$$< B >:= \int_Q \int_{P_1} \int_{P_2} B f d\mathbf{p} d\mathbf{P} d\mathbf{q} \quad , \tag{3.67}$$

where Q, P_1 and P_2 is configuration space, momentum space related to $\mathbf{p}$ and momentum space related to $\mathbf{P}$, respectively.

In Owens' model it is assumed, that a rouleau can either disaggregate or aggregate with another rouleau. Rouleaux are in the model represented as Hookean elastic dumbbells. If a rouleau is composed of k red blood cells it is said, that it is a k-mer. We introduce the following notation for relevant quantities of Owens' model.

- number density of k-mers

$$N_k \tag{3.68}$$

- the scaled number density of RBCs

$$N_0 = \sum_{k=1}^{\infty} kN_k \tag{3.69}$$

- the scaled number density of rouleaux

$$M = \sum_{k=1}^{\infty} N_k \tag{3.70}$$

- the average rouleau size

$$n = n(N_0, M) = \frac{N_0}{M} \tag{3.71}$$

Reversible polymer network theory assumes that aggregation is a Brownian process proportional to the equilibrium number density $N_{k,0}$. Owens supposed also that disaggregation of k-mers is proportional to N_k. We write down an equation, which corresponds to (3.64)

$$\frac{DN_k}{Dt} = D_{tr,k}\Delta N_k - \frac{1}{2\zeta_k}\nabla\nabla : \boldsymbol{\tau}_k + h_k N_{k,0} - g_k N_k, \tag{3.72}$$

where h_k and g_k are aggregation and fragmentation rate coefficients, ζ_k is the k-dependent friction factor and

$D_{tr,k} = \frac{(k_BT+\kappa)_k}{2\zeta_k}$ is translational (thermal and convective) diffusivity for k-mers. As k-mer consists of k cells Owens chose

$$(k_BT + \kappa)_k = k(k_BT + \kappa) \qquad \text{and} \qquad \zeta_k = k\zeta, \tag{3.73}$$

where the term k_BT corresponds to small Brownian contribution and the constants κ takes into account collisions with other cells.

Hence we can replace $D_{tr,k}$ with

$$D_{tr} = \frac{k_BT + \kappa}{2\zeta}. \tag{3.74}$$

The equations corresponding to (3.65) for orientation tensor of k-mers

$$\begin{aligned} < \overset{\nabla}{\mathbf{qq}} >_k = & D_{tr,k}\Delta < \mathbf{qq} >_k + \frac{(4k_BT + \kappa)_k N_k}{\zeta}\mathbf{I} - \frac{4K}{\zeta} < \mathbf{qq} >_k \\ & + h_k < \mathbf{qq} >_{k,0} - g_k < \mathbf{qq} >_k . \end{aligned} \tag{3.75}$$

If we use the Kramers equation

$$\boldsymbol{\tau}_k = K < \mathbf{qq} > -kN_k(k_BT + \kappa)\boldsymbol{I}, \tag{3.76}$$

we get from (3.72) and (3.75) using (3.76) the following equation for the stress tensor of k-mer $\boldsymbol{\tau_k}$

$$\boldsymbol{\tau_k} + \mu_k \overset{\nabla}{\boldsymbol{\tau_k}} - D_{tr}\mu_k(\Delta\boldsymbol{\tau_k} + (\nabla\nabla : \boldsymbol{\tau_k}))\boldsymbol{I} = kN_k(k_BT + \kappa)\mu_k\mathbf{D}, \tag{3.77}$$

where we defined the relaxation time of k-mer

$$\mu_k = \frac{k\lambda_H}{1 + g_k k\lambda_H}. \tag{3.78}$$

In the previous work of Owens [7] it was chosen

$$g_k N_k = \frac{1}{2}\sum_{i=1}^{k-1} F_{i,k-i}N_k + \sum_{j=1}^{\infty} K_{k,j}N_kN_j \tag{3.79}$$

and

$$h_k N_{k,0} = \frac{1}{2}\sum_{i=1}^{k-1} K_{i,k-i}N_iN_{k-i} + \sum_{j=1}^{\infty} F_{k,j}N_{k+j}, \tag{3.80}$$

where $K_{i,j}$ is an aggregation kernel representing the rate at which i-mer and j-mer coalesce to form $(i+j)$-mer. On the other hand $F_{i,j}$ is a fragmentation kernel standing for the rate an i-mer and an j-mer is created by breaking up of $(i+j)$-mer. We choose the kernels to be functions of shear rate only, i.e. $a(\dot\gamma)$, $b(\dot\gamma)$. The next simplifying assumption concerns the position of reaction sites on a k-mer. They interact only at the end points of the rouleaux. The fragmentation coefficient equation (3.79) then becomes

$$g_k = \frac{b(\dot\gamma)(k-1)}{2} + a(\dot\gamma)\sum_{j=1}^{\infty} N_j, \tag{3.81}$$

whereas the aggregation coefficient equation (3.80) is modified to

$$h_k = \frac{a(\dot\gamma)}{2N_{k,0}}\sum_{i=1}^{k-1} N_iN_{k-i} + \frac{b(\dot\gamma)}{N_{k,0}}\sum_{j=1}^{\infty} N_{k+j}. \tag{3.82}$$

Just now we have an immense number of constitutive equations (3.77) for each k-mer. Instead of computing with this multi-mode model, we choose an average relaxation time, i.e. the relaxation time of an average rouleaux n: $\bar\mu := \mu_n$ (See (3.71) and (3.78)). After we performed this simplification, we can convert our equations to the simplified form in the following way.
By multiplying (3.72) with k, summing from $k = 1$ to ∞ we get

$$\frac{DN_0}{Dt} = D_{tr}\Delta N_0 - \frac{D_{tr}}{(k_BT + \kappa)}\nabla\nabla : \boldsymbol{\tau}. \tag{3.83}$$

By summing (3.77) from $k = 1$ to ∞ we get

$$\boldsymbol{\tau} + \bar\mu \overset{\nabla}{\boldsymbol{\tau}} - D_{tr}\bar\mu(\Delta\boldsymbol{\tau} + (\nabla\nabla : \boldsymbol{\tau}))\boldsymbol{I} = N_0(k_BT + \kappa)\bar\mu\mathbf{D}, \tag{3.84}$$

where

$$\boldsymbol{\tau} = \sum_{k=1}^{\infty}\boldsymbol{\tau_k}. \tag{3.85}$$

The evolution equation for number density of aggregates is reached by summing (3.72) from $k = 1$ to ∞

$$\frac{DM}{Dt} = D_{tr}\Delta M - \frac{D_{tr}}{(k_B T + \kappa)}\nabla\nabla : \boldsymbol{\sigma} - \frac{a(\dot{\gamma})}{2}M^2 + \frac{b(\dot{\gamma})}{2}(N_0 - M), \tag{3.86}$$

where

$$\boldsymbol{\sigma} = \sum_{k=1}^{\infty} \frac{\boldsymbol{\sigma}_k}{k}, \tag{3.87}$$

is a tensor quantity, which satisfies

$$\boldsymbol{\sigma} + \bar{\mu}\, \overset{\nabla}{\boldsymbol{\sigma}} - D_{tr}\bar{\mu}(\Delta\boldsymbol{\sigma} + (\nabla\nabla : \boldsymbol{\sigma}))\boldsymbol{I} = M(k_B T + \kappa)\bar{\mu}\mathbf{D}. \tag{3.88}$$

We have to close the system of equations for ($\mathbf{u}$, p, N_0, M, $\boldsymbol{\sigma}$, $\boldsymbol{\tau}$). We do so by adding the equations for linear momentum conservation and for conservation of mass:

$$\rho\frac{D\mathbf{u}}{Dt} = -\nabla p + \eta_N\Delta\mathbf{u} + \operatorname{div}\boldsymbol{\tau}, \tag{3.89}$$

$$\operatorname{div}\mathbf{u} = 0, \tag{3.90}$$

where p is the pressure, ρ is the blood density and η_N is the constant plasma viscosity.

Non-dimensionalization of the nonhomogeneous model

We perform non-dimensionalization of equations (3.83), (3.86), (3.84),(3.88), (3.89) and (3.90) using the following rescaling of variables similarly to [69]

$$\hat{N}_0 = \frac{N_0}{N_{av}} \quad , \quad \hat{M} = \frac{M}{N_{av}} \quad , \quad \hat{\mathbf{x}} = \frac{\mathbf{x}}{L} \quad , \quad \hat{\mathbf{u}} = \frac{\mathbf{u}}{U} \quad , \tag{3.91}$$

$$\hat{t} = \frac{tU}{L} \quad , \quad \hat{\boldsymbol{\tau}} = \frac{\boldsymbol{\tau}L}{\eta_t U} \quad , \quad \hat{p} = \frac{pL}{\eta_t U} \quad , \tag{3.92}$$

where U is the characteristic velocity, L is the characteristic length, N_{av} is the average number density of cells, η_t is the characteristic value of the total blood viscosity:

$$\eta_t = N_{av}(k_B T + \kappa)\lambda_H + \eta_p, \tag{3.93}$$

where the first term is the characteristic value for the RBC viscosity, whereas the second term is the characteristic value of plasma viscosity.

We introduce the following dimensionless numbers

- The Reynolds number

$$Re = \frac{\rho U L}{\eta_t} \tag{3.94}$$

- The Deborah number

$$De = \frac{\lambda_H U}{L} \tag{3.95}$$

- The Peclet number

$$Pe = \frac{UL}{D_{tr}} \tag{3.96}$$

- The ratio of plasma to total viscosity

$$\beta = \frac{\eta_p}{\eta_t} \tag{3.97}$$

After introducing the rescaling and identifying the characteristic nondimensional numbers, we arrive, after dropping of hats above scaled variables, at the following set of equations:

$$Re\frac{\partial \mathbf{u}}{\partial t} + Re\mathbf{u}\cdot\nabla\mathbf{u} = -\nabla p + \operatorname{div}\boldsymbol{\tau} + \beta\Delta\mathbf{u}, \tag{3.98}$$

$$\operatorname{div}\mathbf{u} = 0, \tag{3.99}$$

$$\frac{\partial N_0}{\partial t} + \mathbf{u}\cdot\nabla N_0 = \frac{1}{Pe}\Delta N_0 - \frac{1}{1-\beta}\frac{De}{Pe}\nabla\nabla : \boldsymbol{\tau}, \tag{3.100}$$

$$\frac{\partial M}{\partial t} + \mathbf{u}\cdot\nabla M = \frac{1}{Pe}\Delta M - \frac{1}{1-\beta}\frac{De}{Pe}\nabla\nabla : \boldsymbol{\sigma} - 0.5\alpha(\dot\gamma)\frac{N_0}{n}M + 0.5b(\dot\gamma)(N_0 - M), \tag{3.101}$$

$$\boldsymbol{\tau} + De\bar\mu(\dot\gamma, N_0, M)\overset{\triangledown}{\boldsymbol{\tau}} - \frac{De}{Pe}\bar\mu(\dot\gamma, N_0, M)(\Delta\boldsymbol{\tau} + (\nabla\nabla : \boldsymbol{\tau})\boldsymbol{I}) = (1-\beta)\bar\mu(\dot\gamma, N_0, M)N_0\boldsymbol{D}, \tag{3.102}$$

$$\boldsymbol{\sigma} + De\bar\mu(\dot\gamma, N_0, M)\overset{\triangledown}{\boldsymbol{\sigma}} - \frac{De}{Pe}\bar\mu(\dot\gamma, N_0, M)(\Delta\boldsymbol{\sigma} + (\nabla\nabla : \boldsymbol{\sigma})\boldsymbol{I}) = (1-\beta)\bar\mu(\dot\gamma, N_0, M)M\boldsymbol{D}. \tag{3.103}$$

In the next course of the work we will drop the bar over μ, i.e. $\bar\mu$ becomes μ.

3.3 Modelling blood coagulation

3.3.1 Review of models of blood coagulation

As was said in the Section 2.2 the whole process of blood coagulation consists of four phases - vasoconstriction, *primary haemostasis*, *secondary haemostasis* and fybrinolysis.
Correspondingly the models of blood coagulation could be divided into platelet plug formation models, blood clot formation models, fybrinolysis models. We are mostly interested in the modelling of primary haemostasis, i.e. platelet plug formation, as it is the focus of this work. We will however describe the models

of blood clot formation. We are doing so not only for completeness, but also because the fact, that primary haemostasis happens (almost) concurrently with secondary hemostasis. This concurrency is often taken into account in models of blood coagulation, where both processes are captured in one model. We will also describe the stabilization of the clot during the blood coagulation process in this work. For that purpose we use the model of [70] and [2].
Yet another categorization is elaborated in [71]. We will stick to this review in the following. First classification in [71] is based on the spatial scales of processes, which a model is able to capture. Second classification groups together models, which are able to describe specific physical processes of the blood coagulation process.

Classification of models based on scales of processes, which they describe In [71] the categorization according to scale is started with sub-microscale models, which have characteristic dimensions at sub-cellular scale, i.e. to order of 0.1 μm. At this level the interactions among proteins and macromolecules are captured.
Higher level of description of the coagulation process provide miscroscale models with characteristic dimensions 1-10μm. These models describe behaviour of platelets, erythrocytes and other microparticles in great detail. This can be useful for description of blood coagulation in microvessels, where the continuum hypothesis does not hold.

Macroscale Models In [71] are macroscale models identified by validity of the continuum hypothesis. Characteristic scales are above 100μm. The blood is no longer comprehended at a particulate level. Instead macroscopic variables and parameters are enough representative for description of the blood flow.
We have already made a remark in Section 3.2.2 on the comprehensive model of blood coagulation of [72], [57]. Both blood and clot are modeled as viscoelastic materials, whose constitutive equations were developed using the thermodynamic framework of [58], [32], [31]. The model of coagulation of [57] comprises of concentrations of 23 chemical species obeying convection-diffusion-reaction equations. The reaction kinetics is captured using reaction terms in the bulk of flow and flux boundary conditions defined on the site of injury for subset of the species. The set of reactions ends with creation of fibrin, which causes steep increase of clot viscosity. In this way the coupling flow-chemistry is introduced.
In [72] and [57] the activation of platelets can proceed in two ways - biochemical and rheological. The rheological activation depends on so called activation number, which is assigned to each platelet. The activation number depends on the length of exposure of a platelet to elevated shear stress.

Classification of models based on features, which they describe This grouping of models relies on different physical phenomena captured in the models. In [71] the following groups are described

- Biochemistry (Only) Models

- Biochemistry and Flow Models
- Biochemistry and Flow and Structure Models

In [73] a similar splitting of models is introduced. There are two basic categories - ODE's models and PDE's models. The biochemistry (only) models category from [71] is almost identical with ODE's models of [73].
A coagulation process model begins to be more complicated with introduction of flow as new chemical species and platelets are carried to the site of injury, on the one hand. On the other hand the blood flow carries away the agents of the coagulation process. What is more, this carrying away is very important during the process of fibrinolysis.
The third item in the list Biochemistry and Flow an Structure Models represents models, which try to capture the mechanical properties of clot or influence of clot on the blood flow. One of the models in this category is the model of [6], [74] and [3], which we will treat in the next section in detail. Afterwards we review the model of Storti [1]. We review the constitutive model for blood clot of Kempen [2]t as well. We will modify or extend all three models in the further course of this thesis.

Models of coagulation used in our work

We propose three new coagulation models witch could be seen as extensions of already developed models. We use namely

- Weller's model of blood coagulation, [3], [6]
- Storti's model of *primary hemostasis*, [8], [1]
- Kempen's model of *secondary hemostasis*, [2]

In the next paragraphs we review the models in order to be able to formulate the extensions in further course of this work.

Weller's model of clot growth Let us introduce the basic setting of the free boundary problem, see Fig. 3.2.

In this picture we have the time independent parts, namely inflow I, non-reactive wall Σ and outflow O. The blood flowing from the inflow I carries new platelets, some of which get incorporated on the moving boundary Γ_t into the developing thrombus Ω_s. As the thrombus grows the area of flowing blood Ω_t reduces. Hence the growing clot affects the flow.
Firstly we define the domains, T is the end time of simulation:

- inflow boundary: $I_T := I \times (0, T]$
- outflow boundary: $O_T := O \times (0, T]$
- non-reactive wall $\Sigma_T := \Sigma \times (0, T]$
- time dependent area of blod flow: $\Omega_T := \bigcup_{0<t\leq T} \Omega_t \times \{t\}$
- moving boundary: $\Gamma_T := \bigcup_{0<t\leq T} \Gamma_t \times \{t\}$

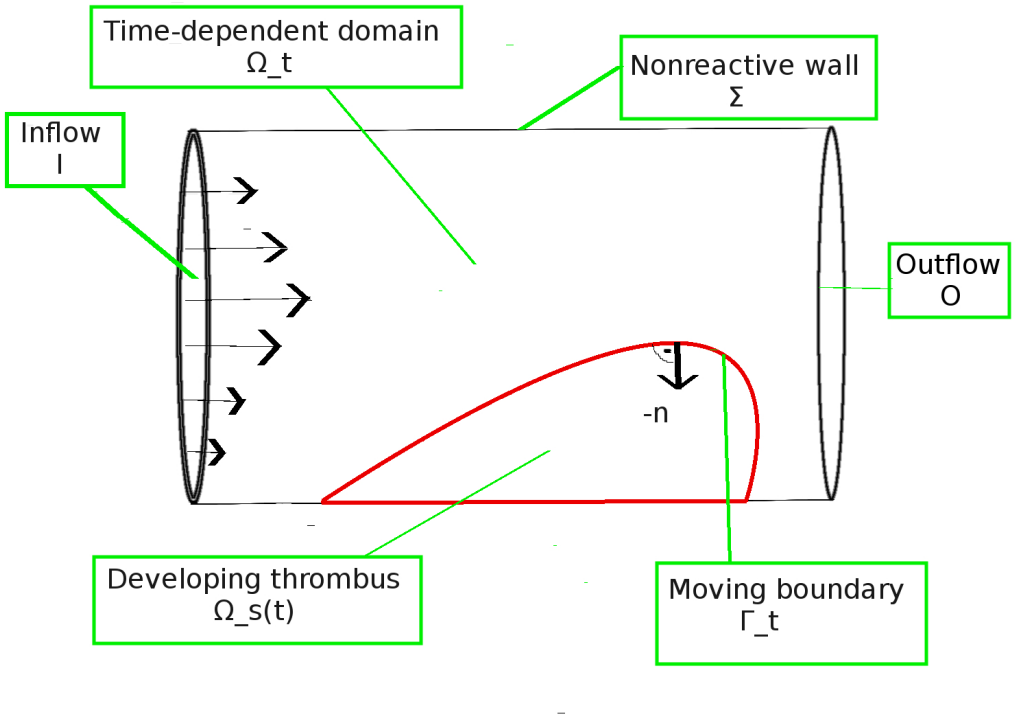

Figure 3.2: Computational domain of Weller's model

Relevant equations are then formulated in these domains. The model contains Navier-Stokes equations for the blood, as blood is taken as a Newtonian fluid with the constant kinematic viscosity ν. In the blood are distributed blood platelets, which obey a transport equation.
The free boundary model then reads, the Navier-Stokes part:

$$\begin{aligned}
\frac{\partial \mathbf{u}}{\partial t} - \nu\Delta\mathbf{u} + \mathbf{u}\cdot\nabla\mathbf{u} + \nabla p &= \mathbf{b} && \text{in} \quad \Omega_T, \\
\nabla\cdot\mathbf{u} &= 0 && \text{in} \quad \Omega_T, \\
\mathbf{u} &= 0 && \text{on} \quad \Gamma_T \cup \Sigma_T, \\
\mathbf{u} &= \mathbf{u}_D && \text{on} \quad I_T, \\
\nu\frac{\partial \mathbf{u}}{\partial \mathbf{o}} &= p\cdot\mathbf{o} && \text{on} \quad O_T, \\
\mathbf{u}(t=0) &= \mathbf{u}_0 && \text{in} \quad \Omega_0,
\end{aligned} \tag{3.104}$$

where $\mathbf{u}$ it the velocity of blood, p is the pressure, $\mathbf{b}$ is the body force field, like gravity, $\mathbf{o}$ is the unit outer normal to the outflow boundary O. $\mathbf{u}_D$ is the Dirichlet boundary condition imposed on velocity on the inflow I, $\mathbf{u}_0$ is the initial condition on velocity.

The transport equation for platelet concentration w looks in the following manner:

$$\frac{\partial w}{\partial t} - D\Delta w + \mathbf{u}\cdot\nabla w = 0 \qquad \text{in} \quad \Omega_T, \tag{3.105}$$

$$D\frac{\partial w}{\partial \mathbf{n}} = kw \qquad \text{on} \quad \Gamma_T, \tag{3.106}$$

$$\frac{\partial w}{\partial \mathbf{n}} = 0 \qquad \text{on} \quad \Sigma_T \cup O_T,$$

$$w = w_D \qquad \text{on} \quad I_T,$$

$$w(t=0) = w_0 \qquad \text{in} \quad \Omega_0,$$

where D is the constant diffusivity, $\mathbf{u}$ is the velocity field obtained from the solution of the Navier-Stokes equations, $\mathbf{n}$ it the unit outer normal to the reactive interface Γ_T. w_D is the Dirichlet boundary condition on platelets, w_0 is the initial condition on platelets.
r is the adhesion rate, which depends on shear stress s, to be defined later on:

$$r := \kappa_1 + \kappa_2 s. \tag{3.107}$$

The growth velocity $\mathbf{u_i}$ is supposed to be antiparallel to platelet gradient, i.e. the proportionality constant α is chosen as positive:

$$\mathbf{u_i} = \alpha\nabla w \qquad \text{on} \quad \Gamma_T. \tag{3.108}$$

We use now the main idea of the level set method (for details see [75] and [76]) - the moving interface Γ_T can be represented implicitly as the zero level set of a function ϕ, whose sign can serve to distinguish the domains of *fluid* blood $\Omega_f(t) := \Omega_t$ and emerging thrombus $\Omega_s(t)$. To be more specific, the different parts of the domain are constituted by

$$\Omega_f(t) = \{x \in \Omega^* : \phi(x,t) > 0\}, \qquad \Gamma_t(t) = \{x \in \Omega^* : \phi(x,t) = 0\}, \tag{3.109}$$

$$\Omega_s(t) = \{x \in \Omega^* : \phi(x,t) < 0\},$$

where $\Omega^* = \Omega_f(t) \cup \Gamma_t(t) \cup \Omega_s(t)$. It follows from the definition of ϕ, that the transport equation

$$\frac{\partial \phi}{\partial t} + \mathbf{u_i}\cdot\nabla\phi = 0 \qquad \text{on} \quad \Gamma_T. \tag{3.110}$$

has to be fulfilled along the moving interface. The natural extension to the whole domain Ω^* can be formulated as

$$\frac{\partial \phi}{\partial t} + \alpha k D^{-1} w\,|\nabla\phi| = 0 \qquad \text{in} \quad \Omega^*. \tag{3.111}$$

At time $t = 0$, the level set function is initialized to the signed distance function, that is

$$\phi(x,0) := \begin{cases} \text{dist}(x,\Gamma_0) & x \in \Omega_t \cup \Gamma_0, \\ -\text{dist}(x,\Gamma_0) & x \in \Omega_s(0). \end{cases} \tag{3.112}$$

Weller substituted the following term obtained by integration by parts over the interface Γ_t

$$\int_{\Gamma_t} \left(-\nu\frac{\partial \mathbf{u}}{\partial \mathbf{n}} + p\mathbf{n}\right)\cdot\boldsymbol{\psi}\, dS \tag{3.113}$$

Figure 3.3: Problem settings

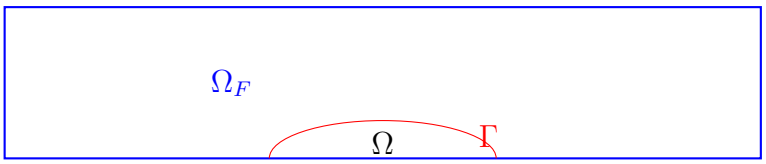

by the following expression

$$\beta(h) \int_{\Gamma_t} \mathbf{u} \cdot \boldsymbol{\psi} dS, \tag{3.114}$$

where β is a function depending on the cell size h so that $\beta(h) \to \infty$ as $h \to 0$. $\boldsymbol{\psi}$ is a vector test function. The velocity field is extended to Ω_s to fullfill $\mathbf{u} = \mathbf{0}$ in Ω_s, which leads to the additional term $\int_{\Omega_s} \mathbf{u} \cdot \boldsymbol{\psi} dx$. The pressure is harmonically extended into the solid. On the part of boundary $\partial\Omega_s(t) \setminus \Gamma_t$ is imposed the homogeneous Dirichlet boundary condition on $\mathbf{u}$.

Storti's model of clot growth

Chemistry part of the model Let us now imagine the situation in the Figure 3.3, where Ω_F, Ω and Γ represent the flowing blood domain, the clot domain and the interface domain, respectively.

The model of Storti is based on the model of [77] and [78]. Before we dive into the biochemical and rheological model of Storti presented in [1], [8] and [79] we shortly describe the rough idea of the model.

Simply said, in the model several biochemical species appear together with two populations of blood platelets - activated and unactivated. On the occurence of the wall injury it is triggered the system of biochemical reactions in which participate both flowing chemical species and blood platelets. The unactivated platelets become activated by influence of some of the chemical species and other already activated platelets. The activated platelets form a flux which causes the growth of the area filled with the activated platelets, the clot. Let us now formalize these ideas.

We trace seven species in the blood flow, it is a continuum model therefore we are interested in their concentrations:

1. Unactivated platelets c_{up}(PLT/ml),
2. Activated platelets c_{ap}(PLT/ml),
3. Adenosine diphosphate c_{adp} (μM),
4. Thromboxane c_{tx} (μM),
5. Prothrombin c_{pt} (μM),
6. Thrombin c_{th} (μM),
7. Antithrombin c_{at} (μM),

where PLT is the number of platelets and μM = nmol/ml.
Convection, diffusion and reaction of all species can be expressed in this generic equation

$$\frac{\partial \mathbf{c}}{\partial t} + (\mathbf{u} \cdot \nabla)\mathbf{c} = \mathbb{D}\Delta\mathbf{c} + \mathbf{S}(\mathbf{c}) \qquad \text{in} \quad \Omega_F, \tag{3.115}$$

where $\mathbf{c}$ is the vector of all seven species, i.e. $\mathbf{c} = (c_{up}, c_{ap}, c_{adp}, c_{tx}, c_{pt}, c_{th}, c_{at})$, $\mathbb{D}$ is the diagonal matrix with diffusivities of each species on diagonal, i.e. $\mathbb{D} = \text{diag}(D_{up}, D_{ap}, D_{adp}, D_{tx}, D_{pt}, D_{th}, D_{at})$. $\mathbf{S}(\mathbf{c})$ is the vector of reaction terms of all seven species,
i.e. $\mathbf{S}(\mathbf{c}) = (S_{up}(\mathbf{c}), S_{ap}(\mathbf{c}), S_{adp}(\mathbf{c}), S_{tx}(\mathbf{c}), S_{pt}(\mathbf{c}), S_{th}(\mathbf{c}), S_{at}(\mathbf{c}))$. $\mathbf{u}$ is the blood flow velocity. A summary of source terms in $\mathbf{S}(\mathbf{c})$ for each species, which will be described below, is given in Table 3.1.
In the coagulation model of [1],[8] and [79] the velocity field $\mathbf{u}$ is obtained by solution of Navier-Stokes equations in Ω_F.
The reaction terms for the unactivated and activated platelets look simple

$$S_{up} = -k_{pa} c_{up} \tag{3.116}$$

and

$$S_{ap} = k_{pa} c_{up}, \tag{3.117}$$

where the first order reaction rate k_{pa} is defined in the following manner

$$k_{pa} = \begin{cases} 0 & \text{if} \quad f_{act} < 1, \\ \frac{f_{act}}{\tau_{pa}} & \text{if} \quad f_{act} \geq 1, \end{cases} \tag{3.118}$$

where τ_{pa} is a characteristic time constant and f_{act} is a function defined by

$$f_{act} = \frac{c_{adp}}{c_{adp,crit}} + \frac{c_{tx}}{c_{tx,crit}} + \frac{c_{th}}{c_{th,crit}}, \tag{3.119}$$

where $c_{adp,crit}$, $c_{tx,crit}$ and $c_{th,crit}$ are the critical values of ADP, thromboxane and thrombin. Their values are in Table 5.9. The ADP, thromboxane and thrombin are responsible for the activation of resting platelets. If their concentration is high enough, the function (3.118) becomes positive and the process of activation of resting platelets is set off. Therefore this function is responsible for the activation of resting platelets by the activating chemicals.
The reaction terms for ADP and thromboxane are taken as

$$S_{adp} = \lambda_{adp} k_{pa} c_{up} \tag{3.120}$$

and

$$S_{tx} = s_{pj} c_{ap} - k_{1j} c_{tx}, \tag{3.121}$$

where λ_{adp} is the quantity of ADP produced from one activated platelet, s_{pj} stands for rate of the creation of thromboxane by activated platelets, k_{1j} is the rate of inhibition of thromboxane.
The reaction terms of the thrombin system are given by

$$S_{pt} = -\gamma c_{pt}(\phi_a c_{ap} + \phi_u c_{up}) \tag{3.122}$$

for prothrombin,

$$S_{th} = \gamma c_{pt}(\phi_a c_{ap} + \phi_u c_{up}) - k_{2j} c_{at} c_{th} \tag{3.123}$$

for thrombin and

$$S_{at} = -k_{2j} c_{at} c_{th} \tag{3.124}$$

for antithrombin, where ϕ_a and ϕ_u stand for rate of synthesis of thrombin from prothrombin at the surface of activated and resting platelets, respectively.

β is a conversion factor, k_{2j} is the rate at which creation of thrombin is inhibited by antithrombin.

$$\mathbb{D}\frac{\partial \mathbf{c}}{\partial \mathbf{n}} = \mathbf{R}(\mathbf{c}, \mathbf{f}) \qquad \text{on} \quad \Gamma, \tag{3.125}$$

where $\mathbf{R}(\mathbf{c}, \mathbf{f})$ is the vector of adhesion or release term for each species, i.e.

$$\mathbf{R}(\mathbf{c}, \mathbf{f}) = (R_{up}(\mathbf{c}, \mathbf{f}), R_{ap}(\mathbf{c}, \mathbf{f}), R_{adp}(\mathbf{c}, \mathbf{f}), R_{tx}(\mathbf{c}, \mathbf{f}), R_{pt}(\mathbf{c}, \mathbf{f}), R_{th}(\mathbf{c}, \mathbf{f})) \tag{3.126}$$

where $\mathbf{f}$ is the vector of the surface quantities, which undergo development, i.e. $\mathbf{f} = (f_s, M_{as}, M_r, M_{at})$. The components of vector $\mathbf{f}$ are specified below. The summary of flux terms for all species in $\mathbf{c}$ is given in Table 3.2.

The boundary condition for unactivated platelets stands for attachment of the platelets to the injured wall

$$D_{up}\frac{\partial c_{up}}{\partial n} = f_s k_{rs} c_{up} \qquad \text{on} \quad \Gamma, \tag{3.127}$$

where f_s is a saturation function of the reacting surface, which will be described below. k_{rs} is the reaction constant capturing adherence of unactivated platelets to the reactive surface.

The boundary condition for activated platelets takes into account both attachment to the injured wall and adherence of activated platelets to each other

$$D_{ap}\frac{\partial c_{ap}}{\partial n} = f_s k_{as} c_{ap} + \frac{M_{as}}{M_\infty} k_{aa} c_{ap} \qquad \text{on} \quad \Gamma, \tag{3.128}$$

where k_{as} and k_{aa} is the adherence constant of activated platelets to the damaged wall and to each other, respectively. M_{as} is the portion of the surface occupied by activated platelets, to be specified below. M_∞ is the total capacity of the surface for platelets. It is the maximal number of platelets that can bind to a certain area.

In the boundary conditions the possibility is taken into account, that the wall is saturated with platelets. In such a case only attachment of activated platelets to each other can happen. It is done by introduction of the function $f_s = f_s(x, t)$, which is developing according to the following equation

$$\begin{cases} \frac{\partial f_s}{\partial t} = -\left(\frac{k_{rs}}{M_\infty} c_{up} + \frac{k_{as}}{M_\infty} c_{ap}\right) f_s \qquad \text{on} \quad \Gamma, \\ f_s|_{t=0} = 1 \qquad \text{on} \quad \Gamma. \end{cases} \tag{3.129}$$

As was said, the boundary condition (3.128) depends on the portion of the total surface coverage occupied by activated platelets M_{as}. It develops according

$$\begin{cases} \frac{\partial M_{as}}{\partial t} = \theta f_s k_{rs} c_{up} + k_{as} f_s c_{ap} + k_{pa} M_r \qquad \text{on} \quad \Gamma, \\ M_{as}|_{t=0} = 0 \qquad \text{on} \quad \Gamma, \end{cases} \tag{3.130}$$

where θ is the fraction of adhering resting platelets, which get activated on contact with the reactive surface. In the equation (3.130) the portion of the total surface coverage occupied by unactivated platelets M_r appears. It obeys the following equation

$$\begin{cases} \frac{\partial M_r}{\partial t} = (1-\theta) f_s k_{rs} c_{up} - k_{pa} M_r & \text{on} \quad \Gamma, \\ M_r|_{t=0} = 0 & \text{on} \quad \Gamma. \end{cases} \tag{3.131}$$

The activated platelets release ADP and thromboxane, which means, that we have an influx of these chemicals into the area around the clot.
The boundary condition on ADP is

$$D_{adp} \frac{\partial c_{adp}}{\partial n} = -\lambda_{adp} (\theta f_s k_{rs} c_{up} + k_{pa} M_r) \qquad \text{on} \quad \Gamma, \tag{3.132}$$

whereas the boundary condition on thromboxane is

$$D_{tx} \frac{\partial c_{tx}}{\partial n} = -s_{pj} M_{at} \qquad \text{on} \quad \Gamma, \tag{3.133}$$

which stipulates, that thromboxane is generated because of the total amount of activated platelets participating in the clot M_{at}. M_{at} contains both activated platelets adhered to the injury and activated platelets bound to each other. Its development is described by the following equation

$$\begin{cases} M_{at} = \theta f_s k_{rs} c_{up} + f_s k_{as} c_{ap} + \frac{k_{aa}}{M_\infty} M_{as} c_{ap} + k_{pa} M_r & \text{on} \quad \Gamma, \\ M_{at}|_{t=0} = 0 & \text{on} \quad \Gamma. \end{cases} \tag{3.134}$$

The thrombin cycle on the injury site does not contain antithrombin, i.e. we have

$$D_{pt} \frac{\partial c_{pt}}{\partial n} = \gamma (\phi_a M_{at} + \phi_r M_r) c_{pt} \qquad \text{on} \quad \Gamma, \tag{3.135}$$

and

$$D_{th} \frac{\partial c_{th}}{\partial n} = -\gamma (\phi_a M_{at} + \phi_r M_r) c_{pt} \qquad \text{on} \quad \Gamma. \tag{3.136}$$

Table 3.1: Overview of elements of reaction terms vector $\mathbf{S}(\mathbf{c})$ depending on concentrations in $\mathbf{c}$

Species name	conc.	conc. units	formula for the reaction term S
Resting platelets	c_{up}	$PLTml^{-1}$	$-k_{pa} c_{up}$
Activated platelets	c_{ap}	$PLTml^{-1}$	$+k_{pa} c_{up}$
ADP	c_{adp}	μM	$\lambda_j k_{pa} c_{up}$
Thromboxane	c_{tx}	μM	$s_{pj} c_{ap} - k_{1j} c_{tx}$
Prothrombin	c_{pt}	μM	$-\beta c_{pt} (\phi_a c_{ap} + \phi_u c_{up})$
Thrombin	c_{th}	μM	$\beta c_{pt} (\phi_a c_{ap} + \phi_u c_{up}) - k_{2j} c_{at} c_{th}$
Antithrombin	c_{at}	μM	$-\beta k_{2j} c_{at} c_{th}$

Table 3.2: Overview of flux terms in $\mathbf{R}(\mathbf{c}, \mathbf{f})$

Species name	concentration	formula for the Robin condition R
Resting platelets	c_{up}	$f_s k_{rs} c_{up}$
Activated platelets	c_{ap}	$f_s k_{as} c_{ap} + \frac{M_{as}}{M_\infty} k_{aa} c_{ap}$
ADP	c_{adp}	$-\lambda_j(\theta f_s k_{rs} c_{up} + k_{pa} M_r)$
Thromboxane	c_{tx}	$-s_{pj} M_{at}$
Prothrombin	c_{pt}	$\beta(\phi_a M_{at} + \phi_r M_r) c_{pt}$
Thrombin	c_{th}	$-\beta(\phi_a M_{at} + \phi_r M_r) c_{pt}$
Antithrombin	c_{at}	0

Plug growth influences the rheology model In [1], [8] and [79] Storti imposes the Poiseuille profile as the boundary condition on the velocity field. The flow is governed by the ALE-reformulated Navier-Stokes equations, which will be shown later.
For the ALE formulation it is necessary to know the velocity of the grid, which is determined by the velocity of the clot growth. For that purpose Storti defined the flux of deposited bounded platelets j_{bp} as

$$j_{bp} = -\frac{\partial c_{bp}}{\partial t}, \tag{3.137}$$

where c_{bp} is defined as the quantity of deposited bounded platelets on the surface of clot. Its development can be obtained from the Robin boundary conditions (3.127) and (3.128) getting

$$\frac{\partial c_{bp}}{\partial t} = f_s k_{rs} c_{up} + \left(f_s k_{as} + \frac{M_{as}}{M_\infty} k_{aa} \right) c_{ap}. \tag{3.138}$$

Using this equation and the definition (3.137) we arrive at the following equation

$$j_{bp} = -f_s k_{rs} c_{up} - \left(f_s k_{as} + \frac{M_{as}}{M_\infty} k_{aa} \right) c_{ap}. \tag{3.139}$$

We define similarly to [1, 8] and [79] the displacement of the interface $\mathbf{d}$ as

$$\frac{d}{dt}\mathbf{d} = \mathbf{u_i} = j_{bp} V_p \, \mathbf{n}, \tag{3.140}$$

where $\mathbf{u_i}$ is the velocity of the growth, V_p is the volume of a single platelet and $\mathbf{n}$ is the normal vector to the clot interface. Storti introduces the parameter α_V, which takes into account, that among the platelets in the clot there is some space. Hence we modify (3.140) followingly

$$\frac{d}{dt}\mathbf{d} = \mathbf{u_i} = j_{bp}(1 + \alpha_V) V_p \, \mathbf{n}. \tag{3.141}$$

ALE framework for the clot growth We define moving curvilinear coordinates $\tilde{\boldsymbol{\zeta}}$ which are related to the spatial coordinates $\mathbf{x}$ by the function $\hat{\mathbf{x}}$

$$\mathbf{x} = \hat{\mathbf{x}}(\tilde{\boldsymbol{\zeta}}, t). \tag{3.142}$$

The function $\mathbf{c} = \mathbf{c}(\mathbf{x}, t)$ can be then expressed with respect to the moving coordinate system as

$$\mathbf{c}(\mathbf{x}, t) = \hat{\mathbf{c}}(\hat{\mathbf{x}}(\tilde{\boldsymbol{\zeta}}, t)) \equiv \bar{\mathbf{c}}(\tilde{\boldsymbol{\zeta}}, t). \tag{3.143}$$

We define the grid time derivative

$$\frac{\delta \mathbf{c}}{\delta t} = \frac{\partial \mathbf{c}}{\partial t}|_{\tilde{\boldsymbol{\zeta}}=const} = \frac{\partial \bar{\mathbf{c}}}{\partial t} \quad , \tag{3.144}$$

which by the chain rule becomes

$$\frac{\delta \mathbf{c}}{\delta t} = \frac{\partial \hat{\mathbf{c}}}{\partial t} + \frac{\partial \hat{\mathbf{x}}}{\partial t} \cdot \nabla \hat{\mathbf{c}}. \tag{3.145}$$

Realising that $\frac{\partial \hat{\mathbf{c}}}{\partial t}$ is the local time derivative $\frac{\partial \mathbf{c}}{\partial t}$ and defining the grid velocity as

$$\mathbf{w} = \frac{\partial \hat{\mathbf{x}}}{\partial t} \tag{3.146}$$

we reformulate (3.145) in the following manner

$$\frac{\delta \mathbf{c}}{\delta t} = \frac{\partial \mathbf{c}}{\partial t} + \mathbf{w} \cdot \nabla \hat{\mathbf{c}} \quad , \tag{3.147}$$

which in the Eulerian formulation, where the grid is fixed, i.e. $\mathbf{w} = 0$ reduces to

$$\frac{\delta \mathbf{c}}{\delta t} = \frac{\partial \mathbf{c}}{\partial t} \quad . \tag{3.148}$$

On the other hand we have the following equation for the Lagrangian formulation, where $\mathbf{w} = \mathbf{u}$, i.e. the grid velocity equals to the fluid velocity:

$$\frac{\delta \mathbf{c}}{\delta t} = \frac{\partial \mathbf{c}}{\partial t} + \mathbf{u} \cdot \nabla \hat{\mathbf{c}} \quad , \tag{3.149}$$

From the equations (3.147) and (3.149) we get

$$\dot{\mathbf{c}} = \frac{\delta \mathbf{c}}{\delta t} + (\mathbf{u} - \mathbf{w}) \cdot \nabla \mathbf{c}. \tag{3.150}$$

Our generic convection-diffusion-reaction equations (3.115) can then be reformulated as follows

$$\frac{\partial \mathbf{c}}{\partial t} + ((\mathbf{u} - \mathbf{w}) \cdot \nabla)\mathbf{c} = \mathbb{D}\Delta \mathbf{c} + \mathbf{S}(\mathbf{c}). \tag{3.151}$$

Taking into account the growth model the following Navier-Stokes equations are to be solved

$$\begin{cases} \rho \frac{\partial \mathbf{u}}{\partial t} + \rho((\mathbf{u} - \mathbf{w}) \cdot \nabla)\mathbf{u} = -\nabla p + \eta \Delta \mathbf{u}, \\ \operatorname{div} \mathbf{u} = 0, \end{cases} \tag{3.152}$$

where $\mathbf{u}$ and p are the blood velocity and pressure, respectively. ρ and η the density and the viscosity of blood, respectively. Looking at the equation for the displacement of the clot surface (3.141) we deduce the specific form of the grid velocity:

$$\mathbf{w} = j_{bp}(1 + \alpha_V)V_p \mathbf{n}, \tag{3.153}$$

where the flux j_{bp} is given by (3.139).
In [8] was assumed, that the emerging clot is a rigid solid. The plug clot poses an obstacle to the blood flow, so the blood can not flow through the area of clot.
Another approach was chosen in [79], where the clot was taken as an elastic solid with neo-Neookean constitutive relation. Namely in the area of clot the following momentum and mass balance equations were assumed:

$$\operatorname{div} \boldsymbol{T} = \mathbf{0} \qquad \text{in} \quad \Omega, \tag{3.154}$$

$$J - 1 = 0 \qquad \text{in} \quad \Omega, \tag{3.155}$$

where the Cauchy stress tensor $\boldsymbol{T}$ for the incompressible material (as we have (3.155)) takes the following form:

$$\boldsymbol{T} = -p\mathbf{I} + \boldsymbol{S}. \tag{3.156}$$

J is defined as

$$J = \det(\mathbf{F}), \tag{3.157}$$

i.e. it captures change of volume of reference configuration into the current configuration . The neo-Hookean constituve relations then reads as

$$\boldsymbol{S} = G\left(\mathbf{B} - \mathbf{I}\right), \tag{3.158}$$

where G is the shear modulus and $\mathbf{B} = \mathbf{F}\mathbf{F}^T$, where $\mathbf{F}$ is the deformation gradient tensor.

The interaction between the blood and the clot is two-fold:

- fluid-solid coupling
  the blood effects the clot by the traction force computed from the total stress tensor of the viscous fluid $\boldsymbol{T}_F$:

  $$\mathbf{t}_F = \boldsymbol{T}_F \mathbf{n}, \tag{3.159}$$

  where $\boldsymbol{T}_F = -p\mathbf{I} + 2\eta\mathbf{D}$.

- solid-fluid coupling
  based on the traction force of the fluid (3.159) one computes using the equations for the solid the displacement of the solid $\delta\mathbf{x}$. The clot is moved accordingly, which causes the change of fluid domain.

Kempen's constitutive model of clot

Kempen developed a nonlinear viscoelastic constitutive equation for blood clot. It captures rheological properties of several types of clots - whole blood clot, platelet rich plasma clot and platelet poor plasma. However it remains on the phenomenological level of description, where the different rheological behaviour of the mentioned types of clot is described by change of seven fit parameters.
The model was fitted against clots in experimental cone-plate rheometer. It is based on the idea of in parallel connected elements - an elastic spring, a viscous dashpot and two Maxwell elements, see Fig. 3.5.

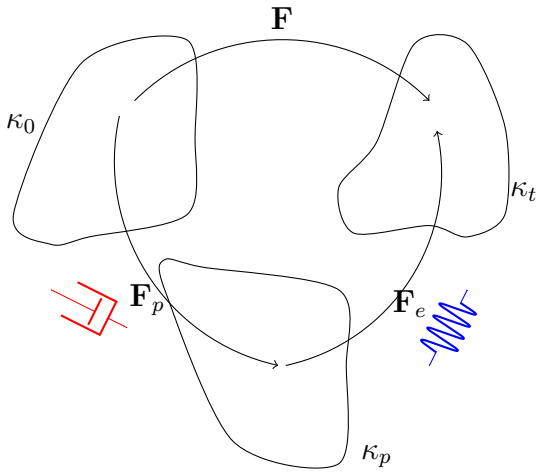

Figure 3.4: Scheme of configurations

Kinematics Assume we have a solid material. Then its changes of shape and volume are described using the deformation gradient tensor $\mathbf{F}$. The deformed line element $\mathbf{dx}$ is related to the underformed state $\mathbf{dX}$ in the following manner:

$$\mathbf{dx} = \mathbf{F}\mathbf{dX}. \tag{3.160}$$

We split the the deformation gradient $\mathbf{F}$ into an inelastic part $\mathbf{F}_p$ and an elastic part $\mathbf{F}_e$, see Figure 3.4,

$$\mathbf{F} = \mathbf{F}_e\mathbf{F}_p. \tag{3.161}$$

The inelastic part $\mathbf{F}_p$ deforms the undeformed state to a relaxed stress-free state. This is a state, at which we would arrrive, when we removed all loads from the material line element. The elastic part $\mathbf{F}_e$ transforms the stress-free state into the deformed state.
We define the Finger tensor $\mathbf{B}$ followingly:

$$\mathbf{B} = \mathbf{F}\mathbf{F}^T. \tag{3.162}$$

We define the Finger tensor $\mathbf{B}_e$ for the elastic deformation:

$$\mathbf{B} = \mathbf{F}_e\mathbf{F}_e^T \tag{3.163}$$

We define the velocity gradient tensor $\mathbf{L}$

$$\mathbf{L} = \dot{\mathbf{F}}\mathbf{F}^{-1}, \tag{3.164}$$

which can be additively decomposed into the elastic part $\mathbf{L}_e$ and the inelastic part $\mathbf{L}_p$:

$$\mathbf{L} = \mathbf{L}_e + \mathbf{L}_p, \tag{3.165}$$

where

$$\mathbf{L}_e = \dot{\mathbf{F}}_e\mathbf{F}_e^{-1} \tag{3.166}$$

and

$$\mathbf{L}_p = \dot{\mathbf{F}}_e\dot{\mathbf{F}}_p\mathbf{F}_p^{-1}\mathbf{F}_e^{-1} \tag{3.167}$$

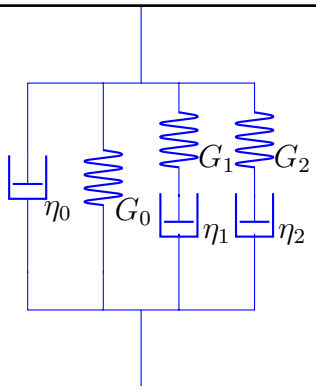

Figure 3.5: Schema of rheological model of Kempen

We decompose both parts of the velocity gradient, i.e. $\mathbf{L}_e$, $\mathbf{L}_p$, followingly

$$\mathbf{L}_e = \mathbf{D}_e + \mathbf{\Omega}_e, \tag{3.168}$$

$$\mathbf{L}_p = \mathbf{D}_p + \mathbf{\Omega}_p \tag{3.169}$$

where $\mathbf{D}_e$ and $\mathbf{D}_p$ are the symmetric rate of deformation tensor for the elastic part of deformation and for the viscous part of deformation, respectively. The symbol $\mathbf{\Omega}_e$ and $\mathbf{\Omega}_p$ represent the skew-symmetric spin tensor for the elastic part of deformation and for the viscous part of deformation, respectively.

In order to have a unique stress free state, it is assumed, that the inelastic deformation happens spin free:

$$\mathbf{\Omega}_p = \mathbf{0} \tag{3.170}$$

and all rotations are contained in the elastic part of deformation

$$\mathbf{\Omega} = \mathbf{\Omega}_e. \tag{3.171}$$

Constitutive model The connection of the viscos dashpot, elastic spring and two Maxwell elements, see Figure 3.5, is described by the following equation

$$\boldsymbol{\tau}_{clot} = \boldsymbol{\tau}_v + \boldsymbol{\tau}_e + \sum_{i=1}^{2} \boldsymbol{\tau}_{ve,i}, \tag{3.172}$$

where $\boldsymbol{\tau}_v$, $\boldsymbol{\tau}_e$ and $\boldsymbol{\tau}_{ve,i}$ are the contributions from the viscous dashpot, elastic spring and Maxwell elements, respectively. Model captures change of the clot behaviour from viscoelastic fluid-like to viscoelastic solid-like.
The viscous element reads as

$$\boldsymbol{\tau}_v = 2\left(\eta_N + f_v(t) f_{vi}(I_B)\eta_{00}\right)\mathbf{D}, \tag{3.173}$$

where η_N is the plasma viscosity, $I_B = \mathrm{tr}\mathbf{B}$, η_{00} is the value of viscosity η_0 of the mature clot, which was obtained from the experiment in [2] and the function $f_v(t)$ is changing with time according to

$$f_v(t) = \begin{cases} 0 & \text{if} \quad t \leq t_0, \\ \left(1 - e^{-\frac{(t-t_0)}{t_c}}\right) & \text{if} \quad t > t_0, \end{cases} \tag{3.174}$$

where t_0 is a delay period needed for formation of fibrin network and t_c is a time constant. In (3.173) the function f_{vi} captures nonlinear viscous dissipation

$$f_{vi}(I_B) = 1 + k_2(I_B - 3), \tag{3.175}$$

i.e. it is a growing function of the deformation. k_2 is a fit parameter.
The elastic spring element contribution in (3.172) reads as

$$\boldsymbol{\tau}_e = f_e(t)x_0 f_{ss}(I_B)G_{00}(\mathbf{B} - \mathbf{I}), \tag{3.176}$$

where G_{00} is the value of the modulus G_0 at the end of formation of the blood clot, obtained from the experiment in [2], and the function $f_e(t)$ is a growing function of time:

$$f_e(t) = f_v(t)^2. \tag{3.177}$$

Function $f_{ss}(I_B)$ in (3.176) causes, that the model is able take into account the fact, that clot stiffness increases with the strain.

$$f_{ss}(I_B) = (1 + k_1(I_B - 3))^{n_1}, \tag{3.178}$$

where n_1 is a fit parameter. The contribution from viscoelastic, Maxwell, modes in (3.172) reads as

$$\boldsymbol{\tau}^e_{ve,i} = x_i G_i(\mathbf{B}_{e,i} - \mathbf{I}), \qquad i = 1, 2 \quad , \tag{3.179}$$

where G_i are fitting parameters. x_i are state parameters undergoing time development depending on the history of deformation according to the following equation

$$\dot{x_i} = \begin{cases} -c_x(x_i - x_{i,\infty}) & \text{if} \quad x_i > x_{i,\infty}, \\ 0 & \text{if} \quad x_i \leq x_{i,\infty}, \end{cases} \tag{3.180}$$

where

$$x_{i,\infty} = e^{-a}\sqrt{I_{B_{e,i}} - 3} \tag{3.181}$$

is the value of x_i corresponding to certain strain and c_x and a are fit parameters.

Hence we assume, that the elastic behaviour of the viscoelastic modes is neo-Hookean-like, whereas the inelastic behaviour is described by the following equation for the inelastic rate of deformation:

$$\boldsymbol{\tau}^v_{ve,i} = 2\eta_i \boldsymbol{D}_{p,i}, \qquad i = 1, 2. \tag{3.182}$$

Using the fact $\boldsymbol{\tau}_{ve,i} = \boldsymbol{\tau}^e_{ve,i} = \boldsymbol{\tau}^v_{ve,i}$ we get the classical Maxwell relations for these two modes.

3.3.2 Weller's model using diffuse interface method

The sharp interface method, the level-set method, introduced in the paragraph on the original model of Weller provides an elegant solution, how to compute useful quantities, like the normal vector to the interface, the characteristic function of the interface, the Heaviside function of the flow domain. These quantities are needed for numerical computations.
For the numerical computations it is however required smearing out, approximation, of the level-set function by a smoothed function. We have tried to circumvent this issue by using the phase-field method, because the phase-field is already implicitly smooth.

Interface tracking using the phase-field method The most important advantages of the phase-field approach in comparison with the level-set method are:

- no necessity of artificial smearing of the characteristic and Heaviside function for numerical computations as the phase field is implicitly smeared by the phase field equation to be specified below
- the phase-field function does not require the reinitalization procedure, which is necessary for the signed distance function of the level-set method

At the heart of our phase-field formulation are the following Cahn-Hilliard equations

$$\frac{\partial c}{\partial t} + \mathbf{u} \cdot \nabla c - \operatorname{div} \mathbb{M} \nabla \mu = 0 \qquad \text{in} \quad \Omega^*, \tag{3.183}$$

$$\mu - \frac{1}{\epsilon^2} W'(c) + \Delta c = 0 \qquad \text{in} \quad \Omega^*, \tag{3.184}$$

where c is the phase field, with values between -1 and 1, μ is the chemical potential, $W'(c)$ is derivative of the double-well potential $W(c)$, $\mathbb{M}$ is the mobility, ϵ is the interface thickness.

Therefore we solve a system of two equations, which is by one more than in the case of the level set method.

The Cahn-Hilliard equations are to be solved in the whole computational domain Ω^*. The velocity $\mathbf{u}$ is given as the sum of the external part $\mathbf{u_e}$, originating from flow of the fluid, and internal component $\mathbf{u_i}$, stemming from the growth of interface due to the influx of platelets, i.e. $\mathbf{u} = \mathbf{u_e} + \mathbf{u_i}$.

We take the growth velocity as in (3.108)

$$\mathbf{u_i} = \alpha \nabla w. \tag{3.185}$$

We rewrite the Robin boundary condition (3.106) on the platelet field w followingly

$$D \frac{\partial w}{\partial \mathbf{n}} = kw = D\mathbf{n} \cdot \nabla w, \tag{3.186}$$

as we will need this form in the derivation of modified phase-field equation.

We release the term $\mathbf{u_e}$, as we neglect mechanical influence of blood flow on the growing thrombus, i.e. $\mathbf{u} = \mathbf{u_i}$. We manipulate the equation (3.183) in the following manner

$$\begin{aligned} &\frac{\partial c}{\partial t} + \mathbf{u_i} \cdot \nabla c - \operatorname{div} \mathbb{M} \nabla \mu = \frac{\partial c}{\partial t} + \mathbf{u_i} \cdot \nabla c - \operatorname{div} \mathbb{M} \nabla \mu \\ &= \frac{\partial c}{\partial t} + \alpha \nabla w \cdot \nabla c - \operatorname{div} M \nabla \mu = \frac{\partial c}{\partial t} + \alpha \nabla w \cdot \frac{\nabla c}{|\nabla c|} |\nabla c| - \operatorname{div} \mathbb{M} \nabla \mu \\ &= \frac{\partial c}{\partial t} + \alpha \nabla w \cdot \mathbf{n} |\nabla c| - \operatorname{div} \mathbb{M} \nabla \mu = \frac{\partial c}{\partial t} + \alpha D^{-1} k w |\nabla c| - \operatorname{div} \mathbb{M} \nabla \mu = 0, \end{aligned} \tag{3.187}$$

where we used the fact, that the following relation holds for the phase-field function c

$$\mathbf{n} = \frac{\nabla c}{|\nabla c|}. \tag{3.188}$$

The term $|\nabla c|$ is due to its delta function like behaviour substituted by a different expression described below. Finally we get this equation:

$$\frac{\partial c}{\partial t} - \nabla \cdot \mathbb{M}\nabla\mu = \alpha D^{-1} k w |\nabla \varphi_\varepsilon(c)| \qquad \text{in} \quad \Omega^*, \tag{3.189}$$

$$\mu - \frac{1}{\epsilon^2} W'(c) + \Delta c = 0 \qquad \text{in} \quad \Omega^*, \tag{3.190}$$

where $|\nabla \varphi_\varepsilon| = \frac{(\varphi_\varepsilon)^2}{\varepsilon} e^{c/\varepsilon}$ features delta function behaviour, as $\varphi_\epsilon(c) = \frac{1}{1+e^{c/\varepsilon}}$, where ε is a constant regularization parameter, r is the adhesion rate:

$$r = \kappa_1 + \kappa_2 s, \tag{3.191}$$

where the shear stress s is given as

$$s = \|\boldsymbol{\tau}_\tau\|_{l^2} = \|\boldsymbol{\tau} - \boldsymbol{\tau}_n\|_{l^2} = \|2\nu \mathbf{D}\mathbf{n} - \boldsymbol{\tau}_n\|_{l^2}, \tag{3.192}$$

where $\boldsymbol{\tau}_n = (\boldsymbol{\tau} \cdot \mathbf{n})\mathbf{n}$ and $\mathbf{n}$ is the normal to the interface given by (3.188).

Transport of platelets using phase-field framework

We have two areas in our computational domain, which have to be described by the transport equation of platelets. It is the fluid area Ω_t and the solid area Ω_s of the clot, see Figure 3.2. For simplicity we do not track the further development of the platelets, which are incorporated into the solid, the thrombus. Therefore we suppose, that the density of platelets in the solid does not have meaning for us. On the interface between the solid Ω_s and the fluid Ω_t we impose the Neumann-boundary condition using the specific procedure developed in [80].
We will briefly outline the framework and then we use it in our case. Our starting point is the transport equation formulated by Weller, i.e. equation (3.105).
Let us have the following equation

$$\Delta u = f \qquad \text{in} \quad \Omega_t \tag{3.193}$$

equipped with the Robin boundary condition

$$\nabla u \cdot \mathbf{n} = k(u - g) \qquad \text{on} \quad \Gamma_t, \tag{3.194}$$

where g is a function $g : \Gamma_t \to \mathbb{R}$ and $k \in \mathbb{R}$. Li et al. in [80] developed the following approximation for this problem using the phase field method (for details see [80] section 2.5, Approximation 2)

$$\operatorname{div}(\phi \nabla u) + \frac{1}{\epsilon} B(\phi) k (u - g) = \phi f \qquad \text{in} \quad \Omega^*, \tag{3.195}$$

where $B(\phi) = \phi^2(1-\phi)^2$. The variable ϕ is interrelated with our phase-field variable c from above using the following formula

$$\phi(c) = \frac{c+1}{2} \begin{cases} 1 & c = 1, \\ 0 & c = -1. \end{cases} \tag{3.196}$$

In [80] it is analyzed the behaviour of the approximation (3.195) in detail. In the work [80] it is introduced the possibility of application of this treatment of boundary conditions to other types of equations.
We will hence reformulate the transport equation (3.105) with the boundary equation (3.106) in the following manner

$$\frac{\partial(\phi w)}{\partial t} - D\,\mathrm{div}(\phi\nabla w) + \mathrm{div}(\phi w\mathbf{u}) + \frac{1}{\epsilon}B(\phi)kw = 0 \qquad \text{in} \quad \Omega^*. \tag{3.197}$$

3.3.3 A modification of the model of Storti

As was said in section 3.2.1 blood does behave under certain conditions as a non-Newtonian fluid. Storti assumed in his model, that blood is a Newtonian fluid, hence Navier-Stokes equation described its behaviour.
We aspire to capture on the one hand the platelet plug development, on the other hand we do not want to neglect the non-Newtonian features of blood.
In the next sections we develop a phase-field model of platelet plug evolution, next we introduce the non-homogeneous model of blood. Afterwards we modify the activation criterion of platelets (3.118).

The phase-field method in the model of Storti

Convection, diffusion and reaction of each species can be expressed using the generic equation (3.115), which is supplemented with Robin-type boundary condition (3.125). The equation is to be solved in the area of flowing blood Ω_F, the boundary condition is imposed on the moving interface Γ, see Figure 3.3.
In the model shown in section 3.3.1 we had to solve the evolution equations defined only on the the moving interface Γ, (3.129), (3.130), (3.131) and (3.134). We abstract from their specific forms and formulate a generic equation as

$$\frac{\partial\mathbf{f}}{\partial t} = \mathbf{P}(\mathbf{c},\mathbf{f}) \qquad \text{on} \quad \Gamma, \tag{3.198}$$

where $\mathbf{f}$ is the vector of the surface quantities, which undergo development, i.e. $\mathbf{f} = (f_s, M_{as}, M_r, M_{at})$.

At the beginning of the wound healing process the interface Γ lies in the injured part of the vessel wall, but as the clot grows the interface Γ moves correspondingly. Let us now rephrase the model with use of techniques taken from diffuse interface modelling. We define the Heaviside function in the following manner

$$H = \begin{cases} 1 & \text{in} \quad \Omega_F, \\ 0 & \text{in} \quad \Omega. \end{cases} \tag{3.199}$$

We will however use in our computations an order parameter ϕ obtained from the phase field using (3.196). The order parameter now attains the values 0, 1 as the Heaviside function (3.199), the transition from one value to another is however smooth, not abrupt.

Using it we rewrite the generic equation of our model (3.115) as

$$\frac{\partial(\phi\mathbf{c})}{\partial t} + \phi\mathbf{u}\cdot\nabla\mathbf{c} = \mathbb{D}\,\mathrm{div}(\phi\nabla\mathbf{c}) + \phi\mathbf{S}(\mathbf{c}) \quad \text{in} \quad \Omega_F \cup \Omega. \tag{3.200}$$

Similarly we can rewrite specific 2-D equations defined only on the interface Γ (3.198) as

$$\frac{\partial \mathbf{f}}{\partial t} = \delta_\Gamma \mathbf{P}(\mathbf{c}, \mathbf{f}), \quad \text{in} \quad \Omega_F \cup \Omega, \tag{3.201}$$

where δ_Γ is the regularized delta function of the interface Γ fulfilling

$$\int_\Gamma f d\Gamma = \int_{\Omega \cup \Omega_F} f \delta_\Gamma d\Omega. \tag{3.202}$$

We face now the question, how to incorporate the Robin boundary conditions into the framework described in the previous chapter. We try to use the ideas outlined by Lowengrub et al. [80]. Lowengrub provides several approximations of Dirichlet, Neumann and Robin boundary values for the following problem

$$-\Delta u = f \qquad \text{on} \quad \Omega_F \tag{3.203}$$

equipped with the Robin boundary condition

$$\nabla u \cdot \mathbf{n} = k(u - g) \qquad \text{on} \quad \partial\Gamma, \tag{3.204}$$

where k is a constant, g is a function defined on the interface Γ.
The system is then approximated on $\Omega_F \cup \Omega$ in the following manner

$$\operatorname{div}(\phi \nabla u) + \epsilon k (u - g) |\nabla \phi|^2 = \phi f \qquad \text{on} \quad \Omega_F \cup \Omega, \tag{3.205}$$

where the order parameter ϕ varies smoothly between 0 (for the domain Ω) and 1 (for the domain Ω_F). In [80] is this procedure used for parabolic equations as well. The Robin conditions in our model are characteristic for each species' equation. It is therefore necessary to write down specific equations for each concentration.
For the initial smooth approximation of the order field ϕ we use the formula

$$\phi(\mathbf{x}, t) = \frac{1}{2}\left[1 + \tanh\left(\frac{r(\mathbf{x}, t)}{2\sqrt{2}\epsilon}\right)\right], \tag{3.206}$$

where $r(\mathbf{x}, t)$ is the signed distance function to Γ set to be positive in Ω_F.
The interface can be defined as set $\Gamma(t) = \{\mathbf{x} \in \Omega \cup \Omega_F | \phi(\mathbf{x}, t) = 1/2\}$. We will follow the development in [81] by developing the phase-field function c using an advective Cahn-Hilliard equation

$$\frac{\partial c}{\partial t} + \mathbf{u} \cdot \nabla c = \operatorname{div}(\mathbb{M} \nabla \mu), \tag{3.207}$$

where μ is a chemical potential

$$\mu = W'(c) - \epsilon \nabla^2 c. \tag{3.208}$$

In [81] $W(c)$ is defined as $W(c) = \frac{1}{4}(1 + c)^2(1 - c)^2$, i.e. as the double well potential. The mobility $\mathbb{M}$ is supposed to be constant. We didn't address till now the evolution of the clot, i.e. the interface Γ. The velocity of growth of the clot is derived in the same way as in case of (3.141)

$$\mathbf{u_i} = j_{bp}(1 + \alpha_V) V_p \mathbf{n}. \tag{3.209}$$

Let us now turn back to the equation (3.207). We must make sense of the velocity $\mathbf{u}$. Actually we suppose, that velocity is composed of fluid flow component $\mathbf{u}_e$ and interfacial growth component $\mathbf{u_i}$, for which the relation (3.209) was derived. We postulate therefore, that

$$\mathbf{u} = \mathbf{u}_e + \mathbf{u}_i. \tag{3.210}$$

We will now exemplify the use of the decomposition (3.210) by reformulation of the equation (3.207), namely

$$\frac{\partial c}{\partial t} + \mathbf{u} \cdot \nabla c = \frac{\partial c}{\partial t} + j_{bp}(1 + \alpha_V)V_p|\nabla c| + \mathbf{u_f} \cdot \nabla c = \mathrm{div}(\mathbb{M}\nabla\mu), \tag{3.211}$$

where we used the fact, that the normal to the interface $\mathbf{n}$ can be expressed as

$$\mathbf{n} = \frac{\nabla c}{|\nabla c|}. \tag{3.212}$$

The term $|\nabla c|$ is due to its delta function like behaviour substituted by a different expression

$$|\nabla \varphi_\varepsilon| = \frac{(\varphi_\varepsilon)^2}{\varepsilon} e^{c/\varepsilon}, \tag{3.213}$$

where

$$\varphi_\varepsilon(c) = \frac{1}{1 + e^{c/\varepsilon}}, \tag{3.214}$$

where ε is a constant regulatization parameter. Finally we get this equation:

$$\frac{\partial c}{\partial t} + \mathbf{u}_f \cdot \nabla c - \nabla \cdot \mathbb{M}\nabla\mu = -j_{bp}(1 + \alpha_V)V_p|\varphi_\varepsilon(c)| \qquad \text{in} \quad \Omega_F \cup \Omega. \tag{3.215}$$

We will now assume, that the velocity field $\mathbf{u_e}$ is identical with the velocity of blood computed from Navier-Stokes equations $\mathbf{u}$, i.e. $\mathbf{u_e} = \mathbf{u}$.

Shear stress dependent activation criterion

As was explained in section 2.2.3 blood coagulation could be triggered on reactive surface by elevated shear rate values only. We have seen, that model of Storti assumes, that blood platelets could be activated only by chemicals like thromboxane, ADP and thrombin. Storti introduced a threshold like activation function (3.119), which causes the activation to start if there is high enough concentration of mentioned chemical species.
We will however assume, that blood platelets are activated not only by the chemicals, but also by elevated values of shear stress. Hence we modify the activation function (3.119) followingly:

$$f_{act} = \frac{c_{adp}}{c_{adp,crit}} + \frac{c_{tx}}{c_{tx,crit}} + \frac{c_{th}}{c_{th,crit}} + \frac{s}{s_{crit}}, \tag{3.216}$$

where the shear stress is defined in (3.192) in section 3.3.2. The value of s_{crit}, i.e. the critical value of shear stress, is to be specified. Use of (3.216) in the expression for the reaction rate k_{pa} is standard

$$k_{pa} = \begin{cases} 0 & \text{if} \quad f_{act} < 1, \\ \frac{f_{act}}{\tau_{pa}} & \text{if} \quad f_{act} \geq 1. \end{cases} \tag{3.217}$$

3.3.4 Adaptation of Kempen's model for our case

Introduction of clot time

The constitutive model in the section 3.3.1 describes development of rheological properties of the blood clot. The properties change since the clot is formed, they are time-dependent.
Output of model of Storti is a platelet plug. We will assume, that after some time after formation of the plug, the fibrin network starts to evolve. This leads to tremendous change in rheological properties of the clot. The development of the properties is described by the Kempen's model, [2], [70].
The key component of Kempen's model [2], [70] is its dependence on time since the creation of the clot. We introduce into model of platelet plug development a time like variable t_{clot}, so called *clot time*. The variable measures the time which passed since the creation of platelet plug in the current location in the platelet clot.
The *clot time* variable is initialized to zero in the whole computation domain $\Omega \cup \Omega_F$, see Figure 3.3. Once the plug is present in the current area we let the clot time develop according to the following equation:

$$\frac{\partial t_{clot}}{\partial t} = C \qquad \text{in} \quad \Omega, \tag{3.218}$$

where C is a properly chosen constant. In order to extend this equation to the whole computational domain $\Omega \cup \Omega_F$ we need to discern the area of the clot Ω from the area of flowing blood Ω_F. For that purpose we have the Heaviside function H:

$$\frac{\partial t_{clot}}{\partial t} = (1 - H)C \qquad \text{in} \quad \Omega \cup \Omega_F, \tag{3.219}$$

i.e. the clot time t_{clot} will increase only in the area, where the Heaviside function H attains nontrivial values.
We reformulate this equation using the variable ϕ, defined in (3.196):

$$\frac{\partial t_{clot}}{\partial t} = (1 - \phi)C \qquad \text{in} \quad \Omega \cup \Omega_F. \tag{3.220}$$

Eulerian description of development of the deformation gradient tensor

For the computations of rheological properties using the model of Kempen, we need the values of deformation gradient in the area of the thrombus. We need to reformulate standard definition of the deformation gradient in the Eulerian description.
We start with standard definition of the deformation gradient $\mathbf{F}$

$$\mathbf{F} = \frac{\partial \mathbf{x}}{\partial \mathbf{X}}, \tag{3.221}$$

which on time derivation and application of the chain rule results into Eulerian formulation:

$$\dot{\mathbf{F}} = \frac{\partial}{\partial t}\frac{\partial \mathbf{x}}{\partial \mathbf{X}}(\mathbf{X}, t) = \frac{\partial \mathbf{u}}{\partial \mathbf{X}}(\mathbf{X}, t) = \frac{\partial \mathbf{u}}{\partial \mathbf{x}}(\mathbf{x}, t)\frac{\partial \mathbf{x}}{\partial \mathbf{X}}(\mathbf{X}, t), \tag{3.222}$$

which can be written as

$$\frac{\partial \mathbf{F}}{\partial t} + \mathbf{u} \cdot \nabla \mathbf{F} = \nabla \mathbf{u} \mathbf{F}. \tag{3.223}$$

We will solve this equation in the whole area of computation, i.e. in the area of blood flow and in the area of thrombus. The values of the deformation gradient in the area of blood flow are not of interest for us, hence we can define their initial and boundary values quite arbitrarily.
Namely we take as the initial condition in the whole domain the undeformed state, i.e. $\mathbf{F}|_0 = \mathbf{I}$. The boundary condition on inflow to the domain is again the undeformed state, i.e. $\mathbf{F}_{in} = \mathbf{I}$.

3.4 Problem formulation

In the followings sections we sum up the equations to be solved for three cases:

- modified Weller's model, blood as a Newtonian fluid
- modified Storti's model, clot as a Newtonian fluid with high viscosity, blood as a non-Newtonian fluid
- modified Storti's model, clot as a viscoelastic material, blood as a non-Newtonian fluid

3.4.1 Governing equations of modified Weller's model

The whole system of equations

Our system contains the equations of conservation of linear momentum and mass for the fluid

$$\frac{\partial \mathbf{u}}{\partial t} + \mathbf{u} \cdot \nabla \mathbf{u} = -\nabla p + \operatorname{div}(\nu \mathbf{D}(\mathbf{u})) + \mathbf{f} \qquad \text{in} \quad \Omega^*, \tag{3.224}$$

$$\operatorname{div} \mathbf{u} = 0 \qquad \text{in} \quad \Omega^*,$$

it contains the Cahn-Hilliard system of equations, which traces the development of the interface fluid-solid(clot)

$$\frac{\partial c}{\partial t} - \nabla \cdot \mathbb{M} \nabla \mu = \alpha D^{-1} k w |\operatorname{grad} \varphi_\varepsilon| \qquad \text{in} \quad \Omega^*, \tag{3.225}$$

$$\mu - \frac{1}{\epsilon^2} W'(c) + \Delta c = 0 \qquad \text{in} \quad \Omega^*$$

and it contains the transport equation for the platelets

$$\frac{\partial (\phi w)}{\partial t} - D \operatorname{div}(\phi \nabla w) + \operatorname{div}(\phi w \mathbf{u}) + \frac{1}{\epsilon} B(\phi) k w = 0 \qquad \text{in} \quad \Omega^*, \tag{3.226}$$

where ϕ is related to the phase field c using (3.196).

To make the equation (3.226) solvable, we need to add some value to platelets field in the area of solid. Therefore we decide to equip the last equation with the additional term $-(1-\phi)\Delta w$, i.e. an harmonic extension of the platelets field

in the area of the growing thrombus. The equation (3.226) will then have the following form

$$\frac{\partial w}{\partial t} - D\,\mathrm{div}(\phi\nabla w) + \mathrm{div}(\phi w\mathbf{u}) + \frac{1}{\epsilon}B(\phi)kw \; -(1-\phi)\Delta w \; = 0 \qquad \text{in} \quad \Omega^*, \tag{3.227}$$

where the newly added harmonic term is highlighted with the yellow color.

3.4.2 Governing equations of modified Storti's model

Non-homogeneous blood model - flowing blood domain

In Section 3.2.3 we introduced the non-homogeneous model of Owens, which we will use in the following. This model is however applicable for our use case only in the areas of flowing blood. The parts taken up by the the clot will require rather specific treatment.
Let us review the governing equations of the model, which are to be fullfilled in the flowing area (i.e. in the area Ω_F in Fig. 3.3).

$$Re\frac{\partial \mathbf{u}}{\partial t} + Re\mathbf{u}\cdot\nabla\mathbf{u} = -\nabla p + \mathrm{div}\,\boldsymbol{\tau} + \eta_N\Delta\mathbf{u} \quad \text{in} \quad \Omega_F, \tag{3.228}$$

$$\mathrm{div}\,\mathbf{u} = 0 \quad \text{in} \quad \Omega_F, \tag{3.229}$$

$$\frac{\partial N_0}{\partial t} + \mathbf{u}\cdot\nabla N_0 = \frac{1}{Pe}\Delta N_0 - \frac{1}{1-\beta}\frac{De}{Pe}\nabla\nabla : \boldsymbol{\tau} \quad \text{in} \quad \Omega_F, \tag{3.230}$$

$$\begin{aligned}\frac{\partial M}{\partial t} + \mathbf{u}\cdot\nabla M = \frac{1}{Pe}\Delta M - \frac{1}{1-\beta}\frac{De}{Pe}\nabla\nabla : \boldsymbol{\sigma} \\ -0.5\alpha(\dot\gamma)\frac{N_0}{n}M + 0.5b(\dot\gamma)(N_0 - M) \quad \text{in} \quad \Omega_F,\end{aligned} \tag{3.231}$$

$$\begin{aligned}\boldsymbol{\tau} + De\mu(\dot\gamma, N_0, M)\,\overset{\triangledown}{\boldsymbol{\tau}} - \frac{De}{Pe}\mu(\dot\gamma, N_0, M)(\Delta\boldsymbol{\tau} + (\nabla\nabla:\boldsymbol{\tau})\boldsymbol{I}) = \\ (1-\beta)\mu(\dot\gamma, N_0, M)N\mathbf{D} \quad \text{in} \quad \Omega_F,\end{aligned} \tag{3.232}$$

$$\begin{aligned}\boldsymbol{\sigma} + De\mu(\dot\gamma, N_0, M)\,\overset{\triangledown}{\boldsymbol{\sigma}} - \frac{De}{Pe}\mu(\dot\gamma, N_0, M)(\Delta\boldsymbol{\sigma} + (\nabla\nabla:\boldsymbol{\sigma})\boldsymbol{I}) = \\ (1-\beta)\mu(\dot\gamma, N_0, M)M\boldsymbol{D} \quad \text{in} \quad \Omega_F,\end{aligned} \tag{3.233}$$

where we refer to the section 3.2.3 for the explanation of the meaning of the equations.

Non-homogeneous blood model - extension to the whole domain

We have to adjust the non-homogeneous model so, that it can be solved in the whole domain $\Omega_F \cup \Omega$. For that purpose we employ the order parameter ϕ introduced by

(3.196). The non-homogeneous model from the previous section is to be solved in the area $\Omega_F \cup \Omega$:

$$Re\frac{\partial \mathbf{u}}{\partial t} + Re\mathbf{u}\cdot\nabla\mathbf{u} = -\nabla p + \nabla\cdot\mathbf{S} + \eta_N\Delta\mathbf{u} \quad \text{in} \quad \Omega_F\cup\Omega, \tag{3.234}$$

$$\nabla\cdot\mathbf{u} = 0 \quad \text{in} \quad \Omega_F\cup\Omega, \tag{3.235}$$

$$\frac{\partial(\phi N_0)}{\partial t} + \phi\mathbf{u}\cdot\nabla N_0 = \phi\frac{1}{Pe}\Delta N_0 - \phi\frac{1}{1-\beta}\frac{De}{Pe}\nabla\nabla:\boldsymbol{\tau} \quad \text{in} \quad \Omega_F\cup\Omega, \tag{3.236}$$

$$\begin{aligned}\frac{\partial(\phi M)}{\partial t} + \phi\mathbf{u}\cdot\nabla M = \phi\frac{1}{Pe}\Delta M - \phi\frac{1}{1-\beta}\frac{De}{Pe}\nabla\nabla:\boldsymbol{\sigma}\\ - 0.5\phi\alpha(\dot\gamma)\frac{N_0}{n}M + 0.5\phi b(\dot\gamma)(N_0 - M) \quad \text{in} \quad \Omega_F\cup\Omega,\end{aligned} \tag{3.237}$$

$$\begin{aligned}\boldsymbol{\tau} + \phi De\mu(\dot\gamma, N_0, M)\overset{\triangledown}{\boldsymbol{\tau}} - \phi\frac{De}{Pe}\mu(\dot\gamma, N_0, M)(\Delta\boldsymbol{\tau} + (\nabla\nabla:\boldsymbol{\tau})\boldsymbol{I}) =\\ \phi(1-\beta)\mu(\dot\gamma, N_0, M)N_0\boldsymbol{D} \quad \text{in} \quad \Omega_F\cup\Omega,\end{aligned} \tag{3.238}$$

$$\begin{aligned}\boldsymbol{\sigma} + \phi De\mu(\dot\gamma, N_0, M)\overset{\triangledown}{\boldsymbol{\sigma}} - \phi\frac{De}{Pe}\mu(\dot\gamma, N_0, M)(\Delta\boldsymbol{\sigma} + (\nabla\nabla:\boldsymbol{\sigma})\boldsymbol{I}) =\\ \phi(1-\beta)\mu(\dot\gamma, N_0, M)M\boldsymbol{D} \quad \text{in} \quad \Omega_F\cup\Omega,\end{aligned} \tag{3.239}$$

where

$$\mathbf{S} = \phi\boldsymbol{\tau} + (1-\phi)\boldsymbol{\tau}_c \quad \text{in} \quad \Omega_F\cup\Omega, \tag{3.240}$$

where $\boldsymbol{\tau}_c$ is the extra stress tensor of the clot, which we take simply as

$$\boldsymbol{\tau}_c = 2\nu_{big}\mathbf{D}, \tag{3.241}$$

where ν_{big} is the constant viscosity. In this model we assume, that the clot is a Newtonian fluid with large viscosity.
To make equations (3.236) and (3.237) solvable, we need to add some values the fields N_0 and M. Therefore we decide to equip the equation for N_0 and M with the additional term $-\operatorname{div}((1-\phi)\nabla N_0)$ and $-\operatorname{div}((1-\phi)\nabla M)$, respectively. The equation (3.236) will then have the following form:

$$\frac{\partial N_0}{\partial t} + \phi\mathbf{u}\cdot\nabla N_0 \boxed{-\operatorname{div}((1-\phi)\nabla N_0)} = \phi\frac{1}{Pe}\Delta N_0 - \phi\frac{1}{1-\beta}\frac{De}{Pe}\nabla\nabla:\boldsymbol{\tau} \quad \text{in} \quad \Omega_F\cup\Omega, \tag{3.242}$$

whereas the equation (3.237) looks in the following way:

$$\begin{aligned}\frac{\partial M}{\partial t} + \phi\mathbf{u}\cdot\nabla M \boxed{-\operatorname{div}((1-\phi)\nabla M)} = \phi\frac{1}{Pe}\Delta M\\ -\phi\frac{1}{1-\beta}\frac{De}{Pe}\nabla\nabla:\boldsymbol{\sigma} - 0.5\phi\alpha(\dot\gamma)\frac{N_0}{n}M + 0.5\phi b(\dot\gamma)(N_0 - M) \quad \text{in} \quad \Omega_F\cup\Omega.\end{aligned} \tag{3.243}$$

The newly added harmonic terms in (3.242) and (3.243) are highlighted with the yellow color.

Coagulation related quantities

We will now remind reader of equations derived in section 3.3.3. We adapted the generic transport equation for platelets or chemical species c_i (3.115) equipped with the Robin boundary condition (3.125) in the following manner

$$\frac{\partial(\phi \mathbf{c})}{\partial t} + \phi(\mathbf{u} \cdot \nabla \mathbf{c}) = \mathbb{D}\,\mathrm{div}(\phi \nabla \mathbf{c}) + \phi \mathbf{S}(\mathbf{c}) \quad \text{in} \quad \Omega_F \cup \Omega. \tag{3.244}$$

Again we have to assign some value to the fields in $\mathbf{c}$ in the area of clot. Therefore we add the harmonic term as it was done in previous section. Hence the final form of equation to be solved reads as

$$\frac{\partial \mathbf{c}}{\partial t} + \phi(\mathbf{u} \cdot \nabla)\mathbf{c} - \mathrm{div}((1-\phi)\nabla \mathbf{c}) = \mathbb{D}\,\mathrm{div}(\phi \nabla \mathbf{c}) + \phi \mathbf{S}(\mathbf{c}) \quad \text{in} \quad \Omega_F \cup \Omega, \tag{3.245}$$

where the newly added harmonic term is highlighted with the yellow color.
Similarly we have adjusted specific 2-D equations for quantities in $\mathbf{f}$ defined only on interface (3.129),(3.130),(3.131) and (3.134) as

$$\frac{\partial \mathbf{f}}{\partial t} = \delta_\Gamma \mathbf{P}(\mathbf{c}, \mathbf{f}) \quad \text{in} \quad \Omega_F \cup \Omega. \tag{3.246}$$

Movement of the interface

We solve in the following equations in the whole domain $\Omega_F \cup \Omega$ the Cahn-Hilliard system of equations

$$\frac{\partial c}{\partial t} + \mathbf{u} \cdot \nabla c - \nabla \cdot \mathbb{M} \nabla \mu = -j_{bp}(1+\alpha_V) V_p |\varphi_\varepsilon(c)| \qquad \text{in} \quad \Omega_F \cup \Omega. \tag{3.247}$$

$$\mu = W'(c) - \epsilon \Delta c \qquad \text{in} \quad \Omega_F \cup \Omega. \tag{3.248}$$

The equation were derived in the section 3.3.3.
Summary of equations to be solved in each timestep:
We solve the following equations in each timestep: (3.234), (3.235), (3.242), (3.243), (3.238), (3.239), (3.245), (3.246), (3.247) (3.248).
In equation (3.234) we use the constitutive equations given by (3.240).

3.4.3 Modified Storti's model with the viscoelastic constitutive equation for the clot

A substantial part of the model similar to the model summed up in Section 3.4.2. Hence we just refer the reader for some parts of the current model to the corresponding equations in the Section 3.4.2.
Concerning the coagulation related quantities we solve the same set of equations as in 3.4.2. Movement of the interface is described using the equations from Section 3.4.2.
Concerning the non-homogeneous blood model in the flowing blood model we refer to Section 3.4.2 for the equations to be solved. Concerning the non-homogeneous blood model in the extended domain, i.e. in the union of the flowing domain and

the domain with the emerging clot, we solve in the extended domain the system of equations (3.234)-(3.239). However we apply the constitutive equation for the clot originating from the model of Kempen, see Section 3.3.1 and 3.3.4.
The extra stress tensor reads then as

$$\mathbf{S} = \phi\boldsymbol{\tau} + (1-\phi)\boldsymbol{\tau}_c \quad \text{in} \quad \Omega_F \cup \Omega, \tag{3.249}$$

where $\boldsymbol{\tau}_c$ is given by (3.172).
Completely new for this model is the viscoelastic model of the blood clot, which is summed in the following section.

Blood clot rheological properties

The whole extra stress tensor for the blood clot is defined on the whole domain $\Omega_F \cup \Omega$, although we will use this quantity only in the linear momentum equations only for the area of clot Ω. Similar holds for the other quantities leading to computation of the extra stress tensor of the clot below.

$$\boldsymbol{\tau}_{clot} = \boldsymbol{\tau}_v + \boldsymbol{\tau}_e + \sum_{i=1}^{2} \boldsymbol{\tau}_{ve,i} \quad \text{in} \quad \Omega_F \cup \Omega.$$

The viscous element reads as

$$\boldsymbol{\tau}_v = 2\left(\eta_p + f_v(t_{clot}) f_{vi}(I_{\mathbf{B}})\eta_{00}\right)\mathbf{D} \quad \text{in} \quad \Omega_F \cup \Omega. \tag{3.250}$$

where η_p is the plasma viscosity and the function $f_v(t)$ is changing with time according to

$$f_v(t_{clot}) = \begin{cases} 0 & \text{if} \quad t \le t_0, \\ \left(1 - e^{-\frac{(t_{clot}-t_0)}{t_c}}\right) & \text{if} \quad t > t_0, \end{cases}$$

where t_0 is a delay period needed for formation of fibrin network and t_c is a time constant. In (3.250) the function f_{vi} captures nonlinear viscous dissipation

$$f_{vi}(I_B) = 1 + k_2(I_{\mathbf{B}} - 3) \quad \text{in} \quad \Omega_F \cup \Omega,$$

i.e. it is a growing function of the deformation. k_2 is a fit parameter.
The elastic spring element contribution in (3.4.3) reads as

$$\boldsymbol{\tau}_e = f_e(t_{clot}) x_0 f_{ss}(I_{\mathbf{B}}) G_{00}(\mathbf{B} - \mathbf{I}) \quad \text{in} \quad \Omega_F \cup \Omega, \tag{3.251}$$

where the function $f_e(t_{clot})$ is a growing function of time:

$$f_e(t_{clot}) = f_v(t_{clot})^2 \quad \text{in} \quad \Omega_F \cup \Omega.$$

Function $f_{ss}(I_B)$ in (3.251) causes, that the model is able take into account the fact, that clot stiffness increases with the strain.

$$f_{ss}(I_B) = (1 + k_1(I_{\mathbf{B}} - 3))^{n_1} \quad \text{in} \quad \Omega_F \cup \Omega.$$

The contribution from viscoelastic, Maxwell, modes in (3.4.3) reads as

$$\boldsymbol{\tau}_{ve,i} = x_i G_i(\mathbf{B}_{e,i} - \mathbf{I}), \qquad i = 1, 2 \quad \text{in} \quad \Omega_F \cup \Omega, \tag{3.252}$$

where G_i are fitting parameters. x_i are state parameters undergoing time development dependending on the history of deformation accroding to the following equation

$$\dot{x_i} = \begin{cases} -c_x(x_i - x_{i,\infty}), & \text{if} \quad x_i > x_{i,\infty} \\ 0, & \text{if} \quad x_i \leq x_{i,\infty} \end{cases}$$

$$x_{i,\infty} = e^{-a}\sqrt{I_{B,i} - 3}$$

We need to trace the development of deformation gradient tensor:

$$\frac{\partial \mathbf{F}}{\partial t} + \mathbf{u} \cdot \nabla \mathbf{F} = \nabla \mathbf{u} \mathbf{F} \quad \text{in} \quad \Omega_F \cup \Omega. \tag{3.253}$$

The clot time is developed according to the following equation.

$$\frac{\partial t_{clot}}{\partial t} = (1 - \phi)C \quad \text{in} \quad \Omega_F \cup \Omega. \tag{3.254}$$

Summary of equations to be solved in each timestep:
We solve the following equations in each timestep: (3.234), (3.235), (3.242), (3.243), (3.238), (3.239), (3.245), (3.246), (3.247), (3.248), (3.250), (3.251), (3.252), (3.253), (3.254).
In equation (3.234) we use the constitutive equations given by (3.249). For the sake of computation of relevant values of Kempen model we need to perform auxiliary precomputations of both tensor and scalar auxiliary quantities. This procedure is rather an implementation problem, hence we explain the procedure of their computation in the part of this work treating numerical methods, see Section 4.5.

3.5 Summary of the main features of described models

3.5.1 The model originating from Weller

The model is summed up in Section 3.4.1. We have used this model, however we approached the implementation differently. Namely, instead of a sharp interface method, i.e. the level-set method we used a diffuse interface method, i.e. the phase field method.
The advantages of the new approach were mentioned in Section 3.3.2.

3.5.2 The model originating from Storti

The model is summed up in Section 3.4.2. We have used the model of Storti, however we again approached the implementation differently. In this modification we assumed that the platelet clot behaves as a Newtonian fluid with large viscosity. The areas of blood and the emerging clot are discerned by the phase field method. The next difference lies in in substitution of the rheological model for blood. Namely we used the nonhomogeneous model of blood instead of the Newtonian fluid, which was used in the original Storti model.
The phase-field function develops as a result the equations described in Section

3.3.3. The activation function of platelets from Section 3.3.1, (3.119), is modified. In Section 2.2.3 the possibility of activation of platelets by elevated values of shear stress was mentioned.
Hence we modified the function (3.119) so that the activation of platelets can be boosted by elevated values of shear stress, (3.216).

3.5.3 The model originating from Storti and employing Kempen

The model is summed up in Section 3.4.3. We have used the model of Storti and modified it by introducing of the phase field method. The phase-field function develops in the way described in Section 3.3.3, wherein the activation function is modified, see Section 3.5.2.
What is completely new is the introduction of the model of Kempen, see Section 3.3.1. We had to modify the model for our computations, see Section 3.3.4.
The platelet clot is undergoing a development, not only as it is growing, but also by the fact, that its rheological properties change with time. This corresponds to the changeover of the clot from the platelet clot into the blood clot with developed fibrin strands.
The blood in which the coagulation process happens is again captured using a non-homogeneous blood model.

4. Numerical methods

4.1 Numerical methods common to all models

We will now review numerical methods common to all three models, i.e. modified Weller's model, modified Storti's model with the clot as a high viscosity fluid and modified Storti's model with the viscoelastic model of the clot originating from Kempen:

- splitting method
- adaptive timestepping
- resolution of different timescales, recoupling

4.1.1 A splitting method for Navier-Stokes equations

The incompressible Navier-Stokes equations are a saddle point problem. After discretization by finite element method the corresponding matrix to be solved by linear solvers is indefinite.
One of the ways how to tackle this problem is a projection method.
The system is splitted into convection-diffusion equations for the velocity and the Poisson problem for the pressure. There are several ways how to split the Navier-Stokes equations, however we have decided to use the incremental pressure correction scheme (IPCS), [82].
This scheme can be described as follows:
Having the velocity $\mathbf{u}^k$ and pressure p^k from the previous time step we solve firstly for the so called tentative velocity $\mathbf{u}_*^{k+1}$:

$$\frac{\mathbf{u}_*^{k+1} - \mathbf{u}^k}{\Delta t} + N(\mathbf{u}_*^{k+1}) + \nabla p^k - L(\mathbf{u}_*^{k+1}) = 0. \tag{4.1}$$

Afterwards we solve for the new pressure p^{k+1}:

$$\Delta(p^{k+1} - p^k) = \frac{1}{\Delta t} \operatorname{div} \mathbf{u}_*^{k+1}. \tag{4.2}$$

Then we perform the correction of the velocity $\mathbf{u}_*^{k+1}$:

$$\mathbf{u}^{k+1} = \mathbf{u}_*^{k+1} - \Delta t(\nabla p^{k+1} - \nabla p^k). \tag{4.3}$$

In these equations we have used the following notation:

$$L(\mathbf{u}) = 2\operatorname{div}(\nu \mathbf{D}) = \operatorname{div}\left(\nu(\nabla \mathbf{u} + (\nabla \mathbf{u})^T)\right) \tag{4.4}$$

and

$$N(\mathbf{u}) = \mathbf{u} \cdot \nabla \mathbf{u}.$$

4.1.2 An heuristic adaptive time stepping method

Suppose that we are about to solve dynamic equations, such as Navier-Stokes equations or transport equations of some species. We will now assume, for instance, that we have a transport equation for quantity u.
We refer to the work of [83] and [84], for further details on the shown procedure. In the following u denotes the unknown precise solution of the equations, whereas $u_{\Delta t}$ denotes approximate solution obtained using time step size Δt. We want to reach some prescribed tolerance TOL in the solution process:

$$\|u - u_{\Delta t}\| \approx TOL. \tag{4.5}$$

For that purpose we perform an expansion to obtain the local truncation error after one step Δt and one step of length $m\Delta t$, where m is an appropriately chosen integer number.
We will assume, that the error of solution $e(u)$ is independent of the time step size. Then the expansions look followingly:

$$u_{\Delta t} = u + \Delta t^2 e(u) + \mathcal{O}(\Delta t^4) \tag{4.6}$$

and

$$u_{m\Delta t} = u + m^2 \Delta t^2 e(u) + \mathcal{O}(\Delta t^4). \tag{4.7}$$

From the previous two expresions we derive the equation for the error:

$$e(u) \approx \frac{u_{m\Delta t} - u_{\Delta t}}{\Delta t^2 (m^2 - 1)}. \tag{4.8}$$

Suppose now, that we want to get an estimation of the error after one properly chosen timestep Δt_*.
We have

$$u_{\Delta t_*} = u + \Delta t_*^2 e(u) + \mathcal{O}(\Delta t^4). \tag{4.9}$$

We obtain from this equation on rearrangement and substitution from (4.8) the following approximate identity:

$$\|u - u_{\Delta t_*}\| \approx \left(\frac{\Delta t_*}{\Delta t}\right)^2 \frac{\|u_{\Delta t} - u_{m\Delta t}\|}{m^2 - 1} = TOL. \tag{4.10}$$

The estimator of the adaptive time step is then

$$\Delta t_*^2 = TOL \frac{\Delta t^2 (m^2 - 1)}{\|u_{\Delta t} - u_{m\Delta t}\|}. \tag{4.11}$$

We sum up the usage of the estimator in the algorithm scheme 1.

Remark

We don't set the newly obtained timestep to Δt_*, as we want to avoid instability problems. Instead if

- $\Delta t_* << \Delta t$ then $\Delta t_{new} = \Delta t / N$,
- $\Delta t_* >> \Delta t$ then $\Delta t_{new} = \Delta t * N$,

where N is some appropriately chosen integer number.

Algorithm: Adaptive time step

Data: u^n

Result: u^{n+1}

Given the old solution u^n do:

begin

1. Make m small timesteps of size Δt to compute $u_{\Delta t}$.
2. Make one large step of size of size $m\Delta t$ to compute $u_{m\Delta t}$.
3. Evaluate the relative solution changes $\|u_{\Delta t} - u_{m\Delta t}\|$.
4. Calculate the 'optimal' value Δt_* using (4.11) for the next time step.
5. If $\Delta t_* << \Delta t$, reset the solution and go back to step 1, using Δt_* as new timestep.
6. Set $u^{n+1} = u_{\Delta t}$.

end

Algorithm 1: Algorithm for one adaptive time step

4.1.3 Resolution of different time scales, recoupling

We model processes with different time scales. Hence we should expect, that the timesteps obtained using the previous adaptive timestepping algorithm will be different for each process.
After computation of each time iteration using the previous algorithm we take the minimum of all proposed timesteps from (4.11), i.e. for the case of our modification of Weller's model 3.4.1

$$\Delta t_{*FUTURE} = \min\{\Delta t_{*NAVIERSTOKES}, \Delta t_{*PHASE}, \Delta t_{*PLAT}\}, \tag{4.12}$$

whereas for our first modification of model of Storti the expression takes the following form

$$\Delta t_{*FUTURE} = \min\{\Delta t_{*NAVIERSTOKES}, \Delta t_{*PHASE}, \Delta t_{*N_0}, \Delta t_{*M}, \Delta t_{*\boldsymbol{\tau}}, t_{*\boldsymbol{\sigma}}, \Delta t_{*\mathbf{c}}, \Delta t_{*\mathbf{f}}\}, \tag{4.13}$$

whereas the future timestep for the second modification of the model of Storti reads as

$$\Delta t_{*FUTURE} = \min\{\Delta t_{*NAVIERSTOKES}, \Delta t_{*PHASE}, \Delta t_{*N_0}, \Delta t_{*M}, \Delta t_{*\boldsymbol{\tau}}, t_{*\boldsymbol{\sigma}}, \Delta t_{*\mathbf{c}}, \Delta t_{*\mathbf{f}}, \Delta t_{*\mathbf{F}}, \Delta t_{t_{clot}}\}. \tag{4.14}$$

The equations for modelled processes are solved as decoupled. However actually they are coupled.
We will reintroduce the coupling into our system of equations by subiteration. The ending criterion of the subiteration is based on the size of difference of solutions originating from last two subiterations.

4.2 Weller's model

We will now go through the adjustment of the splitting method from Section 4.1.1, afterwards we perform the discretization in space.

4.2.1 The splitting method for the model of Weller

The currently introduced splitting scheme must be adapted for our system which we want to solve. We want to enforce low values of velocity in the area of thrombus. For that purpose we enlarge viscosity in the area of thrombus and we add a Brinkman-like term for the area of thrombus. We set the velocity field to zero in the velocity correction step as well.
Hence we solve the following form of the transport equation for the velocity field

$$\frac{\mathbf{u}_*^{k+1} - \mathbf{u}^k}{\Delta t} + N(\mathbf{u}_*^{k+1}) + \nabla p^k - L_\phi(\mathbf{u}_*^{k+1}) +(1-\phi)\mathbf{u}_*^{k+1} = 0, \tag{4.15}$$

where

$$L_\phi(\mathbf{u}) = \mathrm{div}(2\nu(\phi)\mathbf{D}) = \mathrm{div}\left(\nu(\phi)(\nabla\mathbf{u} + (\nabla\mathbf{u})^T)\right), \tag{4.16}$$

i.e. the viscosity is dependent on the value of ϕ defined by (3.196). The newly added Brinkman term is highlighted with the yellow color.
We perform the mentioned setting of the velocity field to zero in the thrombus area by the modification of the correction velocity step (4.3) in the following manner:

$$\mathbf{u}^{k+1} = \phi\left(\mathbf{u}_*^{k+1} - \Delta t(\nabla p^{k+1} - \nabla p^k)\right), \tag{4.17}$$

which could be seen as a projection of the velocity on the space of velocity with trivial values in the area of thrombus.

4.2.2 Discretization in space

Weak formulation of equations for velocity and pressure

We obtain the weak formulations by formally multiplying the equations by a vector test function $\mathbf{v}$ or scalar function q from appropriate spaces defined later.
We will define the following notation for the inner products of tensor, vector and scalar functions:

$$(\mathbf{A}, \mathbf{B} = \int_{\Omega^*} \mathbf{A} : \mathbf{B} dx, \qquad (\mathbf{u}, \mathbf{v}) = \int_{\Omega^*} \mathbf{u}\cdot\mathbf{v} dx, \qquad (p, q) = \int_{\Omega^*} pq dx. \tag{4.18}$$

We multiply (4.15) by the vector function $\mathbf{v}$ obtaining

$$\left(\frac{\mathbf{u}_*^{k+1} - \mathbf{u}^k}{\Delta t} + \mathbf{u}_{nonlin}\nabla\mathbf{u}_*^{k+1} + (1-\phi)\mathbf{u}_*^{k+1}, \mathbf{v}\right) + \left(\nabla p^k, \mathbf{v}\right) - \left(\mathrm{div}\left(2\nu(\phi)\mathbf{D}(u_*^{k+1})\right), \mathbf{v}\right) = \mathbf{0}, \tag{4.19}$$

where $\mathbf{u}_{nonlin}$ is the velocity solution from the previous Picard iteration. As stopping criterion of the Picard iteration we have chosen norm of residual.

In order to redistribute derivatives evenly between solution and test functions we perform formally integration by parts on diffusion and pressure terms. This leads to

$$\left(\frac{\mathbf{u}_*^{k+1}-\mathbf{u}^k}{\Delta t}+\mathbf{u}_{nonlin}\nabla\mathbf{u}_*^{k+1}+(1-\phi)\mathbf{u}_*^{k+1},\mathbf{v}\right)-\left(p^k,\operatorname{div}\mathbf{v}\right)+(p^k\mathbf{n},\mathbf{v})_\Gamma \\ +\left(2\nu(\phi)\mathbf{D}(\mathbf{u}_*^{k+1}),\nabla\mathbf{v}\right)-\left(2\nu(\phi)\mathbf{D}(\mathbf{u}_*^{k+1})\mathbf{n},\mathbf{v}\right)_\Gamma=\mathbf{0}, \quad (4.20)$$

where $(.,.)_\Gamma$ stands for integral over boundary Γ, defined simarly to (4.18). We have $\mathbf{v}$ equal to zero on Γ_{in} and Γ_{wall}, therefore the boundary integrals on these parts of boundary vanish. We have to handle the boundary terms on Γ_{ouflow}.
We set on outflow

$$2\nu(\phi)\mathbf{D}(\mathbf{u}_*^{k+1})\mathbf{n}=\mathbf{0} \qquad \text{on} \quad \Gamma_{ouflow}, \quad (4.21)$$

therefore in the equation (4.20) only the boundary integral with pressure corresponding to the ouflow part of boundary Γ_{ouflow} remains.
We will now turn our attention to the Poisson problem for pressure (4.2). We multiply the equation by a test function q and integrate formally by parts, getting

$$-\left(\nabla(p^{k+1}-p^k),\nabla q\right)+\left(\nabla(p^{k+1}-p^k)\cdot\mathbf{n},q\right)_{\partial\Omega}=\frac{1}{\Delta t}\left(\operatorname{div}\mathbf{u}_*^{k+1},q\right). \quad (4.22)$$

In this case we have to deal with implicit use of a boundary condition. The application of homogeneous Neuman condition $\frac{\partial p}{\partial\mathbf{n}}=0$ leads to singular matrix to be solved by linear solver. One of workarounds to tackle this issue is to prescribe additional boundary condition on pressure $p=0$ on Γ_{out}.
We supply now the definition of the relevant function spaces for tentative velocity and pressure.
Test space for tentative velocity:

$$\mathbf{V}'=\mathbf{H}_0^1=\left\{\mathbf{v}\in\left[H^1(\Omega^*)\right]^3,\mathbf{v}|_{\Gamma_{in}\cup\Gamma_{wall}}=\mathbf{0}\right\}. \quad (4.23)$$

Trial space for tentative velocity:

$$\mathbf{V}=\mathbf{H}_D^1(\Omega^*)=\left\{\mathbf{v}\in\left[H^1(\Omega^*)\right]^3,\mathbf{v}|_{\Gamma_{in}\cup\Gamma_{wall}}=\mathbf{u}_D\right\}, \quad (4.24)$$

where $\mathbf{u}_D$ on inflow is the prescribed parabolic profile, whereas we impose no-slip condition on walls, i.e. $\mathbf{u}_D|_{wall}=\mathbf{0}$. The test and trial space for the weak formulation (4.22) of Poisson problem (4.2) are identical:

$$Q=\left\{q\in H^1(\Omega),q|_{\Gamma_{out}}=0\right\}. \quad (4.25)$$

We have chosen the finite element spaces for the velocity and pressure in the following manner:

$$\mathbf{V}'_h=\left\{\mathbf{v}\in\left[H^1(\Omega^*)\right]^3,\mathbf{v}|_K\in[Q_2(K)]^3,\mathbf{v}|_{\Gamma_{in}\cup\Gamma_{wall}}=\mathbf{0}\right\}, \quad (4.26)$$

$$\mathbf{V}_h=\left\{\mathbf{v}\in\left[H^1(\Omega^*)\right]^3,\mathbf{v}|_K\in[Q_2(K)]^3,\mathbf{v}|_{\Gamma_{in}\cup\Gamma_{wall}}=\mathbf{u}_D\right\}, \quad (4.27)$$

and

$$Q_h = \left\{ q \in H^1(\Omega^*), q|_K \in Q_1(K), q|_{\Gamma_{out}} = 0 \right\} \tag{4.28}$$

In the case of the velocity correction we only multiply the equation (4.17) by test function. Integration by parts is not performed and it is not necessary to discuss boundary conditions.

Weak formulation of the equations for phase-field and chemical potential

We multiply (3.225) by a tuple (ψ_c, ψ_μ) from the appropriate test spaces to be specified later:

$$\begin{aligned} \left(\frac{c^{k+1} - c^k}{\Delta t}, \psi_c \right) - \left(\operatorname{div} \mathbb{M} \nabla \mu^{k+1}, \psi_c \right) &= \left(\alpha D^{-1} k w |\nabla \varphi_\epsilon|, \psi_c \right), \\ \left(\mu^{k+1} - \frac{1}{\epsilon^2} W'(c^{k+1}) + \Delta c^{k+1}, \psi_\mu \right) &= 0. \end{aligned} \tag{4.29}$$

We impose the following boundary conditions on the system

$$\mathbb{M} \nabla \mu^{k+1} \cdot \mathbf{n} = 0 \quad \text{on} \quad \Gamma \tag{4.30}$$

and

$$\nabla c^{k+1} \cdot \mathbf{n} = 0 \quad \text{on} \quad \Gamma_{wall} \cup \quad \Gamma_{out}, \tag{4.31}$$

where Γ is boundary of the computational domain. This leads to zero boundary terms after performing formal integration by parts of equations 4.29:

$$\begin{aligned} \left(\frac{c^{k+1} - c^k}{\Delta t}, \psi_c \right) + \left(\mathbb{M} \nabla \mu^{k+1}, \nabla \psi_c \right) &= \left(\alpha D^{-1} k w |\nabla \varphi_\varepsilon|, \psi_c \right), \\ \left(\mu^{k+1} - \frac{1}{\epsilon^2} W'(c^{k+1}), \psi_\mu \right) - \left(\nabla c^{k+1}, \nabla \psi_\mu \right) &= 0. \end{aligned} \tag{4.32}$$

Test and trial space for the phase field c:

$$\Psi_c = \left\{ c \in H^1(\Omega^*), c|_{\Gamma_{in}} = c_D \right\} \tag{4.33}$$

$$\Psi_c' = \left\{ c \in H^1(\Omega^*), c|_{\Gamma_{in}} = 0 \right\} \tag{4.34}$$

Test and trial space for the chemical potential μ

$$\Psi_\mu' = \Psi_\mu = H^1(\Omega^*). \tag{4.35}$$

We have chosen the finite element spaces in the following manner:

$$\Psi_{ch}' = \left\{ c \in H^1(\Omega^*), c|_K \in Q_1(K), c|_{\Gamma_{in}} = 0 \right\} \tag{4.36}$$

and

$$\Psi_{ch} = \left\{ c \in H^1(\Omega^*), c|_K \in Q_1(K), c|_{\Gamma_{in}} = c_D \right\} \tag{4.37}$$

for the phase field and

$$\Psi_{\mu h} = \Psi_{\mu h}' = \left\{ \mu \in H^1(\Omega^*), \mu|_K \in Q_1(K) \right\} \tag{4.38}$$

for the chemical potential.

Weak formulation of the transport equation for platelets

We multiply (3.227) by the test function Ψ_w from the appropriate space to be specified later:

$$\begin{aligned}&\left(\frac{w^{k+1}-w^k}{\Delta t} - D\mathrm{div}(\phi\nabla w^{k+1}) + \mathrm{div}(\phi w^{k+1}\mathbf{u}), \Psi_w\right)\\ &+ \left(\frac{1}{\epsilon}B(\phi)kw^{k+1} - (1-\phi)\Delta w^{k+1}, \Psi_w\right) = 0 \qquad \text{in} \quad \Omega^*.\end{aligned} \tag{4.39}$$

After integration by parts and application of no-flux boundary condition we obtain the following weak formulation.

$$\begin{aligned}&\left(\frac{w^{k+1}-w^k}{\Delta t} + \mathrm{div}(\phi w^{k+1}\mathbf{u}) + \frac{1}{\epsilon}B(\phi)kw^{k+1}, \Psi_w\right) +\\ &\left((1-\phi)\nabla w^{k+1}, \nabla\Psi_w\right) - \left((1-\phi)\nabla w^{k+1}\cdot\mathbf{n}, \Psi_w\right)_{\Gamma_{outflow}}\\ &+ D\left(\phi\nabla w^{k+1}, \nabla\Psi_w\right) - D\left(\phi\nabla w^{k+1}\cdot\mathbf{n}, \Psi_w\right)_{\Gamma_{outflow}} = 0 \qquad \text{in} \quad \Omega^*\end{aligned} \tag{4.40}$$

Test space for the platelets field w:

$$\Psi'_w = \left\{w \in H^1(\Omega^*), w|_{\Gamma_{in}} = 0\right\}. \tag{4.41}$$

Trial space for the platelets field w:

$$\Psi_w = \left\{w \in H^1(\Omega^*), w|_{\Gamma_{in}} = w_D\right\}. \tag{4.42}$$

We have chosen the finite element spaces in the following manner:

$$\Psi'_{wh} = \left\{w \in H^1(\Omega^*), w|_K \in Q_1(K), w|_{\Gamma_{in}} = 0\right\} \tag{4.43}$$

and

$$\Psi_{wh} = \left\{w \in H^1(\Omega^*), w|_K \in Q_1(K), w|_{\Gamma_{in}} = w_D\right\}. \tag{4.44}$$

4.3 Viscoelastic model of blood flow

We have introduced a splitting method for the Navier-Stokes equations in Section 4.1.1. Our system of equations (3.228) contains however additional elastic stress tensor term. In order to successfully solve the viscoelastic problem, we use the DEVSS framework. Hence we will have to treat the new terms originating from DEVSS method.

4.3.1 DEVSS

In order to increase convergence in viscoelastic flow simulations one can increase coercivity of the elliptic operator in the momentum equation (3.228). An auxiliary variable $\mathbf{d}$ is added to the system of equations to retain consistency of it:

$$Re\frac{\partial\mathbf{u}}{\partial t} + Re\mathbf{u}\cdot\nabla\mathbf{u} + \nabla p - \mathrm{div}\,\boldsymbol{\tau} - (\eta_N + \omega)\,\mathrm{div}\,\mathbf{D}(\mathbf{u}) = -\omega\,\mathrm{div}\,\mathbf{d}, \tag{4.45}$$

$$\mathbf{d} = D(\mathbf{u}), \tag{4.46}$$

where ω is properly chosen constant.

In [23] this approach is discussed in comparison with other methods, like EVSS. We reformulate (4.45) for our splitting method:

$$\frac{\mathbf{u}_*^{k+1} - \mathbf{u}^k}{\Delta t} + N(\mathbf{u}_*^{k+1}) + \nabla p^k - L_{DEVSS}(\mathbf{u}_*^{k+1}) - \operatorname{div} \boldsymbol{\tau}^k = -\omega \operatorname{div} \mathbf{d}^k, \tag{4.47}$$

where

$$L_{DEVSS}(\mathbf{u}) = \operatorname{div}((\eta_N + \omega))(\nabla \mathbf{u} + (\nabla \mathbf{u})^T). \tag{4.48}$$

The nonlinear term needs special treatment. There is possibility to use an extrapolation from the previous time step for linearization, however we have decided to linearize the convective term using Picard iteration. We have chosen the norm of residual as the termination criterion of the iteration.

4.3.2 Note on boundary conditions

We have to deal with boundary conditions in the nonhomogeneous model, i.e. boundary conditions for N_0, M, $\boldsymbol{\tau}$ and $\boldsymbol{\sigma}$ in equations (3.230), (3.231), (3.232) and (3.233), respectively. Generally, we set a Dirichlet boundary condition on the inflow and a no-flux condition on the solid walls for each of the variables. We now iterate over the variables in order to show, which values we set on the inflow and wall boundaries. At inflow we set Dirichlet boundary condition for N_0 and M. Further we assume, that if we define fluxes

$$\mathbf{J}_{N_0} = \frac{1}{Pe}\nabla N_0 - \frac{1}{1-\beta}\frac{De}{Pe}\operatorname{div} \boldsymbol{\tau} \tag{4.49}$$

and

$$\mathbf{J}_M = \frac{1}{Pe}\nabla M - \frac{1}{1-\beta}\frac{De}{Pe}\operatorname{div} \boldsymbol{\sigma}, \tag{4.50}$$

then we assume no-flux boundary conditions on the walls, i.e. it holds

$$\mathbf{J}_{N_0} \cdot \tilde{\mathbf{n}} = 0 \tag{4.51}$$

and

$$\mathbf{J}_M \cdot \tilde{\mathbf{n}} = 0, \tag{4.52}$$

where $\tilde{\mathbf{n}}$ is the unit outer normal to the wall.

The situation is not so simple in for the case of tensor quantities $\boldsymbol{\tau}$ and $\boldsymbol{\sigma}$. At inflow we impose the following Dirichlet boundary conditions

$$\boldsymbol{\tau}_D = \frac{1-\beta}{De} N_0 Q_0 \mathbf{t}\mathbf{t} - \frac{1-\beta}{De} N_0 \mathbf{I} \tag{4.53}$$

and

$$\boldsymbol{\sigma}_D = \frac{1-\beta}{De} M Q_0 \mathbf{t}\mathbf{t} - \frac{1-\beta}{De} M \mathbf{I}, \tag{4.54}$$

where $\mathbf{t}$ is the tangent vector to the flow on the inflow. N_0 and M are the prescribed values at inflow defined above. Q_0 is length of a Hookean dumbbell. The expressions

(4.53) and (4.53) originate from well known Kramers expression, also mentioned in section 3.2.3.

We have to deal with the values of the tensor quantities $\boldsymbol{\tau}$ and $\boldsymbol{\sigma}$ on the walls as well. We define corresponding fluxes

$$\boldsymbol{J}_{\boldsymbol{\tau}} = \frac{De}{Pe}\mu(\dot{\gamma}, N_0, M)(\nabla\boldsymbol{\tau} + (\operatorname{div}\boldsymbol{\tau})\mathbf{I}) \tag{4.55}$$

and

$$\boldsymbol{J}_{\boldsymbol{\sigma}} = \frac{De}{Pe}\mu(\dot{\gamma}, N_0, M)(\nabla\boldsymbol{\sigma} + (\operatorname{div}\boldsymbol{\sigma})\mathbf{I}) \tag{4.56}$$

then we assume no-flux boundary condition on the walls, i.e. it holds

$$\boldsymbol{J}_{\boldsymbol{\tau}}\tilde{\mathbf{n}} = \mathbf{0} \tag{4.57}$$

and

$$\boldsymbol{J}_{\boldsymbol{\sigma}}\tilde{\mathbf{n}} = \mathbf{0}, \tag{4.58}$$

i.e. product of flux, which is tensor of third order with outer normal vector. Hence the result is the tensor of second order.

4.3.3 Discretization in space - flowing blood domain

We use the finite element method for the spatial discretization of our partial differential equations.
We present firstly the variational formulation of our problem. We use splitting methods for both rheological and biochemical part of our model. We will treat them separately.

Weak formulation of the equations for velocity and pressure

We multiply (4.47) by the vector function $\mathbf{v}$ obtaining

$$\begin{aligned}\left(\frac{\mathbf{u}_*^{k+1} - \mathbf{u}^k}{\Delta t} + \mathbf{u}_{nonlin}\nabla\mathbf{u}_*^{k+1}, \mathbf{v}\right) + \left(\nabla p^k, \mathbf{v}\right) - \left(\operatorname{div}(2(\eta_N + \omega)\mathbf{D}\mathbf{u}_*^{k+1}), \mathbf{v}\right) \\ = \left(\operatorname{div}\boldsymbol{\tau}^{\mathbf{k}}, \mathbf{v}\right) - \left(\omega \operatorname{div}\mathbf{d}^k, \mathbf{v}\right)\end{aligned} \tag{4.59}$$

In order to redistribute derivatives evenly between trial and test functions we perform formally integration by parts on diffusion and pressure terms. This leads to

$$\begin{aligned}&\left(\frac{\mathbf{u}_*^{k+1} - \mathbf{u}^k}{\Delta t} + \mathbf{u}\nabla\mathbf{u}_*^{k+1}, \mathbf{v}\right) - \left(p^k, \operatorname{div}\mathbf{v}\right) + (p^k\mathbf{n}, \mathbf{v})_\Gamma + \left(2(\eta_N + \omega)\mathbf{D}(\mathbf{u}_*^{k+1}), \nabla\mathbf{v}\right) \\ &- \left(2(\eta_N + \omega)\mathbf{D}(\mathbf{u}_*^{k+1})\mathbf{n}, \mathbf{v})\right)_\Gamma = \left(\operatorname{div}\boldsymbol{\tau}^{\mathbf{k}}, \mathbf{v}\right) + \left(\omega\mathbf{d}^k, \nabla\mathbf{v}\right),\end{aligned} \tag{4.60}$$

where $(.,.)_\Gamma$ stands for integral over boundary Γ. We have $\mathbf{v}$ equal to zero on Γ_{in} and Γ_{wall}, therefore the boundary integrals on these parts of boundary vanish. We have to handle the boundary terms on $\Gamma_{outflow}$.
We set on outflow

$$2(\eta_N + \omega)\mathbf{D}(\mathbf{u}_*^{k+1})\mathbf{n} = \mathbf{0} \qquad \text{on} \quad \Gamma_{outflow}, \tag{4.61}$$

therefore in the equation (4.60) only the boundary integral with pressure corresponding to the ouflow part of boundary Γ_{ouflow} remains.
We will now turn our attention to the Poisson problem for pressure (4.2). We multiply the equation by a test function q and integrate formally by parts, getting

$$-\left(\nabla(p^{k+1}-p^k),\nabla q\right)+\left(\nabla(p^{k+1}-p^k)\cdot\mathbf{n},q\right)_\Gamma=\frac{1}{\Delta t}\left(\operatorname{div}\mathbf{u}_*^{k+1},q\right). \tag{4.62}$$

In this case we have to deal with implicit use of a boundary condition. The application of the homogeneous Neuman condition $\frac{\partial p}{\partial \mathbf{n}}=0$ leads to singular matrix to be solved by linear solver. One of workarounds to tackle this issue is to prescribe additional boundary condition on pressure $p=0$ on Γ_{out}.
We now supply the definition of the relevant function spaces for tentative velocity and pressure.
Test space for tentative velocity:

$$\mathbf{V}'=\mathbf{H}_0^1=\left\{\mathbf{v}\in\left[H^1(\Omega)\right]^3,\mathbf{v}|_{\Gamma_{in}\cup\Gamma_{wall}}=\mathbf{0}\right\}. \tag{4.63}$$

Trial space for tentative velocity:

$$\mathbf{V}=\mathbf{H}_D^1(\Omega)=\left\{\mathbf{v}\in\left[H^1(\Omega)\right]^3,\mathbf{v}|_{\Gamma_{in}\cup\Gamma_{wall}}=\mathbf{u}_D\right\}. \tag{4.64}$$

The test and trial space for the weak formulation (4.62) of Poisson problem (4.2) are identical:

$$Q=\left\{q\in H^1(\Omega),q|_{\Gamma_{out}}=0\right\}. \tag{4.65}$$

In the case of the velocity correction we only multiply the equation (4.17) by test function. Integration by parts is not performed and it is not necessary to discuss boundary conditions.
We chose the following finite element spaces:

$$\mathbf{V}'_h=\left\{\mathbf{v}\in\left[H^1(\Omega)\right]^3,\mathbf{v}|_K\in\left[Q_2(K)\right]^3,\mathbf{v}|_{\Gamma_{in}\cup\Gamma_{wall}}=\mathbf{0}\right\}, \tag{4.66}$$

$$\mathbf{V}_h=\left\{\mathbf{v}\in\left[H^1(\Omega)\right]^3,\mathbf{v}|_K\in\left[Q_2(K)\right]^3,\mathbf{v}|_{\Gamma_{in}\cup\Gamma_{wall}}=\mathbf{u}_D\right\}, \tag{4.67}$$

and

$$Q_h=\left\{q\in H^1(\Omega),q|_K\in Q_1(K),q|_{\Gamma_{out}}=0\right\} \tag{4.68}$$

Weak formulation of the equations for red blood cell stress tensor

We multiply (3.232)by a tensor test function $\boldsymbol{\chi}$ from the proper space and integrate formally by parts:

$$\begin{aligned}&\left(\boldsymbol{\tau}+De\mu(\dot\gamma,N_0,M)\overset{\triangledown}{\boldsymbol{\tau}},\boldsymbol{\chi}\right)+\left(\frac{De}{Pe}\left(\nabla\boldsymbol{\tau}+(\operatorname{div}\boldsymbol{\tau})\mathbf{I}\right),\nabla(\mu(\dot\gamma,N_0,M)\boldsymbol{\chi})\right)\\&-\left(\frac{De}{Pe}\mu(\dot\gamma,N_0,M)(\nabla\boldsymbol{\tau}+(\operatorname{div}\boldsymbol{\tau})\mathbf{I})\mathbf{n},\boldsymbol{\chi}\right)_{\Gamma_{outflow}}=((1-\beta)N_0\boldsymbol{D},\boldsymbol{\chi})\end{aligned} \tag{4.69}$$

Test space for the red blood cell stress field $\boldsymbol{\tau}$:

$$\boldsymbol{\Psi}'_{\boldsymbol{\tau}} = \left\{ \boldsymbol{\tau} \in \left[H^1(\Omega_F) \right]^{3\times 3}, \boldsymbol{\tau}|_{\Gamma_{in}} = \mathbf{0} \right\}. \tag{4.70}$$

Trial space for the red blood cell stress field $\boldsymbol{\tau}$:

$$\boldsymbol{\Psi}_{\boldsymbol{\tau}} = \left\{ \boldsymbol{\tau} \in \left[H^1(\Omega_F) \right]^{3\times 3}, \boldsymbol{\tau}|_{\Gamma_{in}} = \boldsymbol{\tau}_D \right\}, \tag{4.71}$$

where $\boldsymbol{\tau}_D$ is defined by (4.53).
We chose the following finite element spaces:

$$\boldsymbol{\Psi}'_{\boldsymbol{\tau}h} = \left\{ \boldsymbol{\tau} \in \left[H^1(\Omega_F) \right]^{3\times 3}, \boldsymbol{\tau}|_K \in \left[Q_1(K) \right]^{3\times 3}, \boldsymbol{\tau}|_{\Gamma_{in}} = \mathbf{0} \right\} \tag{4.72}$$

and

$$\boldsymbol{\Psi}_{\boldsymbol{\tau}h} = \left\{ \boldsymbol{\tau} \in \left[H^1(\Omega_F) \right]^{3\times 3}, \boldsymbol{\tau}|_K \in \left[Q_1(K) \right]^{3\times 3}, \boldsymbol{\tau}|_{\Gamma_{in}} = \boldsymbol{\tau}_D \right\}. \tag{4.73}$$

Weak formulation of the equations for aggregate stress tensor

We multiply (3.233)by a tensor test function $\boldsymbol{\chi}$ from the proper space and integrate formally by parts:

$$\begin{aligned} &\left(\boldsymbol{\sigma} + De\mu(\dot{\gamma}, N_0, M)\, \overset{\triangledown}{\boldsymbol{\sigma}}, \boldsymbol{\chi} \right) + \left(\frac{De}{Pe} \left(\nabla\boldsymbol{\sigma} + (\operatorname{div}\boldsymbol{\sigma})\mathbf{I} \right), \nabla(\mu(\dot{\gamma}, N_0, M)\boldsymbol{\chi}) \right) \\ &- \left(\frac{De}{Pe}\mu(\dot{\gamma}, N_0, M)(\nabla\boldsymbol{\sigma} + (\operatorname{div}\boldsymbol{\sigma})\mathbf{I})\mathbf{n}, \boldsymbol{\chi} \right)_{\Gamma_{outflow}} = ((1-\beta)M\boldsymbol{D}, \boldsymbol{\chi}) \end{aligned} \tag{4.74}$$

Test space for the aggregate stress field $\boldsymbol{\sigma}$:

$$\boldsymbol{\Psi}'_{\boldsymbol{\sigma}} = \left\{ \boldsymbol{\sigma} \in \left[H^1(\Omega_F) \right]^{3\times 3}, \boldsymbol{\sigma}|_{\Gamma_{in}} = \mathbf{0} \right\}. \tag{4.75}$$

Trial space for the aggregate stress field $\boldsymbol{\sigma}$:

$$\boldsymbol{\Psi}_{\boldsymbol{\sigma}} = \left\{ \boldsymbol{\sigma} \in \left[H^1(\Omega_F) \right]^{3\times 3}, \boldsymbol{\sigma}|_{\Gamma_{in}} = \boldsymbol{\sigma}_D \right\}, \tag{4.76}$$

where $\boldsymbol{\sigma}_D$ is defined by (4.54).

We have chosen the finite element spaces in the following manner:

$$\boldsymbol{\Psi}'_{\boldsymbol{\sigma}h} = \left\{ \boldsymbol{\sigma} \in \left[H^1(\Omega_F) \right]^{3\times 3}, \boldsymbol{\sigma}|_K \in \left[Q_1(K) \right]^{3\times 3}, \boldsymbol{\sigma}|_{\Gamma_{in}} = \mathbf{0} \right\} \tag{4.77}$$

and

$$\boldsymbol{\Psi}_{\boldsymbol{\sigma}h} = \left\{ \boldsymbol{\sigma} \in \left[H^1(\Omega_F) \right]^{3\times 3}, \boldsymbol{\sigma}|_K \in \left[Q_1(K) \right]^{3\times 3}, \boldsymbol{\sigma}|_{\Gamma_{in}} = \boldsymbol{\sigma}_D \right\}. \tag{4.78}$$

Weak formulation of the equation for the red blood cells field

We multiply (3.230) by a test ψ_{N_0} function from the proper space and integrate formally by parts:

$$\left(\frac{\partial N_0}{\partial t} + \mathbf{u}\cdot\nabla N_0, \psi_{N_0}\right) + \frac{1}{Pe}\left(\nabla N_0, \nabla\psi_{N_0}\right) - \frac{1}{Pe}\left(\nabla N_0\cdot\mathbf{n}, \psi_{N_0}\right)_{\Gamma_{outflow}} = \frac{1}{1-\beta}\frac{De}{Pe}\left(\operatorname{div}\boldsymbol{\tau}, \nabla\psi_{N_0}\right) - \frac{1}{1-\beta}\frac{De}{Pe}\left((\operatorname{div}\boldsymbol{\tau})\cdot\boldsymbol{n}, \psi_{N_0}\right)_{\Gamma_{outflow}}. \tag{4.79}$$

Test space for the red blood cells field N_0:

$$\Psi'_{N_0} = \left\{N_0 \in H^1(\Omega_F), N_0|_{\Gamma_{in}} = 0\right\}. \tag{4.80}$$

Trial space for the red blood cells field N_0:

$$\Psi_{N_0} = \left\{N_0 \in H^1(\Omega_F), N_0|_{\Gamma_{in}} = N_D\right\}. \tag{4.81}$$

We have chosen the finite element spaces in the following manner:

$$\Psi'_{N_0h} = \left\{N_0 \in H^1(\Omega_F), N_0|_K \in Q_1(K), N_0|_{\Gamma_{in}} = 0\right\} \tag{4.82}$$

and

$$\Psi_{N_0h} = \left\{N_0 \in H^1(\Omega_F), N_0|_K \in Q_1(K), N_0|_{\Gamma_{in}} = N_D\right\}. \tag{4.83}$$

Weak formulation of the equation for the aggregates/rouleaux field

We multiply (3.231) by a test ψ_M function from the proper space and integrate formally by parts:

$$\left(\frac{\partial M}{\partial t} + \mathbf{u}\cdot\nabla M, \psi_M\right) + \frac{1}{Pe}\left(\nabla M, \nabla\psi_M\right) - \frac{1}{Pe}\left(\nabla M\cdot\mathbf{n}, \psi_M\right)_{\Gamma_{outflow}} + \left(0.5\alpha(\dot\gamma)M^2, \psi_M\right)\Big) + \left(0.5b(\dot\gamma)M, \psi_M\right)) = \frac{1}{1-\beta}\frac{De}{Pe}\left(\operatorname{div}\boldsymbol{\sigma}, \nabla\psi_M\right) - \frac{1}{1-\beta}\frac{De}{Pe}\left((\operatorname{div}\boldsymbol{\sigma})\cdot\boldsymbol{n}, \psi_M\right)_{\Gamma_{outflow}} + \left(0.5b(\dot\gamma)M, \psi_M\right). \tag{4.84}$$

Test space for the aggregates field M:

$$\Psi'_M = \left\{M \in H^1(\Omega_F), M|_{\Gamma_{in}} = 0\right\}. \tag{4.85}$$

Trial space for the aggregates field M:

$$\Psi_M = \left\{M \in H^1(\Omega_F), M|_{\Gamma_{in}} = M_D\right\}. \tag{4.86}$$

We have chosen the finite element spaces in the following manner:

$$\Psi'_{Mh} = \left\{M \in H^1(\Omega_F), M|_K \in Q_1(K), M|_{\Gamma_{in}} = 0\right\} \tag{4.87}$$

and

$$\Psi_{Mh} = \left\{M \in H^1(\Omega_F), M|_K \in Q_1(K), M|_{\Gamma_{in}} = M_D\right\}. \tag{4.88}$$

4.3.4 Discretization in space - extension to the whole domain

Weak formulation of the equations for red blood cell stress tensor

We multiply (3.238) by a tensor test function $\boldsymbol{\chi}$ from the proper space and integrate formally by parts:

$$\left(\boldsymbol{\tau} + De\phi\mu(\dot{\gamma}, N_0, M)\overset{\triangledown}{\boldsymbol{\tau}}, \boldsymbol{\chi}\right) + \left(\frac{De}{Pe}\left(\nabla\boldsymbol{\tau} + (\operatorname{div}\boldsymbol{\tau})\mathbf{I}\right), \nabla(\phi\mu(\dot{\gamma}, N_0, M)\boldsymbol{\chi})\right) - \left(\frac{De}{Pe}\phi\mu(\dot{\gamma}, N_0, M)(\nabla\boldsymbol{\tau} + (\operatorname{div}\boldsymbol{\tau})\mathbf{I})\mathbf{n}, \boldsymbol{\chi}\right)_{\Gamma_{outflow}} = (\phi(1-\beta)N_0\boldsymbol{D}, \boldsymbol{\chi}) \tag{4.89}$$

Test space for the red blood cell stress field $\boldsymbol{\tau}$:

$$\boldsymbol{\Psi}'_{\boldsymbol{\tau}} = \left\{\boldsymbol{\tau} \in \left[H^1(\Omega_F \cup \Omega)\right]^{3\times 3}, \boldsymbol{\tau}|_{\Gamma_{in}} = \mathbf{0}\right\}. \tag{4.90}$$

Trial space for the red blood cell stress field $\boldsymbol{\tau}$:

$$\boldsymbol{\Psi}_{\boldsymbol{\tau}} = \left\{\boldsymbol{\tau} \in \left[H^1(\Omega_F \cup \Omega)\right]^{3\times 3}, \boldsymbol{\tau}|_{\Gamma_{in}} = \boldsymbol{\tau}_D\right\}, \tag{4.91}$$

where $\boldsymbol{\tau}_D$ is defined by (4.53).
We chose the following finite element spaces:

$$\boldsymbol{\Psi}'_{\boldsymbol{\tau}h} = \left\{\boldsymbol{\tau} \in \left[H^1(\Omega_F \cup \Omega)\right]^{3\times 3}, \boldsymbol{\tau}|_K \in [Q_1(K)]^{3\times 3}, \boldsymbol{\tau}|_{\Gamma_{in}} = \mathbf{0}\right\} \tag{4.92}$$

and

$$\boldsymbol{\Psi}_{\boldsymbol{\tau}h} = \left\{\boldsymbol{\tau} \in \left[H^1(\Omega_F \cup \Omega)\right]^{3\times 3}, \boldsymbol{\tau}|_K \in [Q_1(K)]^{3\times 3}, \boldsymbol{\tau}|_{\Gamma_{in}} = \boldsymbol{\tau}_D\right\}. \tag{4.93}$$

Weak formulation of the equations for aggregate stress tensor

We multiply (3.239)by a tensor test function $\boldsymbol{\chi}$ from the proper space and integrate formally by parts:

$$\left(\boldsymbol{\sigma} + De\phi\mu(\dot{\gamma}, N_0, M)\overset{\triangledown}{\boldsymbol{\sigma}}, \boldsymbol{\chi}\right) + \left(\frac{De}{Pe}\left(\nabla\boldsymbol{\sigma} + (\operatorname{div}\boldsymbol{\sigma})\mathbf{I}\right), \nabla(\phi\mu(\dot{\gamma}, N_0, M)\boldsymbol{\chi})\right) - \left(\frac{De}{Pe}\phi\mu(\dot{\gamma}, N_0, M)(\nabla\boldsymbol{\sigma} + (\operatorname{div}\boldsymbol{\sigma})\mathbf{I})\mathbf{n}, \boldsymbol{\chi}\right)_{\Gamma_{outflow}} = (\phi(1-\beta)M\boldsymbol{D}, \boldsymbol{\chi}) \tag{4.94}$$

Test space for the aggregate stress field $\boldsymbol{\sigma}$:

$$\boldsymbol{\Psi}'_{\boldsymbol{\sigma}} = \left\{\boldsymbol{\sigma} \in \left[H^1(\Omega_F \cup \Omega)\right]^{3\times 3}, \boldsymbol{\sigma}|_{\Gamma_{in}} = \mathbf{0}\right\}. \tag{4.95}$$

Trial space for the aggregate stress field $\boldsymbol{\sigma}$:

$$\boldsymbol{\Psi}_{\boldsymbol{\sigma}} = \left\{\boldsymbol{\sigma} \in \left[H^1(\Omega_F \cup \Omega)\right]^{3\times 3}, \boldsymbol{\sigma}|_{\Gamma_{in}} = \boldsymbol{\sigma}_D\right\}, \tag{4.96}$$

where $\boldsymbol{\sigma}_D$ is defined by (4.54).

We have chosen the finite element spaces in the following manner:

$$\boldsymbol{\Psi}'_{\boldsymbol{\sigma}h} = \left\{ \boldsymbol{\sigma} \in \left[H^1(\Omega_F \cup \Omega) \right]^{3\times 3}, \boldsymbol{\sigma}|_K \in \left[Q_1(K) \right]^{3\times 3}, \boldsymbol{\sigma}|_{\Gamma_{in}} = \mathbf{0} \right\} \tag{4.97}$$

and

$$\boldsymbol{\Psi}_{\boldsymbol{\sigma}h} = \left\{ \boldsymbol{\sigma} \in \left[H^1(\Omega_F \cup \Omega) \right]^{3\times 3}, \boldsymbol{\sigma}|_K \in \left[Q_1(K) \right]^{3\times 3}, \boldsymbol{\sigma}|_{\Gamma_{in}} = \boldsymbol{\sigma}_D \right\}. \tag{4.98}$$

Weak formulation of the convection-diffusion equation for the red blood cells field

We multiply (3.242) by a test ψ_{N_0} function from the proper space and integrate formally by parts:

$$\begin{aligned} &\left(\frac{\partial N_0}{\partial t} + \phi \mathbf{u} \cdot \nabla N_0, \psi_{N_0} \right) + (\nabla N_0, \nabla((1-\phi)\psi_{N_0})) \\ &+ \frac{1}{Pe} (\nabla N_0, \nabla(\phi \psi_{N_0})) - \frac{1}{Pe} (\phi \nabla N_0 \cdot \mathbf{n}, \psi_{N_0})_{\Gamma_{outflow}} \\ =&\frac{1}{1-\beta} \frac{De}{Pe} (\operatorname{div} \boldsymbol{\tau}, \nabla(\phi \psi_{N_0})) - \frac{1}{1-\beta} \frac{De}{Pe} ((\phi \operatorname{div} \boldsymbol{\tau}) \cdot \boldsymbol{n}, \psi_{N_0})_{\Gamma_{outflow}} \end{aligned} \tag{4.99}$$

Test space for the red blood cells field N_0:

$$\Psi'_{N_0} = \left\{ N_0 \in H^1(\Omega_F \cup \Omega), N_0|_{\Gamma_{in}} = 0 \right\}. \tag{4.100}$$

Trial space for the red blood cells field N_0:

$$\Psi_{N_0} = \left\{ N_0 \in H^1(\Omega_F \cup \Omega), N_0|_{\Gamma_{in}} = N_D \right\}. \tag{4.101}$$

We have chosen the finite element spaces in the following manner:

$$\Psi'_{N_0 h} = \left\{ N_0 \in H^1(\Omega_F \cup \Omega), N_0|_K \in Q_1(K), N_0|_{\Gamma_{in}} = 0 \right\} \tag{4.102}$$

and

$$\Psi_{N_0 h} = \left\{ N_0 \in H^1(\Omega_F \cup \Omega), N_0|_K \in Q_1(K), N_0|_{\Gamma_{in}} = N_D \right\}. \tag{4.103}$$

Weak formulation of the equation for the aggregates/rouleaux field

We multiply (3.243) by a test ψ_M function from the proper space and integrate formally by parts:

$$\begin{aligned} &\left(\frac{\partial M}{\partial t} + \phi \mathbf{u} \cdot \nabla M, \psi_M \right) + (\phi \nabla M, \nabla(\psi_M(1-\phi))) + \frac{1}{Pe} (\phi \nabla M, \nabla(\psi_M(1-\phi)) \\ &-\frac{1}{Pe} (\phi \nabla M \cdot \mathbf{n}, \psi_M)_{\Gamma_{outflow}} + \left(0.5\phi\alpha(\dot{\gamma}) M^2, \psi_M \right)) + (0.5\phi b(\dot{\gamma}) M, \psi_M)) = \\ &\frac{1}{1-\beta} \frac{De}{Pe} (\operatorname{div} \boldsymbol{\sigma}, \nabla(\phi \psi_M)) - \phi \frac{1}{1-\beta} \frac{De}{Pe} ((\operatorname{div} \boldsymbol{\sigma}) \cdot \boldsymbol{n}, \psi_M)_{\Gamma_{outflow}} + (0.5\phi b(\dot{\gamma}) M, \psi_M). \end{aligned} \tag{4.104}$$

Test space for the aggregates field M:

$$\Psi'_M = \left\{ M \in H^1(\Omega_F \cup \Omega), M|_{\Gamma_{in}} = 0 \right\}. \tag{4.105}$$

Trial space for the aggregates field M:

$$\Psi_M = \left\{ M \in H^1(\Omega_F \cup \Omega), M|_{\Gamma_{in}} = M_D \right\}. \tag{4.106}$$

We have chosen the finite element spaces in the following manner:

$$\Psi'_{Mh} = \left\{ M \in H^1(\Omega_F \cup \Omega), M|_K \in Q_1(K), M|_{\Gamma_{in}} = 0 \right\}. \tag{4.107}$$

and

$$\Psi_{Mh} = \left\{ M \in H^1(\Omega_F \cup \Omega), M|_K \in Q_1(K), M|_{\Gamma_{in}} = M_D \right\}. \tag{4.108}$$

4.3.5 SUPG stabilization

Convection dominated problems require special numerical treatment as their Galerkin formulation suffers from spurious oscillations not present in their true solution.
The first possibility is to introduce into the system artificial diffusion in all direction. It can however lead to the blurring of sharp layers and non–physical increase of the concentration in some regions.
The SUPG approach which is more physically accurate was therefore proposed. Its crux lies in the introduction of artificial diffusion in streamline upwind direction. Mathematically, the introduction of artificial diffusion can be formulated as a modification of the test function of the convective term. On this basis is developed the SUPG stabilization method for finite element method, but for consistency, the modified test function is applied to all terms of the weak form. In that case, the exact solution of the problem satisfies the weak form.
In our case, the test function $\phi_{\boldsymbol{\tau}}$ for the polymeric part of the stress tensor is modified in the following manner:

$$\psi_{\boldsymbol{\tau}} \to \psi_{\boldsymbol{\tau}} + \alpha_h^{SU} \mathbf{u} \cdot \nabla \psi_{\boldsymbol{\tau}}, \tag{4.109}$$

where α_h^{SU} is a stabilisation parameter, which we take as

$$\alpha_h^{SU} = \frac{h}{\sqrt{1 + \mathbf{u}^2}}, \tag{4.110}$$

where h is the cell diameter.
The test function for aggregate tensor field is modified similarly:

$$\psi_{\boldsymbol{\chi}} \to \psi_{\boldsymbol{\chi}} + \alpha_h^{SU} \mathbf{u} \cdot \nabla \psi_{\boldsymbol{\chi}}. \tag{4.111}$$

The test function for the number concentration of RBCs field N_0 is modified accordingly:

$$\psi_{N_0} \to \psi_{N_0} + \alpha_h^{SU} \mathbf{u} \cdot \nabla \psi_{N_0}. \tag{4.112}$$

The test function for the number concentration of rouleaux field M is modified in similar vein:

$$\psi_M \to \psi_M + \alpha_h^{SU} \mathbf{u} \cdot \nabla \psi_M. \tag{4.113}$$

We do not write the modified test function in the system of equations for simplicity. We will implicitly treat them as modified in the described manner.

4.4 Coagulation related quantities equations and phase field

4.4.1 Discretization in space

Weak formulation of coagulation related quantities - flowing blood domain

We multiply (3.115) by a test $\psi_{\mathbf{c}}$ function from the proper space and integrate formally by parts:

$$\left(\frac{\partial \mathbf{c}}{\partial t} + \mathbf{u}\cdot\nabla\mathbf{c}, \psi_{\mathbf{c}}\right) + \mathbb{D}\left(\nabla\mathbf{c}, \nabla\psi_{\mathbf{c}}\right) - \mathbb{D}\left(\nabla\mathbf{c}\mathbf{n}, \psi_{\mathbf{c}}\right)_{\Gamma_{outflow}} - \left(\mathbf{R}(\mathbf{c},\mathbf{f}), \psi_{\mathbf{c}}\right)_{\Gamma} = \left(\mathbf{S}(\mathbf{c}), \psi_{\mathbf{c}}\right), \tag{4.114}$$

where $\mathbf{R}(\mathbf{c},\mathbf{f})$ is the Robin boundary condition (3.125) and $\mathbf{S}(\mathbf{c})$ is the generic source term introduced in section 3.3.1. Test space for the field $\mathbf{c}$:

$$\mathbf{\Psi}'_{\mathbf{c}} = \left\{\mathbf{c} \in \left[H^1(\Omega_F)\right]^7, \mathbf{c}|_{\Gamma_{in}} = \mathbf{0}\right\}. \tag{4.115}$$

Trial space for the aggregates field $\mathbf{c}$:

$$\mathbf{\Psi}_{\mathbf{c}} = \left\{\mathbf{c} \in \left[H^1(\Omega_F)\right]^7, \mathbf{c}|_{\Gamma_{in}} = \mathbf{c_D}\right\}. \tag{4.116}$$

We have chosen the finite element spaces in the following manner:

$$\mathbf{\Psi}'_{\mathbf{c}h} = \left\{\mathbf{c} \in \left[H^1(\Omega_F)\right]^7, \mathbf{c}|_K \in \left[Q_1(K)\right]^7, \mathbf{c}|_{\Gamma_{in}} = \mathbf{0}\right\} \tag{4.117}$$

and

$$\mathbf{\Psi}_{\mathbf{c}h} = \left\{\mathbf{c} \in \left[H^1(\Omega_F)\right]^7, \mathbf{c}|_K \in \left[Q_1(K)\right]^7, \mathbf{c}|_{\Gamma_{in}} = \mathbf{c_D}\right\}. \tag{4.118}$$

Weak formulation of coagulation related quantities - extension to the whole domain

We multiply (3.244) by a test function $\psi_{\mathbf{c}}$ from the proper space and integrate formally by parts, under assumption of no flux on walls:

$$\begin{aligned}\left(\frac{\partial \mathbf{c}}{\partial t} + \phi\mathbf{u}\cdot\nabla\mathbf{c}, \psi_{\mathbf{c}}\right) + \left((1-\phi)\nabla\mathbf{c}, \nabla\psi_{\mathbf{c}}\right) + \mathbb{D}\left(\phi\nabla\mathbf{c}, \nabla\psi_{\mathbf{c}}\right) \\ -\mathbb{D}\left(\phi\nabla\mathbf{c}\cdot\mathbf{n}, \psi_{\mathbf{c}}\right)_{\Gamma_{outflow}} + \mathbf{D}\left(\mathbf{R}(\mathbf{c},\mathbf{f})_{approx}, \psi_{\mathbf{c}}\right) = \left(\phi\mathbf{S}(\mathbf{c}), \psi_{\mathbf{c}}\right),\end{aligned} \tag{4.119}$$

where $\mathbf{R}(\mathbf{c},\mathbf{f})_{approx}$ is a term originating from approximation of the Robin boundary condition $\mathbf{R}(\mathbf{c},\mathbf{f})$ (3.125) using the framework [80], see equations (3.193)-(3.195).

$\mathbf{S}(\mathbf{c})$ is the generic source term introduced in section 3.3.1.

Test space for the field $\mathbf{c}$:

$$\mathbf{\Psi}'_{\mathbf{c}} = \left\{\mathbf{c} \in \left[H^1(\Omega_F \cup \Omega)\right]^7, \mathbf{c}|_{\Gamma_{in}} = \mathbf{0}\right\}. \tag{4.120}$$

Trial space for the aggregates field $\mathbf{c}$:

$$\mathbf{\Psi_c} = \left\{ \mathbf{c} \in \left[H^1(\Omega_F \cup \Omega) \right]^7, \mathbf{c}|_{\Gamma_{in}} = \mathbf{c_D} \right\}. \tag{4.121}$$

We have chosen the finite element spaces in the following manner:

$$\mathbf{\Psi'}_{\mathbf{c}h} = \left\{ \mathbf{c} \in \left[H^1(\Omega_F \cup \Omega) \right]^7, \mathbf{c}|_K \in [Q_1(K)]^7, \mathbf{c}|_{\Gamma_{in}} = \mathbf{0} \right\} \tag{4.122}$$

and

$$\mathbf{\Psi}_{\mathbf{c}h} = \left\{ \mathbf{c} \in \left[H^1(\Omega_F \cup \Omega) \right]^7, \mathbf{c}|_K \in [Q_1(K)]^7, \mathbf{c}|_{\Gamma_{in}} = \mathbf{c_D} \right\}. \tag{4.123}$$

Surface coagulation quantities

We multiply (3.246) by a test function $\psi_{\mathbf{f}}$ getting

$$\left(\frac{\partial \mathbf{f}}{\partial t}, \psi_{\mathbf{f}} \right) = (\delta_\Gamma \mathbf{P}(\mathbf{c}, \mathbf{f}), \psi_{\mathbf{f}}) \tag{4.124}$$

Test and trial space for the field $\mathbf{f}$:

$$\mathbf{\Psi_f} = \mathbf{\Psi'_f} = \left[H^1(\Omega_F \cup \Omega) \right]^4 \tag{4.125}$$

We have chosen the finite element spaces in the following manner:

$$\mathbf{\Psi}_{\mathbf{f}h} = \mathbf{\Psi}'_{\mathbf{f}h} = \left\{ \mathbf{f} \in \left[H^1(\Omega_F \cup \Omega) \right]^4, \mathbf{f}|_K \in [Q_1(K)]^4 \right\} \tag{4.126}$$

Weak formulation of equations of the movement of the interface

We multiply (3.247) by a tuple (ψ_c, ψ_μ) from the appropriate test spaces:

$$\left(\frac{c^{k+1} - c^k}{\Delta t}, \psi_c \right) - \left(\operatorname{div} \mathbb{M} \nabla \mu^{k+1}, \psi_c \right) = \left(-(1 + \alpha_V) j_{bp} V_p |\varphi_\varepsilon(c)|, \psi_c \right), \tag{4.127}$$

$$\left(\mu^{k+1} - \frac{1}{\epsilon^2} W'(c^{k+1}) + \Delta c^{k+1}, \psi_\mu \right) = 0.$$

We impose the following boundary conditions on the system

$$\mathbb{M} \nabla \mu^{k+1} \cdot \mathbf{n} = 0 \quad \text{on} \quad \Gamma \tag{4.128}$$

and

$$\nabla c^{k+1} \cdot \mathbf{n} = 0 \quad \text{on} \quad \Gamma_{wall} \cup \quad \Gamma_{out}, \tag{4.129}$$

where Γ is boundary of the computational domain. This leads to zero boundary terms after performing formal integration by parts of equations (4.29):

$$\left(\frac{c^{k+1} - c^k}{\Delta t}, \psi_c \right) + \left(\mathbb{M} \nabla \mu^{k+1}, \nabla \psi_c \right) = \left(-j_{bp} (1 + \alpha_V) V_p |\varphi_\epsilon(c)|, \psi_c \right), \tag{4.130}$$

$$\left(\mu^{k+1} - \frac{1}{\epsilon^2} W'(c^{k+1}), \psi_\mu \right) - \left(\nabla c^{k+1}, \nabla \psi_\mu \right) = 0.$$

Test and trial space for the phase field c:

$$\Psi_c = \left\{ c \in H^1(\Omega_F \cup \Omega), c|_{\Gamma_{in}} = c_D \right\} \tag{4.131}$$

$$\Psi_c' = \left\{ c \in H^1(\Omega_F \cup \Omega), c|_{\Gamma_{in}} = 0 \right\} \tag{4.132}$$

Test and trial space for the chemical potential μ

$$\Psi_\mu' = \Psi_\mu = H^1(\Omega_F \cup \Omega). \tag{4.133}$$

We have chosen the finite element spaces in the following manner:

$$\Psi_{ch}' = \left\{ c \in H^1(\Omega_F \cup \Omega)), c|_K \in Q_1(K), c|_{\Gamma_{in}} = 0 \right\} \tag{4.134}$$

and

$$\Psi_{ch} = \left\{ c \in H^1(\Omega_F \cup \Omega)), c|_K \in Q_1(K), c|_{\Gamma_{in}} = c_D \right\} \tag{4.135}$$

for the phase field and

$$\Psi_{\mu h} = \Psi_{\mu h}' = \left\{ \mu \in H^1(\Omega_F \cup \Omega)), \mu|_K \in Q_1(K) \right\}. \tag{4.136}$$

for the chemical potential.

4.5 Numerical methods for the viscoelastic model of blood clot

4.5.1 The algorithm for computation of quantities related the model of Kempen

For the numerical computations of the model introduced in Section 3.3.1 and Section 3.3.4 we need to evaluate the time derivative of inelastic right Cauchy-Green tensor of each mode $\mathbf{C}_{p,i}, \quad i = 1, 2$:

$$\mathbf{C}_{p,i} = \mathbf{F}_p^T \mathbf{F}_p = \mathbf{F}_p^T \mathbf{B}_{e,i}^{-1} \mathbf{F}. \tag{4.137}$$

We perform the time derivative of the previous equations and using the assumption of the spin-free inelastic deformation we arrrive at the following expression:

$$\dot{\mathbf{C}}_{p,i} = 2\mathbf{C}_{p,i}\mathbf{F}^{-1}\mathbf{D}_{p,i}\mathbf{F}, \quad i = 1, 2. \tag{4.138}$$

We need to get values for all terms in the constitutive equation (3.4.3). In order to evaluate $\boldsymbol{\tau}_v$ and $\boldsymbol{\tau}_e$ we need to update the clot time t_{clot} and the Finger tensor $\mathbf{B}$. Hence we solve in eat timestep the following equations:

$$\frac{\partial t_{clot}}{\partial t} = (1 - \phi)C \quad \text{in} \quad \Omega_F \cup \Omega \tag{4.139}$$

and

$$\frac{\partial \mathbf{F}}{\partial t} + \mathbf{u} \cdot \nabla \mathbf{F} = \nabla \mathbf{u} \mathbf{F} \quad \text{in} \quad \Omega_F \cup \Omega, \tag{4.140}$$

the Finger tensor is then given as $\mathbf{B} = \mathbf{F}\mathbf{F}^T$. We insert then the corresponding values into the equations (3.250) and (3.251).
We need to evaluate in (3.4.3) the terms $\boldsymbol{\tau}_{ve,i}, i = 1, 2$, as well. For that purpose we use the following iteration scheme, see [85] for more general settings:

1. Get values from the previous timestep $\mathbf{F}^k$, $\mathbf{C}^k_{p,i}$, $\boldsymbol{\tau}^k_{ve,i}$, x^k_i, $\quad i = 1, 2$, current value $\mathbf{F}^{k+1}$ is obtained from the solution of (4.140).

2. Compute intelastic deformation rates

$$\mathbf{D}^k_{p,i} = \frac{\boldsymbol{\tau}^k_{p,i}}{2\eta_i}, \quad i = 1, 2 \tag{4.141}$$

3. Compute time derivatives of inelastic right Cauchy-Green tensors

$$\dot{\mathbf{C}}^k_{p,i} = 2\mathbf{C}^k_{p,i}(\mathbf{F}^k)^{-1}\mathbf{D}^k_{p,i}\mathbf{F}^k, \quad i = 1, 2 \tag{4.142}$$

4. Compute $\mathbf{C}^{k+1}_{p,i}$, $\quad i = 1, 2$ using

$$\mathbf{C}^{k+1}_{p,i} = \mathbf{C}^k_{p,i} + \dot{\mathbf{C}}^k_{p,i}\Delta t \tag{4.143}$$

5. Compute $\mathbf{B}^{k+1}_{e,i}$, $\quad i = 1, 2$ using

$$\mathbf{B}^{k+1}_{e,i} = \mathbf{F}^{k+1}(\mathbf{C}^{k+1}_{p,i})^{-1}(\mathbf{F}^{k+1})^T \tag{4.144}$$

6. Compute x^{k+1}_i, $\quad i = 1, 2$ using

$$\dot{x_i} = \begin{cases} -c_x(x_i - x_{i,\infty}) & \text{if} \quad x_i > x_{i,\infty} \\ 0 & \text{if} \quad x_i \leq x_{i,\infty} \end{cases} \tag{4.145}$$

$$x_{i,\infty} = e^{-a}\sqrt{I_{B^{k+1}_{e,i}} - 3} \tag{4.146}$$

7. Compute $\boldsymbol{\tau}^{k+1}_{ve,i}$, $\quad i = 1, 2$ using

$$\boldsymbol{\tau}^{k+1}_{ve,i} = x^{k+1}_i G_i \left(\mathbf{B}^{k+1}_{e,i} - \mathbf{I}\right) \tag{4.147}$$

8. Save $\mathbf{C}^{k+1}_{p,i}$ and $\boldsymbol{\tau}^{k+1}_{ve,i}$ for $i = 1, 2$ to be used in the next time step

4.5.2 Discretization in space

Weak formulation of the equation for clot time

We multiply (4.139) by a test function $\psi_{t_{clot}}$ obtaining

$$\left(\frac{t^{k+1}_{clot} - t^k_{clot}}{\Delta t}, \psi_{t_{clot}}\right) = \left((1-\phi)C, \psi_{t_{clot}}\right). \tag{4.148}$$

Test and trial spaces for the scalar clot time were chosen followingly.

$$\Psi_{t_{clot}} = \Psi'_{t_{clot}} = H^1(\Omega \cup \Omega_F). \tag{4.149}$$

$$\Psi_{t_{clot}h} = \Psi'_{t_{clot}h} = \left\{t_{clot} \in H^1(\Omega \cup \Omega_F), t_{clot}|_K \in Q_1(K)\right\} \tag{4.150}$$

Weak formulation of the equations for deformation gradient

We multiply (4.140) by a test function $\boldsymbol{\Upsilon}$ getting

$$\left(\frac{\boldsymbol{F}^{k+1}-\boldsymbol{F}^{k}}{\Delta t}+\mathbf{u}\cdot\nabla\boldsymbol{F}^{k+1}-\nabla\mathbf{u}\boldsymbol{F}^{k+1},\boldsymbol{\Upsilon}\right)=\mathbf{0}. \tag{4.151}$$

Test and trial spaces were chosen followingly.

$$\boldsymbol{\Psi}_{\mathbf{F}}=\left\{\boldsymbol{F}\in\left[H^{1}(\Omega\cup\Omega_{F})\right]^{3\times3},\boldsymbol{F}|_{\Gamma_{in}}=\mathbf{F}_{d}\right\}. \tag{4.152}$$

$$\boldsymbol{\Psi}_{\mathbf{F}}^{'}=\left\{\boldsymbol{F}\in\left[H^{1}(\Omega\cup\Omega_{F})\right]^{3\times3},\boldsymbol{F}|_{\Gamma_{in}}=\mathbf{0}\right\}. \tag{4.153}$$

$$\boldsymbol{\Psi}_{\mathbf{F}h}=\left\{\boldsymbol{F}\in\left[H^{1}(\Omega\cup\Omega_{F})\right]^{3\times3},\boldsymbol{F}|_{K}\in\left[Q^{1}(K)\right]^{3\times3},\boldsymbol{F}|_{\Gamma_{in}}=\mathbf{F}_{d}\right\}. \tag{4.154}$$

$$\boldsymbol{\Psi}_{\mathbf{F}h}^{'}=\left\{\boldsymbol{F}\in\left[H^{1}(\Omega\cup\Omega_{F})\right]^{3\times3},\boldsymbol{F}|_{K}\in\left[Q^{1}(K)\right]^{3\times3},\boldsymbol{F}|_{\Gamma_{in}}=\mathbf{0}\right\}. \tag{4.155}$$

Weak formulation of the equations for left cauchy green tensors

We multiply (4.143) by a test function $\boldsymbol{\Gamma}$ obtaining

$$\left(\mathbf{C}_{p,i}^{k+1},\boldsymbol{\Gamma}\right)=\left(\mathbf{C}_{p,i}^{k}+\dot{\mathbf{C}}_{p,i}^{k}\Delta t,\boldsymbol{\Gamma}\right). \tag{4.156}$$

Test and trial spaces were chosen followingly.

$$\boldsymbol{\Psi}_{\mathbf{C}}=\boldsymbol{\Psi}_{\mathbf{C}}^{'}=\left[H^{1}(\Omega\cup\Omega_{F})\right]^{3\times3}. \tag{4.157}$$

$$\boldsymbol{\Psi}_{\mathbf{C}h}=\boldsymbol{\Psi}_{\mathbf{C}h}^{'}=\left\{\mathbf{C}\in\left[H^{1}(\Omega\cup\Omega_{F})\right]^{3\times3},\mathbf{C}|_{K}\in\left[Q_{1}(K)\right]^{3\times3}\right\} \tag{4.158}$$

Weak formulation of the equation for state parameters

We multiply (4.145) by a test function α getting

$$\left(\frac{x_{i}^{k+1}-x_{i}^{k}}{\Delta t},\Psi_{x_{i}}\right)=\begin{cases}\left(-c_{x}(x_{i}^{k}-x_{i,\infty}),\Psi_{x_{i}}\right) & \text{if} \quad x_{i}^{k}>x_{i,\infty}\\ 0 & \text{if} \quad x_{i}\leq x_{i,\infty}\end{cases} \tag{4.159}$$

Test and trial spaces for the state parameters $x_i, i=1,2$ are chosen as

$$\Psi_{x_{i}}=\Psi_{x_{i}}^{'}=H^{1}(\Omega\cup\Omega_{F}). \tag{4.160}$$

$$\Psi_{x_{i}h}=\Psi_{x_{i}h}^{'}=\left\{x_{i}\in H^{1}(\Omega\cup\Omega_{F}),t_{clot}|_{K}\in Q_{1}(K)\right\} \tag{4.161}$$

5. Computational simulations

5.1 Weller's model of clot growth

We performed computations of the model formulated in Section 3.4.1 on two geometries - the perfusion chamber and the cylinder geometry. Afterwards we present a numerical and scaling study of computations of modified Weller's model.

5.1.1 Perfusion chamber geometry

In our first simulation we have chosen one of the configurations used in [3], [74] and [6]. This configuration originates from the experimental setting of Affeld [86]. In this experiment platelet-rich plasma with pre-activated platelets flows from the inflow of perfusion chamber onto a glass plane. The glass plane is orthogonal to the flow direction at the inflow. The key result of the experiment is, that the deposition of platelets is minute at the point of stagnation point on the glass plane, whereas the site with greatest concentration of deposited platelets shows to be at the place of elevated shear rate. This location appeared to be downstream of the axis of symmetry of the perfusion chamber, i.e. considerably far away from the stagnation point. We solved our model on three differently refined meshes. The coarsest mesh has 26422 cells, the finer mesh has 208786 cells, whereas the finest mesh has 1497304 cells.
You can see the computational meshes of both refinements in Fig. 5.1. Initial values of phase field are rendered in 2D cut of the computational domain for the coarse mesh in Fig. 5.2a, for the finer mesh in Fig. 5.2b and for the finest mesth in Fig. 5.2c.
We have performed computations on all three meshes and we achieved corresponding results on all levels of refinement. In Fig. 5.2d and 5.3d it could be seen, that the clot has grown in the area of clot, which experiences the biggest shear stress. The same behaviour can be observed for the finer mesh, see the Fig. 5.2e and 5.3e. The clot behaves in the same way even for the finest mesh, see Fig. 5.2f and 5.3f. In the pictures of computations on the finer and finest mesh it is apparent, that the shape of emerging clot is smoother, which corresponds to the better resolution of phase field due smaller mesh cells. The location of the most intense growth of clot is also shifted, which could be attributed to the coarseness of the first mesh. We have mentioned, that the clot grows mostly in the area of high shear stress. This statement can be proven by a look in Fig. 5.3d for coarse mesh, in Fig. 5.3e for the finer mesh and in Fig. 5.3f for the finest mesh. In the pictures in Fig. 5.3 are rendered values of velocity field, both as colour on the slice and arrows on the slice. However the most interesting for us is the isosurface of phase field of zero value. We have colored the contour by values of the shear stress field. It is therefore apparent, that the clot grows preferably in the area of high shear stress. This is in accordance with the assumptions of high shear stress thrombosis outlined in Section 2.2.3 .
We have reached similar location of growth of the clot as in [6]. We must however admit, that our results are considerably not so fine as in [6]. Namely, the interface between blood and the clot is rather blurred. This originates from the very basic

assumption of the phase-field - the interface is represented by a no-sharp function. The another reason for the not so sharp location of the interface is the fact, that we computed the problem in fully three dimensional setting. In [3], [74] and [6] was used the cylindrical symmetry of the problem, i.e. Weller solved actually two dimensional problem, for which he could afford different levels of refinement. Saying this, we however aspire to be able to compute similar problems with similar granularity of computational mesh, as was presented [3], [74] and [6]. In the section on scaling of our fully three dimensional implementation of the model we will discuss the possibility of scaling up of our code to rather larger number of cells.

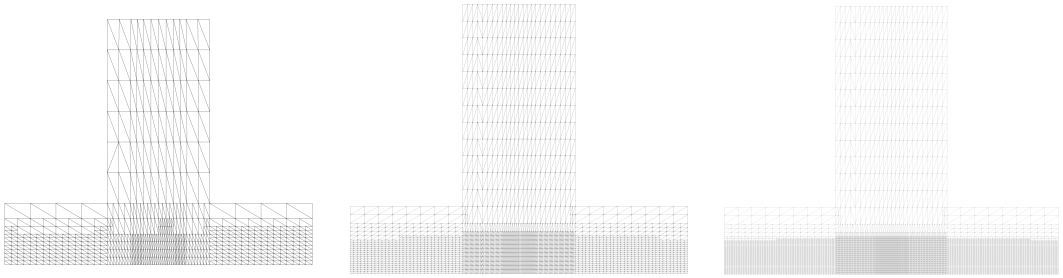

(a) 2D cut of the computational mesh - coarse mesh

(b) 2D cut of the computational mesh - fine mesh

(c) 2D cut of the computational mesh - finest mesh

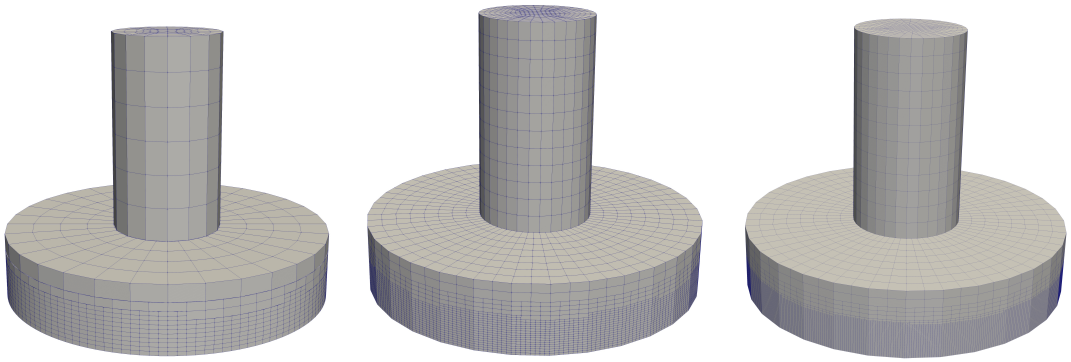

(d) 3D view - coarse grid

(e) 3D view - fine grid

(f) 3D view - finest grid

Figure 5.1: Overview of computational meshes - perfusion chamber

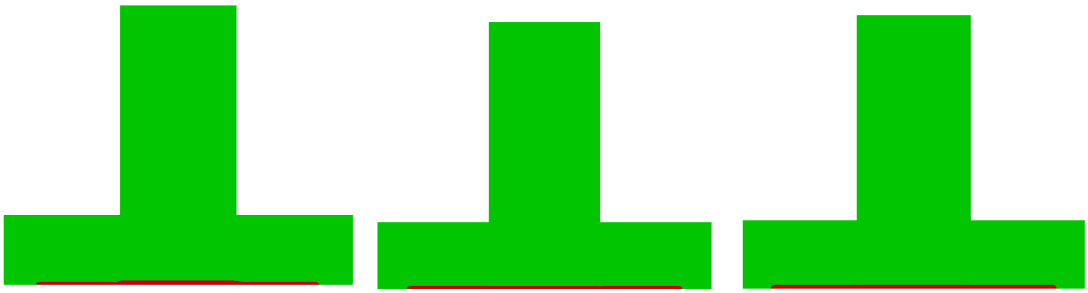

(a) Initial phase field setting - coarse mesh (b) Initial phase field setting - finer mesh (c) Initial phase field setting - finest mesh

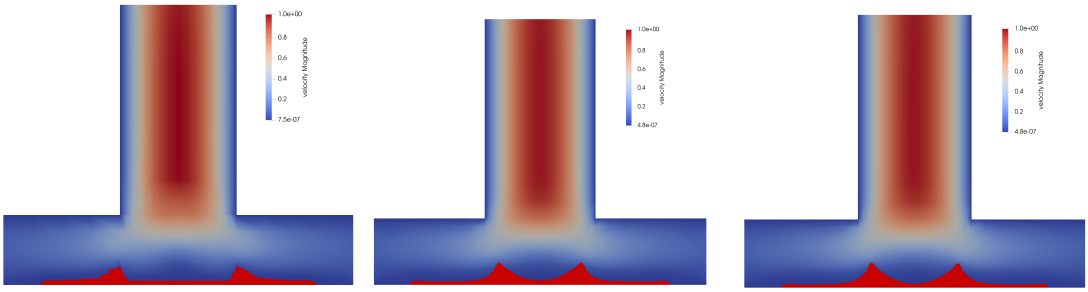

(d) Final state of the phase field - coarse grid (e) Final state of the phase field - finer grid (f) Final state of the phase field - finest grid

Figure 5.2: Initial and final state of phase field - perfusion chamber

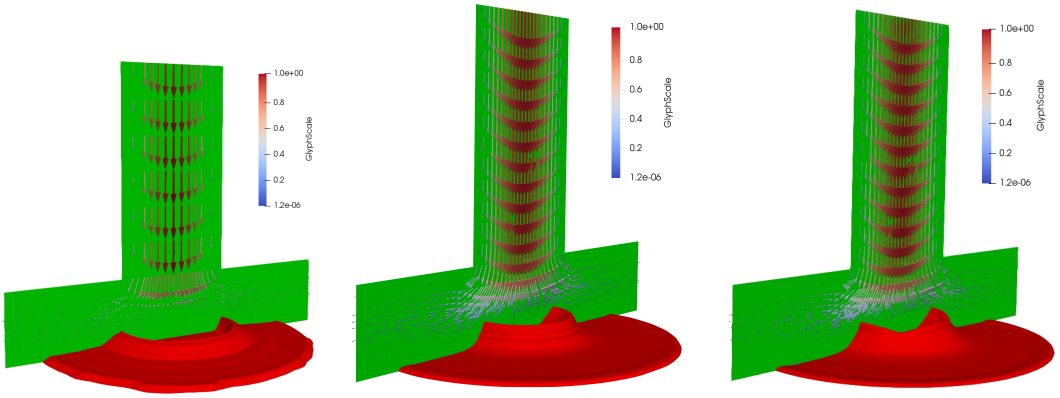

(a) Velocity glyphs and zero phase field isosurface - coarse grid

(b) Velocity glyphs and zero phase field isosurface - finer grid

(c) Velocity glyphs and zero phase field isosurface - finest grid

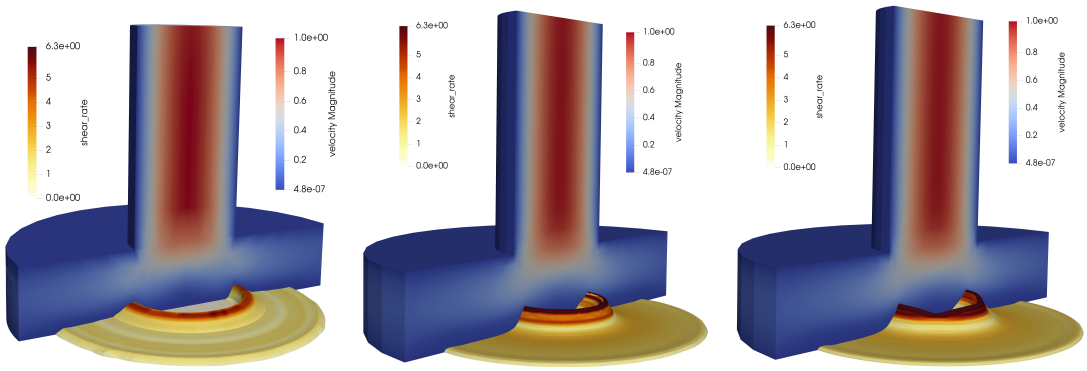

(d) Velocity with shear rate on zero phase field isosurface - coarse grid

(e) Velocity with shear rate on zero phase field isosurface - finer grid

(f) Velocity with shear rate on zero phase field isosurface - finest grid

Figure 5.3: 3D view of the velocity field and shear rate on zero phase field isosurface - perfusion chamber

5.1.2 Cylinder geometry

In our second simulation we solved our system in the cylinder geometry, where the reactive zone is located in the middle symmetrically at the walls . The use case for this geometry could be stented artery as the artificial surface of the stent is reactive.
We solved our model on two differently refined meshed. The coarser one has 20480 cells, whereas the finer mesh has 163840 cells. You can see the computational mesh for the coarse grid and the fine grid in Fig. 5.4.
Initial values of phase field are shown in Fig. 5.5a for the coarse mesh and in Fig. 5.5b for the fine mesh.
We have performed computations on both meshes and we achieved corresponding results on both levels of refinement. In figures 5.5c, 5.6a, 5.6c and 5.6e it could be seen, that the clot has grown in the area of clot, which experiences the biggest shear stress. The same behaviour can be observed for the fine mesh, see figures 5.5d, 5.6b, 5.6d. and 5.6f. In the pictures of computations on the finer mesh it is apparent, that the shape of emerging clot is smoother, which corresponds to the better resolution of phase field due smaller mesh cells.
We have mentioned, that the clot grows mostly in the area of high shear stress. This statement can be proven by a look in Fig. 5.6c. for the coarse mesh and Fig. 5.6d for the finer mesh. In the figures 5.6e and 5.6f are rendered values of velocity field as arrows flowing through the artery narrowed by the clot. However the most interesting for us is the 3D contour of phase field of zero value, see figures 5.6c and 5.6d. We have colored the contour by values of the shear stress field. It is therefore apparent, that the clot grows preferably in the area of high shear stress. This is in accordance with the assumptions of high shear stress thrombosis mentioned in Section 2.2.3.
We would like also comment on the dependence of thrombus growth not only on shear stress, but also on supply of blood platelets. Blood platelets, thrombocytes, are namely an integral part of the high shear rate thrombus.
We take into account the dependence of growth rate on shear rate and thrombocytes inflow by the Robin boundary equation for the platelet field (3.106). The boundary condition depends linearly on the concentration of platelets and the adhesion rate, which grows linearly with shear stress. Therefore we should expect, that the growth of the thrombus starts only after the arrival of thrombocytes on the location of thrombus interface. We can witness this development in the series of steps 1-6 in Fig. 5.7.
We would like to add a note about the results of simulations in the Fig. 5.7. It could seem, that the development of the platelet field does not couple correctly with the development of the phase field (green colour in Fig. 5.7), i.e. the simulation results in nonzero values for platelet field in the area of the developing thrombus. We must however remind the reader, that we have used harmonical extension of the platelet field in the area of thrombus, see the equation (3.227).
Therefore it could be said, that in the area of the thrombus the values of the platelet field are irrelevant to us, as its values are there only supplied for the better solvability of our problem. Hence we do not assign any physical interpretation to the platelet field in the area of the developing thrombus.

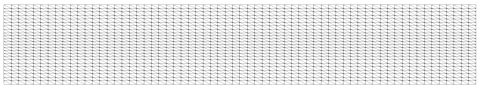

(a) 2D cut of the computational mesh - coarse mesh

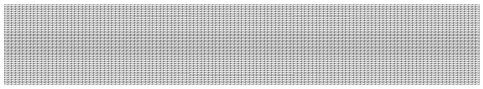

(b) 2D cut of the computational mesh - fine mesh

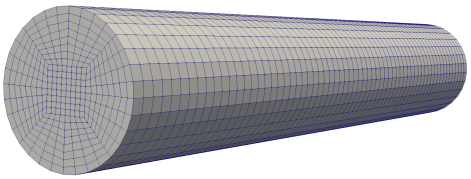

(c) 3D view - coarse grid

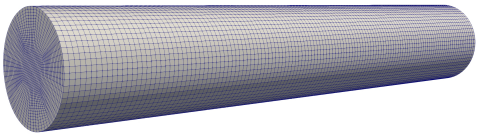

(d) 3D view - fine grid

Figure 5.4: Overview of computational meshes - cylinder

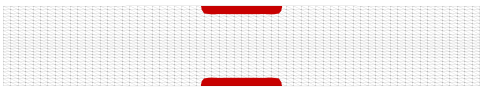

(a) Initial phase field setting - coarse mesh

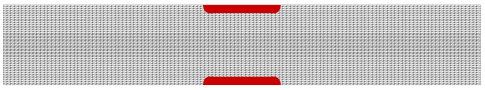

(b) Initial phase field setting - fine mesh

(c) Final state of the phase field - coarse grid

(d) Final state of the phase field - fine grid

Figure 5.5: Initial and final state of the clot - cylinder

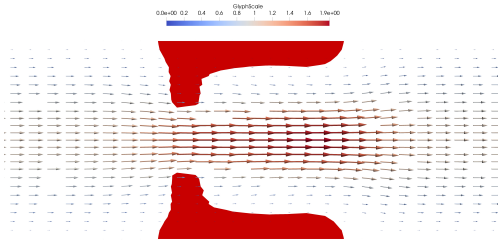

(a) Final state of clot with velocity glyphs - coarse grid

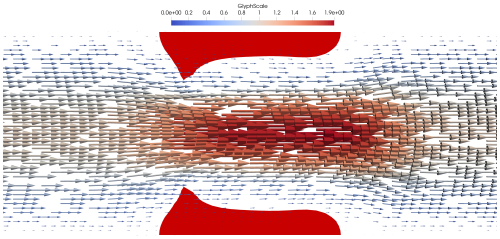

(b) Final state of clot with velocity glyphs - fine grid

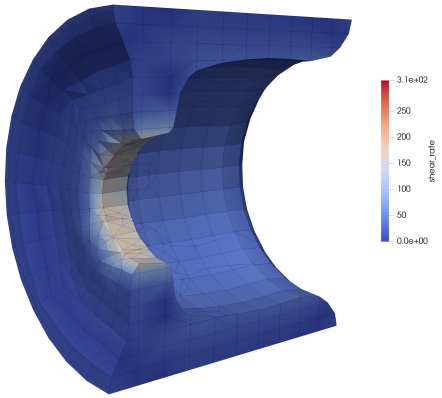

(c) 3D view of emerging thrombus colored by shear rate - coarse grid

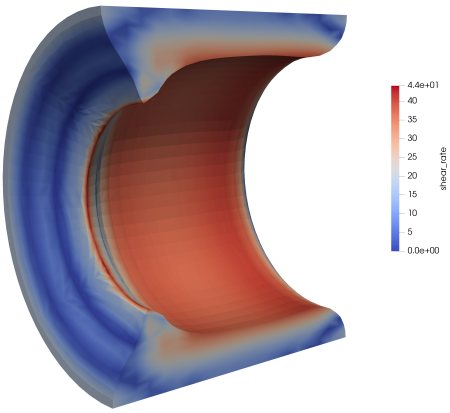

(d) 3D view of emerging thrombus colored by shear rate - fine grid

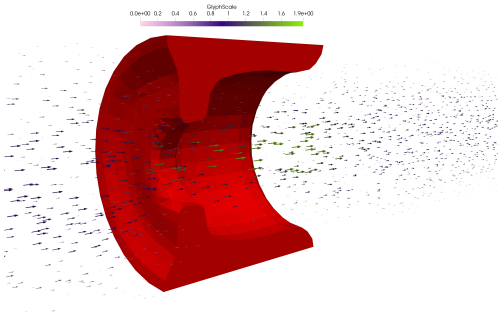

(e) 3D view of emerging thrombus with velocity glyphs - coarse grid

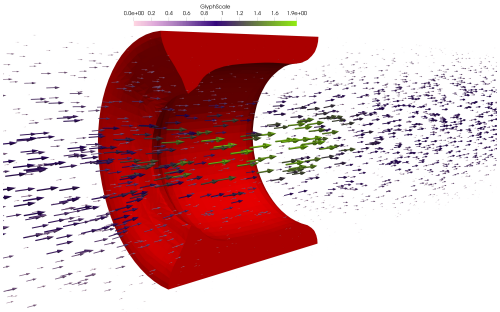

(f) 3D view of emerging thrombus with velocity glyphs - fine grid

Figure 5.6: 2D and 3D views of the clot, the velocity field, shear rate field- cylinder geometry

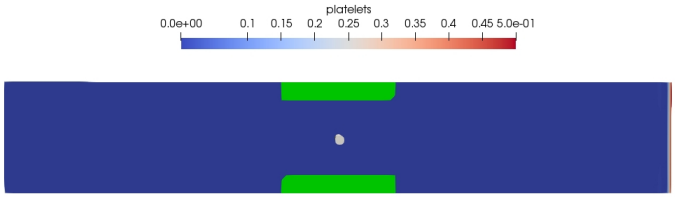

(a) Step 1

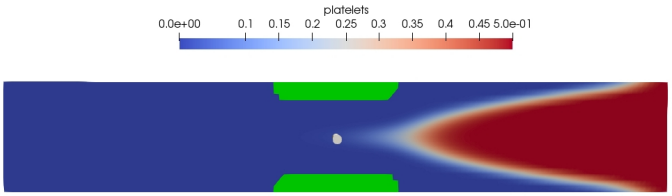

(b) Step 2

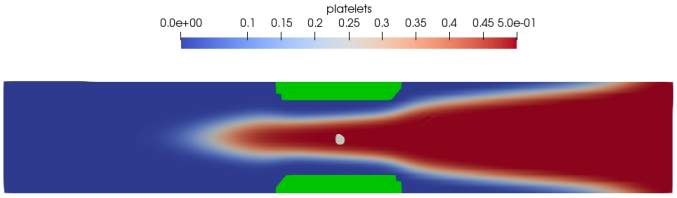

(c) Step 3

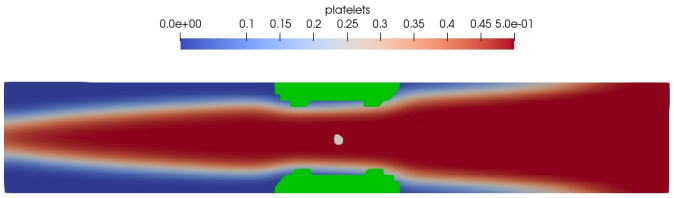

(d) Step 4

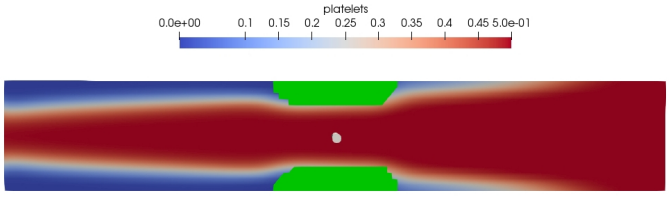

(e) Step 5

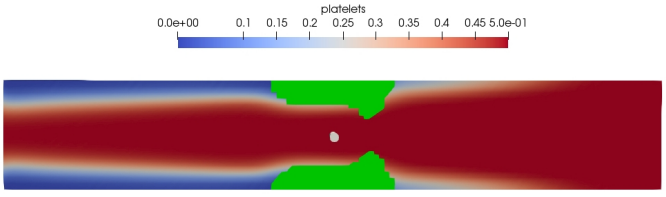

(f) Step 6

Figure 5.7: Development of the phase field and platelet s - cylinder

5.2 Weller's model - scaling, recoupling properties

In the following two sections we want to show numerical and scaling properties of our implementation of the model.

5.2.1 Recoupling of the decoupled equations

We have mentioned in Section 4.1.3, that recoupling iterations are needed for achievement of proper results. The norm of difference of subsequent solutions played the role of the terminating criterion of recoupling subiterations.
We could naturally expect that if we decrease the initial timestep, than the norm of difference of solutions from different recoupling iterations would decrease faster. We performed a simple numerical experiment, which confirms this expectation. We chose the cylindrical geometry with 5120 cells as our computational domain. We performed computations using our adaptive timestepping method until we arrived at fixed time. The number of recoupling iterations in each timestep was now fixed. We denote the solution obtained using n iterations as $\mathbf{u}_n$ for velocity and w_n for platelets. We persisted the solution for $n = 4$ to hard disk in order to be able to compare it with solutions for $n = 1, 2, 3$. The results of the computations are given in the tables 5.1, 5.2, 5.3 and 5.4. From the tables it can be seen, that the convergence to the finest solution is quicker for the smaller initial timestep 0.05 and that the convergence slows down for the larger timesteps 0.1 and 0.2 (see table 5.2 and 5.3). In the case of convergence in Table 5.4 we can see, that it is by several orders smaller than in Table 5.1 for the platelet field. The differences in the velocity field in Table 5.4 decrease at the same pace as in 5.1, but the order of magnitude of the differences is approximately two orders lower. It is however questionable, whether the solution with $n = 4$ for timestep 0.5, see Table 5.4, is a good candidate for comparing convergence of the solution $n = 1, 2, 3$, because it appears, that the convergence in the platelet field w is very slow. Hence it we could doubt about finished convergence for solution w_4.

Table 5.1: $\|\mathbf{u}_4 - \mathbf{u}_n\|, \|w_4 - w_n\|$, $\Delta t = 0.05$

NO. of couplings-n	velocity-$\mathbf{u}$	platelets-w
1	$1.08 \cdot 10^{-4}$	$3.59 \cdot 10^{-8}$
2	$3.59 \cdot 10^{-8}$	$2.11 \cdot 10^{-10}$
3	$4.85 \cdot 10^{-13}$	$1.06 \cdot 10^{-10}$

Table 5.2: $\|\mathbf{u}_4 - \mathbf{u}_n\|, \|w_4 - w_n\|$, $\Delta t = 0.1$

NO. of couplings-n	velocity-$\mathbf{u}$	platelets-w
1	$2.23 \cdot 10^{-2}$	$1.12 \cdot 10^{-4}$
2	$1.72 \cdot 10^{-8}$	$1.72 \cdot 10^{-8}$
3	$1.28 \cdot 10^{-13}$	$4.15 \cdot 10^{-13}$

Table 5.3: $\|\mathbf{u}_4 - \mathbf{u}_n\|, \|w_4 - w_n\|$, $\Delta t = 0.2$

NO. of couplings-n	velocity-$\mathbf{u}$	platelets-w
1	0.24	$9.89 \cdot 10^{-2}$
2	$2.08 \cdot 10^{-8}$	$2.04 \cdot 10^{-10}$
3	$2.30 \cdot 10^{-13}$	$6.72 \cdot 10^{-14}$

Table 5.4: $\|\mathbf{u}_4 - \mathbf{u}_n\|, \|w_4 - w_n\|$, $\Delta t = 0.5$

NO. of couplings-n	velocity-$\mathbf{u}$	platelets-w
1	0.1	0.21
2	$1.03 \cdot 10^{-6}$	0.11
3	$5.86 \cdot 10^{-11}$	$9.87 \cdot 10^{-2}$

5.2.2 Scaling of linear solvers

We have experimented with different combinations of linear solvers and preconditioners. The most demanding processing of linear systems were performed for the solution of the tentative velocity step (4.15) and for the solution of the projection step (4.2). The solution of the projection step results into linear system with symmetric positive definitive matrix. We chose conjugate gradient solver with either ILU or algebraic multigrid as preconditioner. We tried to increase the number of cores, which were used for the solution of the system originating from cylindrical geometry with 5120 cells.

Table 5.5: Solution times in seconds for CG with different preconditioners for the projection step (4.2)

Preconditioner	24 Cores	48 Cores	96 Cores	192 Cores
ILU	0.229	0.411	0.904	1.49
AMG	0.581	0.994	1.53	2.98

We can observe in Table 5.5, that the duration of solution of the projection step increases as we add more cores for solution of the system. This could be attributed to the fact, that the system is quite small and communication prevails with increasing of number of cores.
Discretization of the tentative velocity step does not end with symmetric matrix. Therefore we have to use a more robust solver for the solution of the linear system. We chose GMRES solver equipped with ILU, SOR or algebraic multigrid as preconditioners.

For almost all preconditioners we can observe in Table 5.6 decrease of time of solution with increasing number of cores. The linear system is namely larger than pressure system, hence the scaling up is working. We can however see that for the algebraic multigrid there is a plateaux in the solution time for 96 and 192 cores.

Table 5.6: Solution times in seconds for GMRES with different preconditioners for the tentative velocity step (4.15)

Preconditioner	24 Cores	48 Cores	96 Cores	192 Cores
SOR	67.4	45	24.1	12
ILU	55.7	32.2	17.7	9.7
AMG	81.7	61	43.7	43.8

5.2.3 Strong scaling of our implementation

We have performed series of computations on the cylinder or on the chamber mesh for two different levels of refinement. We were computing until we reached a fixed time limit. We were increasing the number of cores by factor 2 from 24 cores to 768 cores.
We have achieved considerable level of scaling of our computations, however we reached a plateaux and the duration of computations of the problem started to grow (see Table 5.7 and the chart in Figure 5.8) . This could be attributed to the fact, that the communication overhead might start to dominate. That was the case of both refinement levels of chamber grid and of the cylinder geometry.

Table 5.7: Strong scaling - solution times in seconds

	Chamber geometry		Chamber geometry	
Number of Cores	1504 cells	75954 cells	5120 cells	40960 cells
24	3,430	71,000	1,560	
48	1,670	31,700	822	
96	1,020	16,400	456	10,700
192	742	8,820	304	4,710
384	506	4,070	156	459
768	424	7,710	258	2,460

5.2.4 Weak scaling of our implementation

In the case of weak scaling performance tests we started with low number of cells solved on not many cores. We increased then the number of cells and cores by factor 2 in each step in order to allocate to a core fixed amount of work. In Table 5.8 and in the chart in the Figure 5.9 we can see, that with increasing number of cells and cores we do not witness constant level of solution time of our problem. Well scaling code would exhibit here constant function like behaviour. As the solution time almost monotonously growing with number of cells/cores and the jumps to one order higher value for the largest number of cells/processors, we suppose, that the communication of our distributed code is becoming dominant. To improve this behaviour it would be necessary to refactor our current codebase.

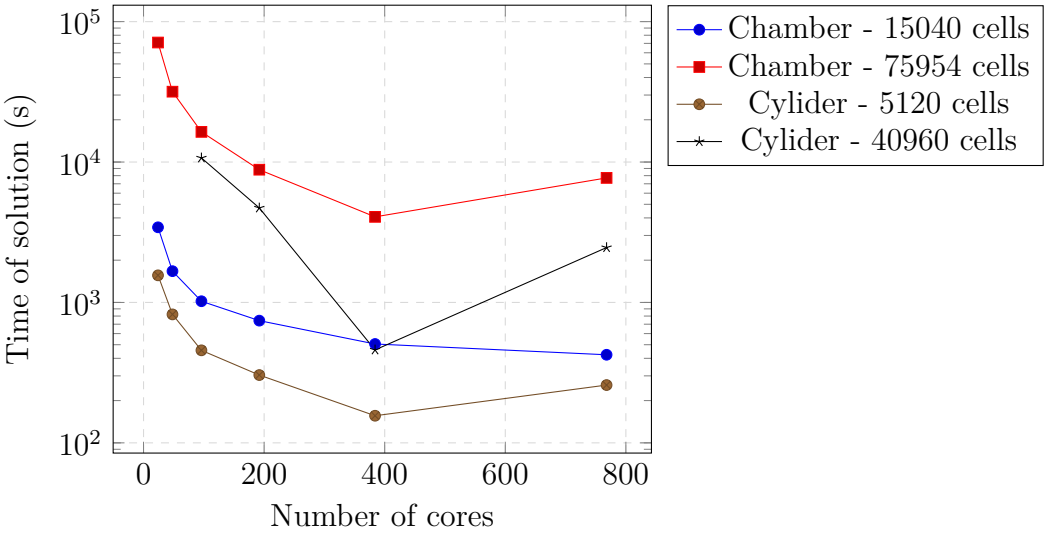

Figure 5.8: Strong scaling

Table 5.8: Weak scaling - solution times in seconds

NO. of cells	NO. of cores	time [s]
640	24	73.3
1,280	48	104
2,560	96	165
5,120	192	204
10,240	384	158
20,480	768	1,310

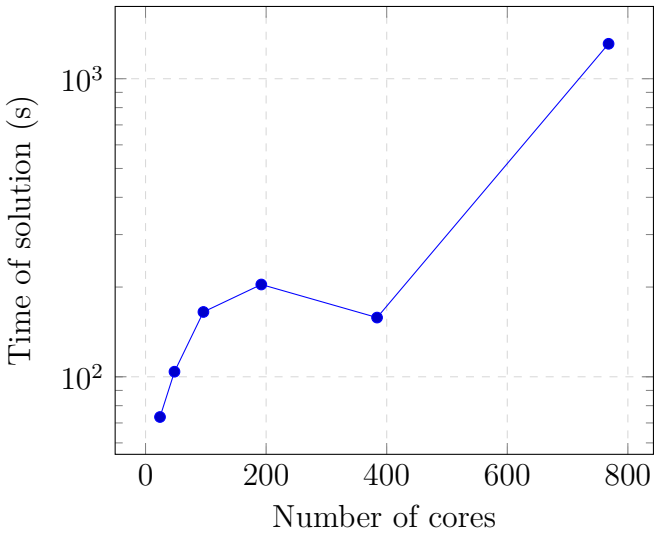

Figure 5.9: Weak scaling

5.3 Modified Storti's model

In the following we show results of computations based on the model from Section 3.4.2. We perform our simulation in the configuration similar to the original configuration of [1]. We have however implemented the model in fully three dimensional setting, therefore the simulation settings can not be fully imitated.
As our computational domain we have chosen the cylinder geometry with 20480 cells, whereas the finer mesh has 163840 cells, see figures 5.10a, 5.10c for the coarse mesh and 5.10b, 5.10d for the fine mesh. For numerical issues with start-up of our splitting method we were increasing the boundary condition on velocity gradually. We have let the simulation start and only after a certain time we set off the process of platelet plug formation. Namely we have let the velocity field develop. The plug is formed on the reactive surface, which is represented as the isosurface of zero phase field value. At the beginning of our simulations the isosurface looks like in figures 5.11a, 5.11c for the coarse mesh and 5.11b, 5.11d for the fine mesh.
After setup of phase field, which could be seen in figures 5.11a, 5.10c and 5.11b, 5.10d, the phase field has direct influence on the flow field. Namely, as it develops, it narrows down the lumen of the vessel. This leads to increase of velocity in the narrowed part of vessel in comparison with the rest of the vessel, where no stenosis is present. You can see the stenosed vessel in figures 5.12a, 5.12c, 5.12e for the coarse grid and the vessel stenosis for fine grid in figures 5.12b, 5.12d, 5.12f. Due to the fact, that the grid is still quite coarse, numerical artefacts can be seen in figures 5.12a, 5.12c in the velocity field. The situation improves once we use the finer grid, see figures 5.12b, 5.12d.
In the figures it can be seen, that the clot starts to develop after the activated platelets arrive or after they were activated from resting platelets at the site of injury, i.e. in the vicinity of zero phase field isosurface.
More plastic view of the flow around the obstacle - clot can be obtained from figures 5.13a, 5.13c and 5.13b, 5.13d. In these pictures it can be seen, that some kind of recirculation zone could be present in the vicinity upstream of the clot.
We have used however uniform refinement of the grid, so we were not able to render the velocity field (here glyphs) in more detail. We have experimented with local refinement in these areas using the tools provided by the library deal.ii [4], see Appendix A for details. We tried different local refinements, however as we use iterative solvers we were not able to solve the corresponding linear system.

(a) 2D cut of the computational mesh - coarse mesh

(b) 2D cut of the computational mesh - fine mesh

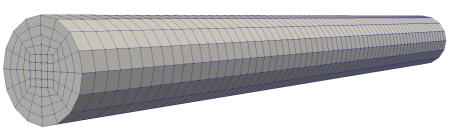

(c) 3D view - coarse grid

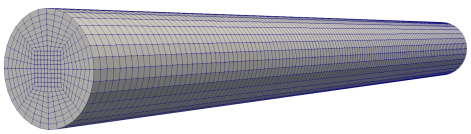

(d) 3D view - fine grid

Figure 5.10: Overview of computational meshes

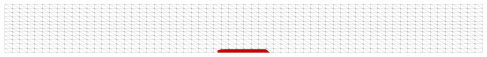

(a) 2D cut of the initial thrombus - coarse mesh

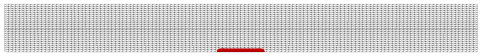

(b) 2D cut of the initial thrombus - fine mesh

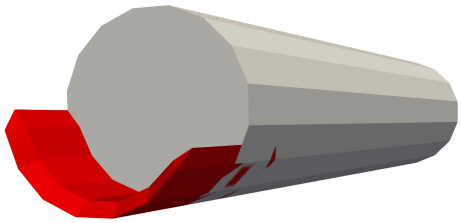

(c) 3D view of initial clot - coarse mesh

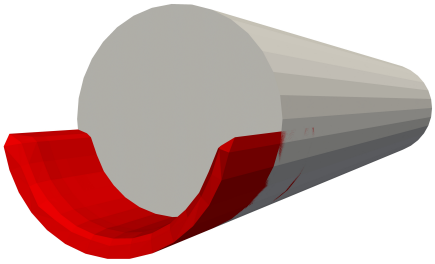

(d) 3D view of initial clot - fine mesh

Figure 5.11: Initial state of clot for both meshes

Table 5.9: Initial values of all species and critical values of the activating species

Species name	concentration	Initial conc.	units	critical values
Resting platelets	c_{up}	0.7×10^8	$PLTml^{-1}$	
Activated platelets	c_{ap}	$0.05c_{up}$	$PLTml^{-1}$	
ADP	c_{adp}	0.0	μM	2.0
Thromboxane	c_{tx}	0.0	μM	0.60
Prothrombin	c_{pt}	1.1	μM	
Thrombin	c_{th}	0.0	μM	9.11×10^{-4}
Antithrombin	c_{at}	2.844	μM	

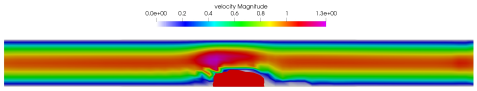

(a) 2D cut of the final thrombus with velocity field - coarse mesh

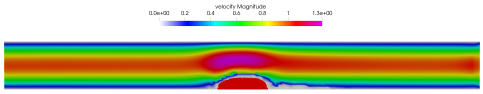

(b) 2D cut of the final thrombus with velocity field - fine mesh

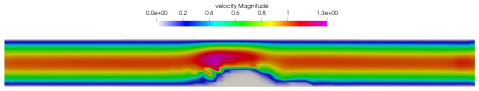

(c) 2D view of final velocity field - coarse mesh

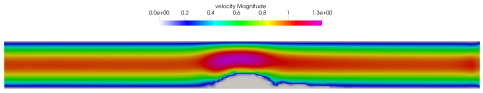

(d) 2D view of final velocity field - fine mesh

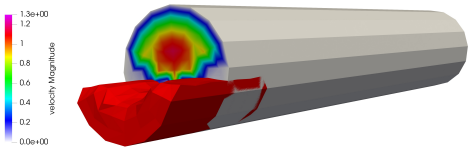

(e) 3D view of final clot and velocity field on clip - coarse mesh

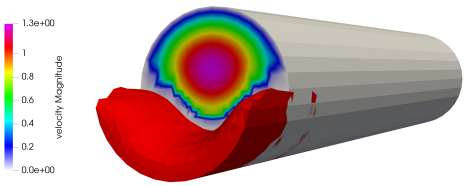

(f) 3D view of final clot and velocity field on clip - fine mesh

Figure 5.12: 2D and 3D views of clot with velocity field

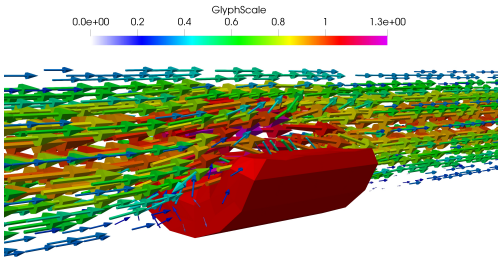

(a) 3D view of velocity glyphs and final clot - coarse mesh

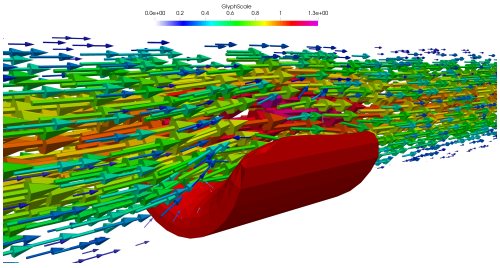

(b) 3D view of velocity glyphs and final clot - fine mesh

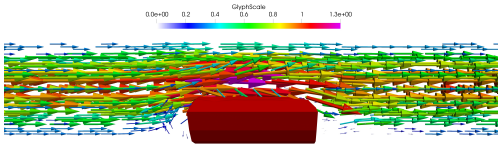

(c) 3D view from side of velocity glyphs and final clot - coarse mesh

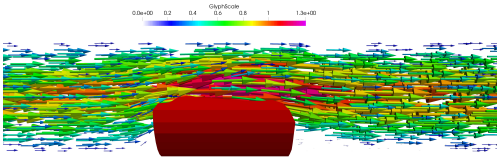

(d) 3D view from side of velocity glyphs and final clot - fine grid

Figure 5.13: Final clot and glyphs of velocity field

5.4 Modified Storti's model and Kempen's model for blood clot

In the following we show results of computations based on the model from Section 3.4.3. In the following we try to compare the results from [79] and [1] with the results from our more complete model. We cannot however fully compare one-to-one the results.
Firstly results of Storti were computed using the neo-Hookean elastic constitutive equations for the platelet clot. However we employ a viscoelastic model for the platelet clot, which develops into the blood clot.
Secondly we perform computations in fully three dimensional settings, in contrast with [79] and [1], where only two dimensional computations were performed.
Thirdly due to the computational expense we run simulations on quite coarse grid, in comparison with two dimensional meshes of [79] and [1].

5.4.1 Influence of blood flow on the shape of clot

We performed two sets of computations for different values of velocity Dirichlet boundary conditions on inflow. In contrast to Storti we can not experiment with tweaking of only one parameter in the constitutive equation (in Storti it was the shear modulus G in (3.158)). Namely the model of Kempen [2] contains seven fit parameters, which we take over from the article.
We are again turning on the velocity field gradually. The plug is formed on the reactive surface, which is represented as the isosurface of zero phase field value. The initial reactive surface is present only after the velocity field establishes.
In the first case we imposed low velocity on the inflow. After certain time the blood clot develops and the narrowed area of blood vessel causes local increase of velocity values. The 2D snapshot of the phase field is in Figure 5.14a, in Figure 5.14a we can see the influence of the clot on the blood flow. The same visualization is shown for the finer grid 5.15a.
3D views of developing thrombus and the velocity field are in figures 5.14b and 5.14c. We can see, that the blood flows around the obstacle, around the clot. Similar behaviour can be observed for the fine grid in figures 5.15b and 5.15c.
In the second case we imposed large velocity on the inflow. After certain time the blood clot develops and the narrowed area of blood vessel causes local increase of velocity values. The 2D snapshot of the phase field is in Figure 5.16a, in Figure 5.16a we can see the influence of the clot on the blood flow. The blood is flowing around the clot even in the case of fine grid, see Fig. 5.17a.
3D views of developing thrombus and the velocity field are in figures 5.16b and 5.16c. We can see, that the blood flows around the obstacle, around the clot.
If we compare the first case with the second case we can see, that the magnitute of inflow velocity has some impact on the shape of the developing clot, this is well to be seen in Figure 5.14a and Figure 5.16a. Change of shape can also be observed on 3D view in Figure 5.14c and Figure 5.16c. On the finer grid the dependence of shape can be mainly observed on 2D views in figures 5.15a and 5.17a.

In the work [79],[8] and [1] clot is thicker at lower velocity at the proximal part, whereas at higher velocity it is thicker at the distal part. Similar behaviour can

be seen in Figure 5.14a and Figure 5.16a. The similar observation can be made from the figures 5.14c and 5.16c. In finer grid this behaviour is not so apparent, see figures 5.15a, 5.15b, 5.15c for the low velocity and figures 5.17a, 5.17b, 5.17c for the high velocity.

We will now compare the shapes of the emerging thrombus in this section with the shapes of clots obtained in Section 5.3. It is visible in figures 5.12b and 5.12d, that the clot is rather smoothed. This phenomenon is to be attributed to the very assumption of the modified Storti model - the clot is taken as a Newtonian fluid with high viscosity. If we now look in the figures referenced in this section, e.g. figures 5.15a, 5.15b, 5.15c for the low velocity and figures 5.17a, 5.17b, 5.17c for the high velocity, we can see, that the viscoelastic material of the clot is able to withstand the drag imposed on the surface of the clot from the flowing blood.

5.4.2 Modified activation criterion for platelets

In Section 3.3.3 we adjusted the activation criterion of platelets to depend not only on concentration of chemical species, but also on the value of the shear stress. We can see in the Figure 5.18a that although already at the beginning time of clotting the shear stress at the surface of the clot is elevated, clotting does not start. This can be visible even at the more advanced time in the Figure 5.18b. This is caused by the fact, that it lasts for certain time until blood platelets, either activated or unactivated, arrive at the place of reactive surface.
Once they arrive the clot starts to develop, see Figure 5.18c. From figures 5.18c, 5.18d and 5.18e it is apparent, that there the distal parts of clot develop more, the clot is thicker there, than the proximal parts of clot. The distal parts experience larger shear stresses, therefore the activation function achieves there larger values, which leads to the speedup of coagulation. On the other hand the proximal part of the clot experiences high shear stresses as well, but the clot is relatively thin there. Part of the platelets which are activated there are carried away to the other areas of surface of the clot, where they can bind in elevated measure.

We can see in Figure 5.19a that although already at the beginning time of clotting the shear stress at the surface of the clot is elevated, clotting does not start. This can be visible even at the more advanced time in Figure 5.19b. This is caused by the fact, that it lasts for certain time until blood platelets, either activated or unactivated, arrive at the place of reactive surface.
Once they arrive the clot starts to develop, see figures 5.19c, 5.19d and 5.19e. In figures 5.19d and 5.19e it is apparent, that there the proximal parts of clot develop more, the clot is thicker there, than the distal parts of clot. The parts experience larger shear stresses, therefore the activation function achieves there larger values, which leads to the speedup of coagulation. On the other hand the distal part of the clot experiences high shear stresses as well, but the clot is relatively thin there. We could not however use one scale, as in the previous case, as the values of shear stress at the beginning of simulation are minute. In Figures 5.20a, 5.20b, 5.20c, 5.20d and 5.20e is rendered the development of the clot with values of shear stress on its surface for the higher velocity.

5.4.3 Comparison with an in-vivo experiment

In [5] an in-vivo experiment was performed on a living mouse. A blood vessel was injured by a laser. Followingly the concentration of platelets, fibrin and tissue factor was tracked using confocal fluorescence imaging.
Although we do not work with the concentration of platelets, fibrin and tissue factor in our model of the clot, we can get an idea, what the shape of the clot should be. We took three pictures from the article [5] so, that our reader can compare the results from the in-vivo experiment and the results from the simulations of our mathematical model.
During the experiments in [5] the target vessels were of size 20-60 μm. We are mostly interested in the bright-field microscopy results. Characteristic size of our computations, i.e. the width of the channel is 0.003cm, which equals to 0.03mm or 30 μm. Therefore we can compare at least roughly results of the in-vivo experiment with outputs of our computational simulations.
In the original work [5] several experiments were done with the same settings. But should we compare the resulting clots, there are some discrepancies originating from some hidden experimental parameters. The parameters are not under control of the experimenter.
We picked two results of in-vivo experiments, focusing on the bright-field microscopy. We compare the results of the experiment with the two settings of our simulations, namely with the slow flow and with fast flow of blood.
We can discern some similarity in the shape of clots, see figures in 5.21 for the fast flow and figures in 5.22 for the slow flow, for the case of coarse grid
In the set of figures in 5.21 we are trying to identify a clot from the in-vivo experiment from the subfigure 5.21a with the results of simulations with faster inlet velocity of blood, see figures 5.21b, 5.21c.
In the set of figures in 5.22 we are trying to identify a clot from the in-vivo experiment from the subfigure 5.22a with computational results originating from imposition of slower inlet velocity, see figures 5.22b, 5.22c.
We can find that the similarity even for the case of slow and fast flow of blood in the fine grid, see figures in 5.24 for the slow flow and figures in 5.23 for the fast flow.

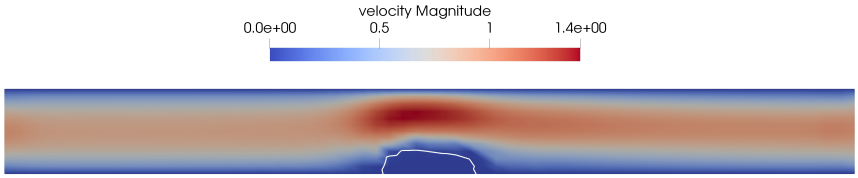

(a) velocity - large scale

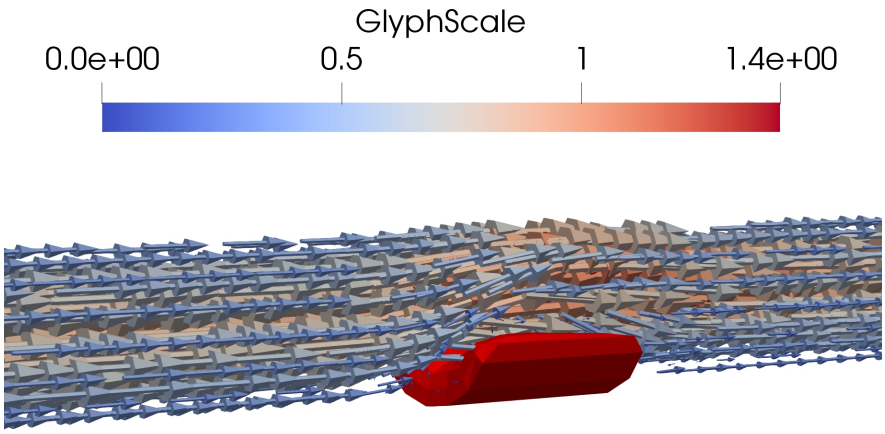

(b) velocity field as arrows

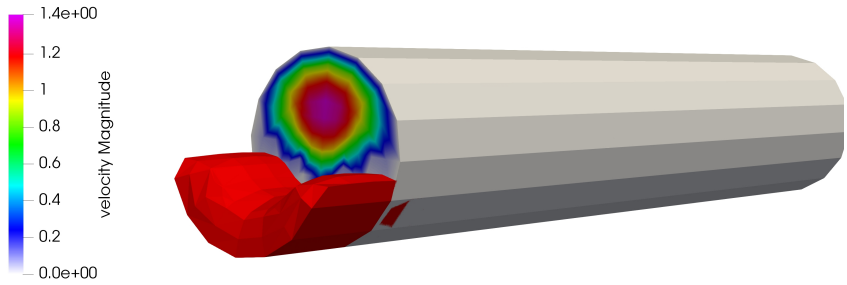

(c) velocity field on 2D cut

Figure 5.14: Developed clot and velocity field at low blood inflow velocity - coarse grid

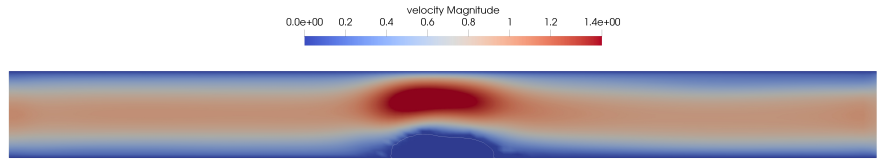

(a) velocity - large scale

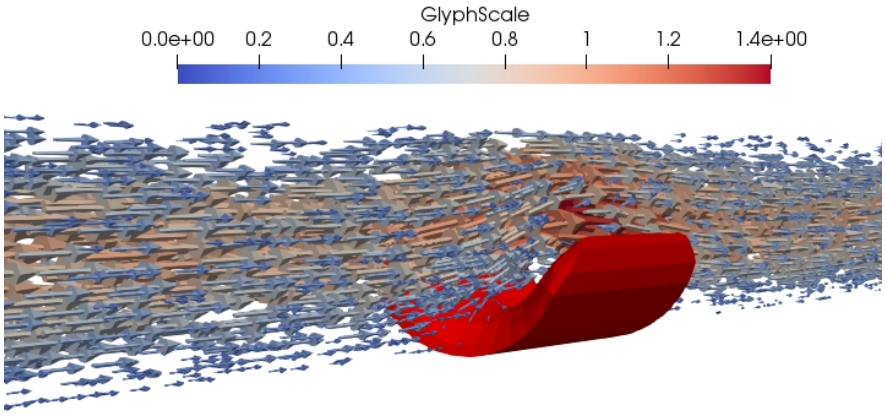

(b) velocity field as arrows

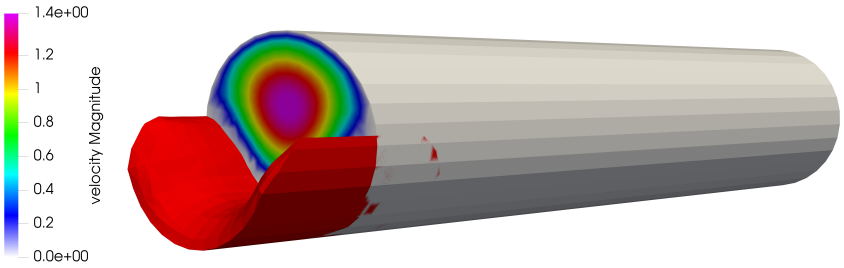

(c) velocity field on 2D cut

Figure 5.15: Developed clot and velocity field at low blood inflow velocity - fine grid

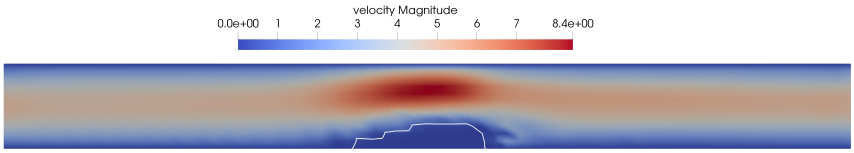

(a) velocity field

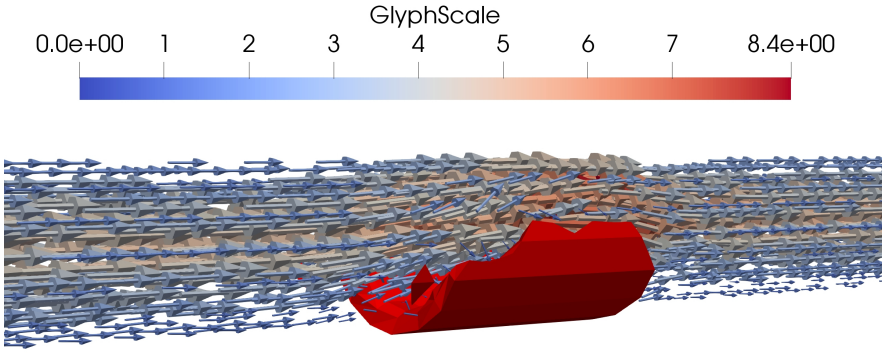

(b) velocity field as arrows velocity

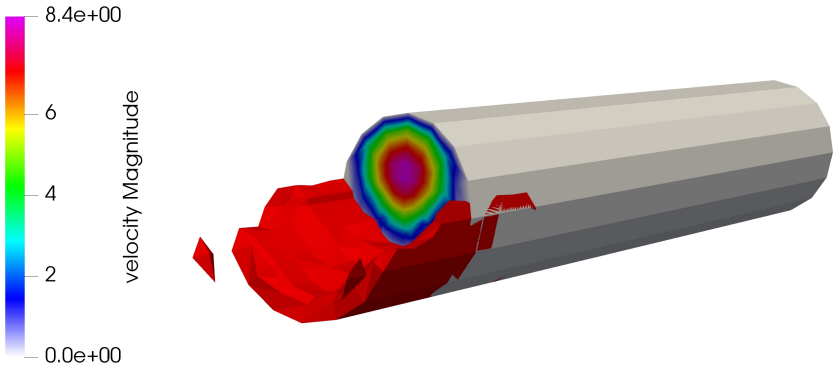

(c) velocity field on 2D cut

Figure 5.16: Developed clot and velocity field at large blood inflow velocity - coarse grid

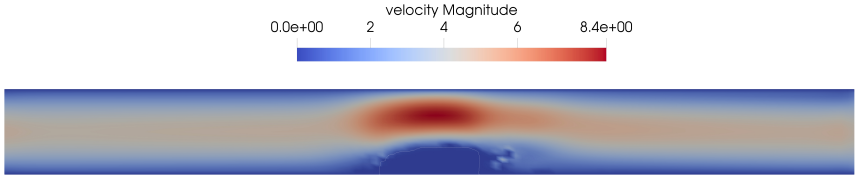

(a) velocity field

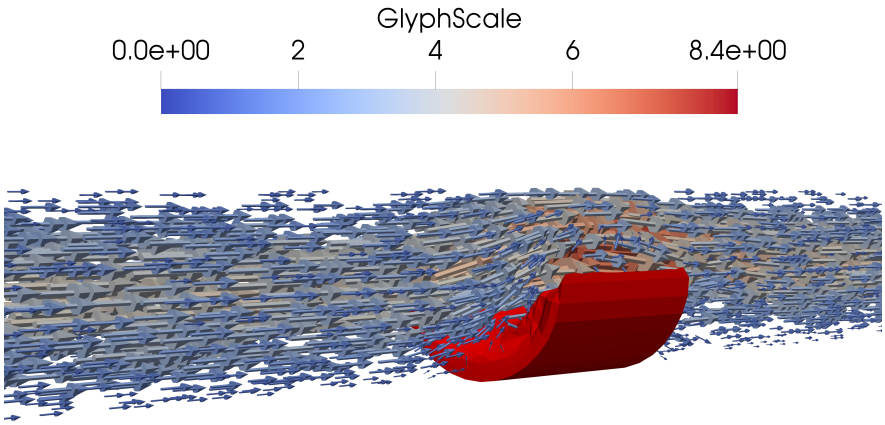

(b) velocity field as arrows velocity

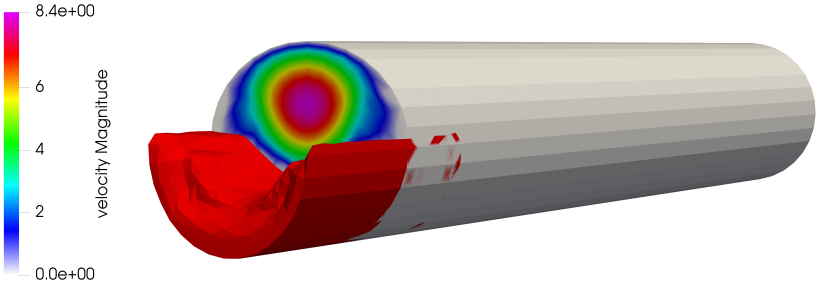

(c) velocity field on 2D cut

Figure 5.17: Developed clot and velocity field at large blood inflow velocity - fine grid

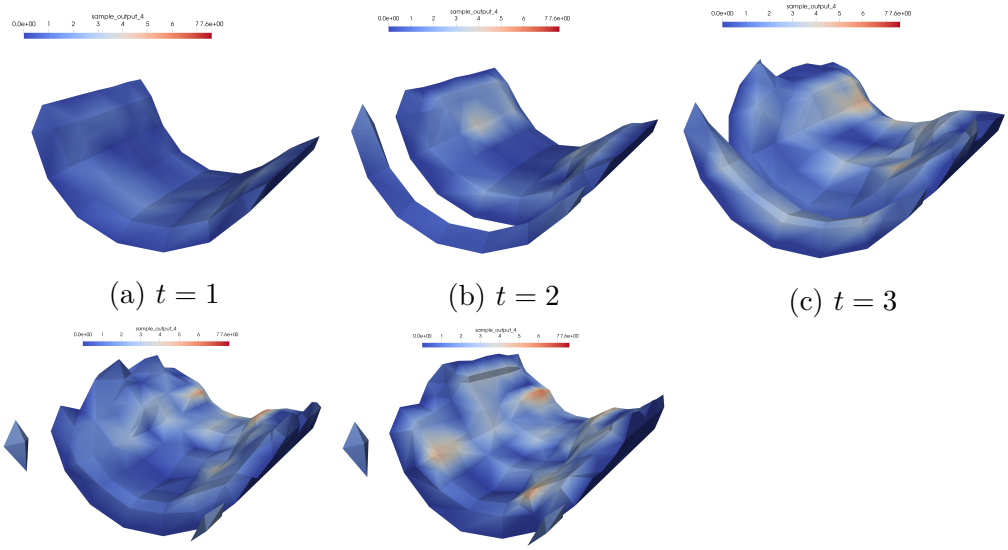

(a) $t = 1$ (b) $t = 2$ (c) $t = 3$

(d) $t = 4$ (e) $t = 5$

Figure 5.18: Phase field isosurface and values of shear stress at different times of the evolution - coarse grid

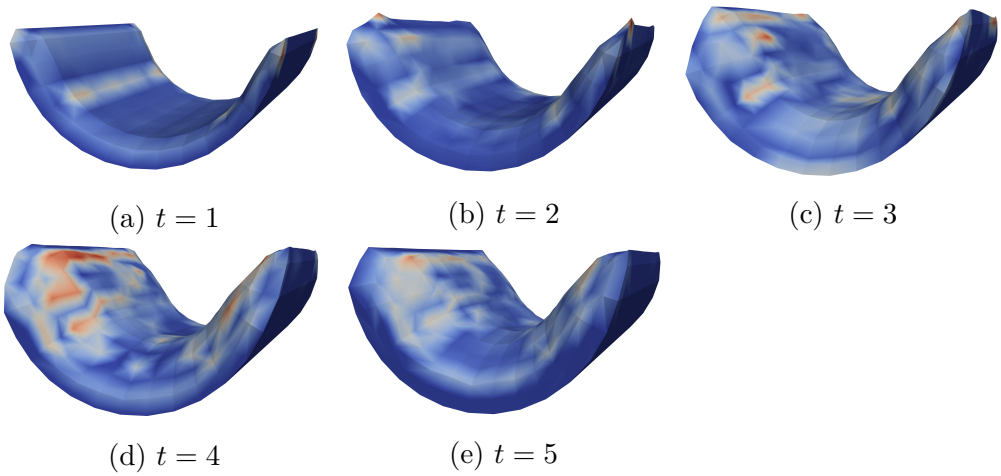

(a) $t = 1$ (b) $t = 2$ (c) $t = 3$

(d) $t = 4$ (e) $t = 5$

Figure 5.19: Phase field isosurface and values of shear stress at different times of the evolution at low velocity - fine grid

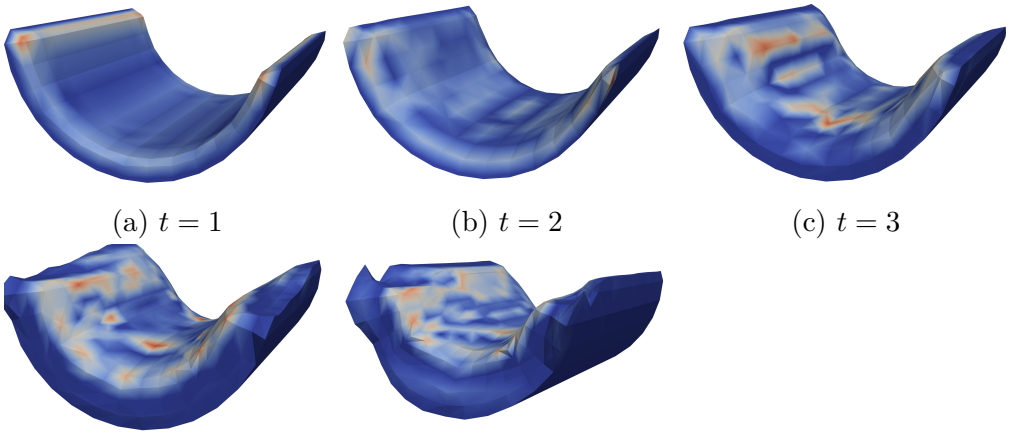

(a) $t = 1$ (b) $t = 2$ (c) $t = 3$

(d) $t = 4$ (e) $t = 5$

Figure 5.20: Phase field isosurface and values of shear stress at different times of the evolution at high velocity - fine grid

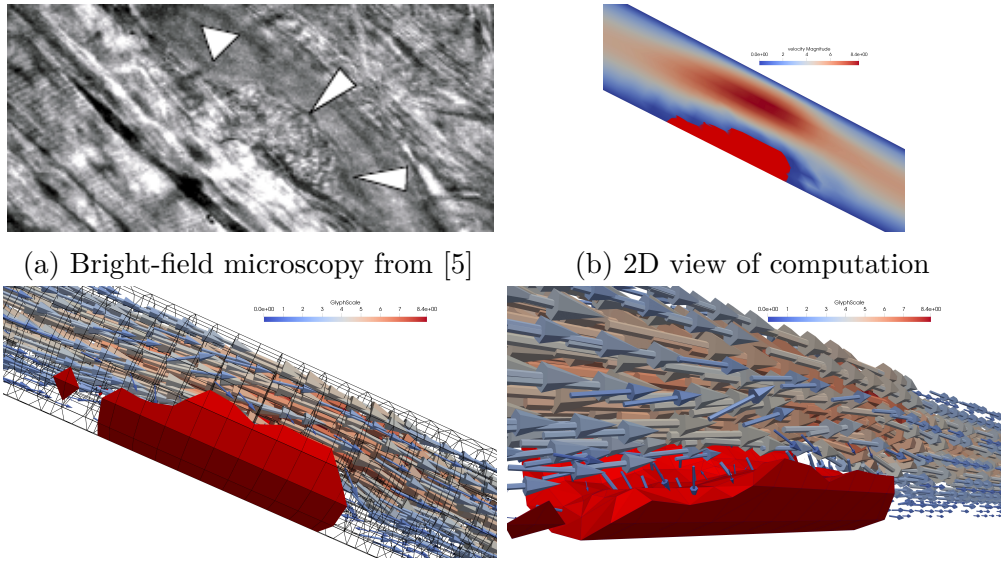

(a) Bright-field microscopy from [5] (b) 2D view of computation

(c) 3D view of computation (d) 3D view of computation

Figure 5.21: Results from bright-field microscopy in [5], comparison with fast flow simulations - coarse grid

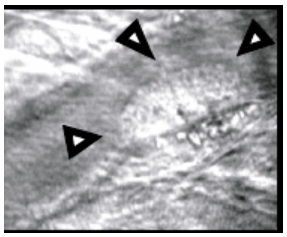

(a) bright-field microscopy from [5]

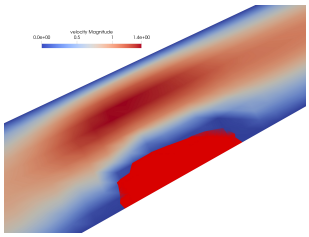

(b) 2D view of computation

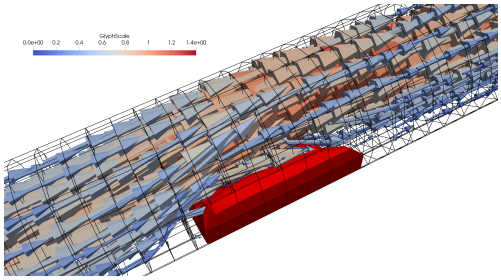

(c) 3D view of computation

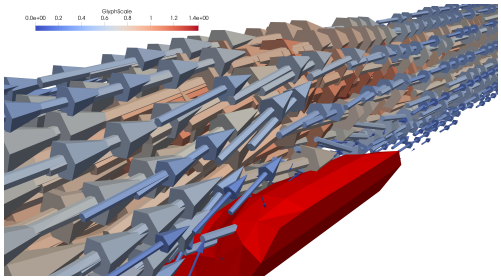

(d) 3D view of computation

Figure 5.22: Results from bright-field microscopy in [5], comparison with slow flow simulations - coarse grid

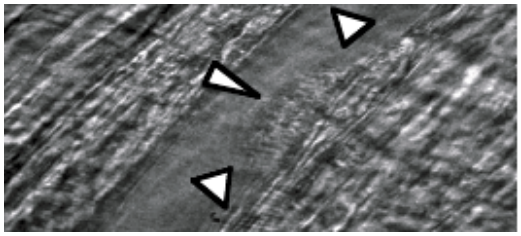

(a) bright-field microscopy from [5]

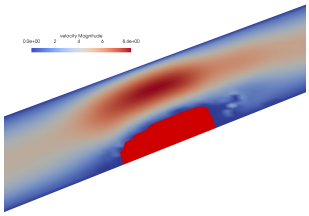

(b) 2D view of computation

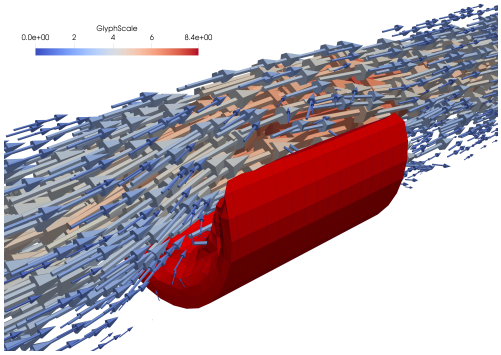

(c) 3D view of computation

Figure 5.23: Results from bright-field microscopy in [5], comparison with fast flow simulations - fine grid

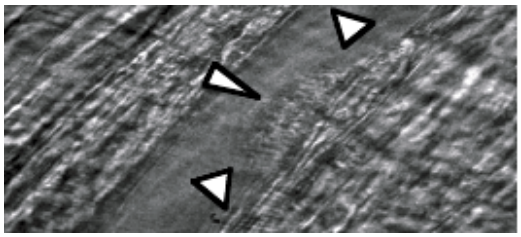

(a) bright-field microscopy from [5]

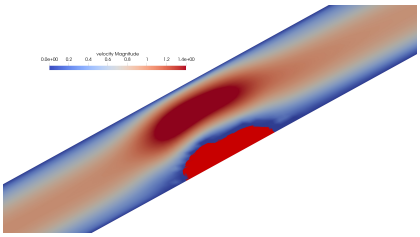

(b) 2D view of computation

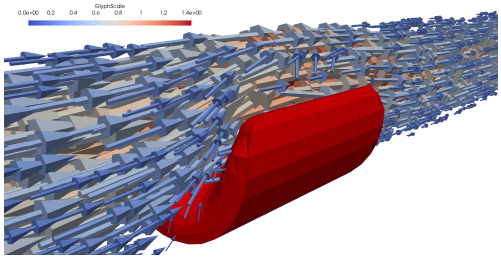

(c) 3D view of computation

Figure 5.24: Results from bright-field microscopy in [5], comparison with slow flow simulations - fine grid

6. Conclusion

6.1 Development of blood coagulation models

In this work we presented our research in the blood coagulation modelling field. As we noted in Introduction we limited ourselves only to two of the phases of blood coagulation, i.e. *primary hemostasis* and *secondary hemostasis*. We have used three available models of the blood coagulation process in our computations:

- Weller's model of coagulation, [3, 6]
- Storti's model of *primary hemostasis*, [8, 1]
- Kempen's model of *secondary hemostasis*, [2]

The blood itself was taken either as a Newtonian fluid or as a viscoelastic fluid using the non-homogeneous model of Owens [7, 65, 66].
The dissertation thesis of Weller [3] has title *Modeling, Analysis, and Simulation of Thrombosis and Hemostasis*. However author admits, that he is modelling only the initial stage of platelet aggregation. Hence the work of Weller could be taken as an important contribution to research of *primary hemostasis*.
We want to draw a line between the model of Weller and Storti [1], studied in this work, and more comprehensive models of blood coagulation such as Anand's model [57] and as Gregg's model [87]. Anand in [57] treats blood and clot as viscoelastic fluids, whereas in [87] the clot is captured in the model via a Brinkman term depending on density of platelets. The term is added to the Navier-Stokes equations.
We implemented the model of Weller using a novel approach, the phase field method. The phase field serves us only as a marker function, i.e. it does not have any thermodynamic meaning. We compared the phase field approach and the original sharp interface method, level-set, method. What we appreciate on the phase field framework is its avoidance of artificial smearing of useful quantities for numerical computations, i.e. the Heaviside function and the delta function. The phase field is namely implicitly smoothed.
We have applied the phase field method to the model of Storti [1] as well. We have however added another three new features in our first model, see Section 3.4.2.
Firstly we treat blood in the model as viscoelastic fluid, whose constitutive equations come from the nonhomogeneous model of Owens [7], [65].
Secondly we have modified the activation function for platelets so, that the resting platelets get activated, if they are exposed to high enough shear stress values.
Thirdly the clot is modelled as a Newtonian fluid with high viscosity.
The ALE implementation of the original model [1] requires remeshing, which has to be done after the movement of the interface platelet clot-blood. This brings several problems with itself. The problem is even more pronounced in three dimensional computations. Using the phase field method we avoid the necessity of remeshing.
What is new in this work, i.e. in the second model from Section 3.4.3, is the ability of our model to describe maturing of the platelet clot into blood clot. For that purpose we used the model of blood clot of [2]. The model takes the clot as a viscoelastic material with time dependent rheological properties.

We had to adjust both the formulation of the problem, i.e. the original equations, and the numerical treatment of the arising problem to suit our requirements. To sum up, our proposed model has the following features.
Firstly we treat blood in the model as viscoelastic fluid, whose constitutive equations comes from the nonhomogeneous model of Owens [7], [65].
Secondly we have modified the activation function for platelets so, that the resting platelets get activated, if they are exposed to high enough shear stress values, see Section 3.3.3.
Thirdly the platelet clot matures into blood clot. This was achieved by incorporation of the model [2] using the adjustments outlined in 3.3.4.
The model [2] was fitted against an experiment in cone-plate rheometer using seven fitting parameters. The question naturally arises, whether our generalization of Kempen's model of blood clot development is valid.

6.2 Development of numerical solvers

Our systems of equations outlined in sections 3.4.1, 3.4.2 and 3.4.3 are large. The equations of the models are intrinsically coupled. However in the solver process we solve each group separately and we reintroduce the coupling by subiterations in each timestep. The stopping criterion of the subiteration is based on the size of difference of solutions originating from last two subiterations. This is combined with a simple adaptive timestepping based on the truncation error estimation outlined in Section 4.1.2. Since the submodels can have different time scales, after computation of each time iteration using the previous algorithm we take the minimum of all proposed timesteps, see Section 4.1.3
The flow subproblem is solved by the incremental pressure correction scheme (IPCS) [82]. All nonlinearities in the equations were treated using the Picard subiteration. The norm of residual was taken as the termination criterion. The linearization of the double well potential in the Cahn-Hilliard equation was performed similarly to [88]. The procedure outlined in [88] results in (semi)-implicit expression for the double well potential derivative discretization. All the implementation is done in the open source finite element library deal.ii [4] with Trilinos [89] as the linear algebra backend, see Appendix A

6.3 Comments on results of simulations

We achieved comparable results with Weller simulations for the case of the perfusion chamber geometry, see Section 5.1.1 . We reached physically reasonable results for the cylinder geometry as well, see Section 5.1.2. In comparison with Weller we were limited a little bit, because we could not achieve such high levels of mesh refinement. In [3] the cylindrical symmetry of the perfusion chamber was used to reduce the problem to two-dimensional computation reducing by that the computational cost.
Our implementation is based on the finite element library deal.ii [4], [90] which enables dimension independent distributed computing.
We have performed a scaling study, which has shown, that our code is not ideally scalable, both weakly and strongly, see Section 5.2. Further refactoring of our

code would be needed in order to arrive at better performance results. There is however always trade-off between performance of the code and its modifiability, maintainability and extensibility.

We have performed simulations of modified Storti's model formulated in Section 3.4.2. The results are shown in Section 5.3.

We have performed simulations of our proposed model from Section 3.4.3 , see Section 5.4.

Besides the study of results of simulations themselves and the comparison of the results with the results from 5.3, we performed a rather simplified visual comparison of our simulations with the results of in-vivo experiment from [5]. Our computations are however simplified in comparison with the settings in [5]. Main differences lie in

- our computational domains and meshes are quite coarse
- the results of [5] took into account the whole process of blood coagulation, whereas we used the biochemistry model of blood coagulation, which relies only on several blood species
- the results of [5] provide different several outputs (see e.g. figures 5.24a, 5.23a, 5.22a, 5.21a) which shows, that in the in-vivo experiment there are some variables, which were not taken into account, i.e. they are not controllable by the setting of the experiment.
- the process of blood clot formation is captured in our model at continuum level. We do not trace the quantities of interest from the experiment in [5] in the area of clot, i.e. fibrin concentration, platelets concentration, tissue factor concentration. The fibrin concentration, which has direct impact on rheological properties of blood clot is taken into account by developing rheological parameters of modified Kempen's model, see 3.4.3

6.4 Final remarks and further research

We implemented our model using the finite element library deal.ii [4] in such a way, that adding new chemical species, new population types of platelets or another constitutive equation for blood or platelet clot should be relatively easy.
In the approach from Section 3.4.2 we have taken the clot as a fluid with high viscosity. However the clot can more likely behave like a viscoelastic material. In the approach from Section 3.4.3 we have used a specific constitutive equation for viscoelastic material of the blood clot, whose rheological parameters undergo development. Our model is however amenable to changing the extra stress tensor of the clot relatively easily.
The platelet plug which forms in model of [1],[8] and [79] can mature in the process of secondary hemostasis into blood clot. That is, what was done using the inclusion of model [2] into our system of equations. The model [2] is rather

phenomenological, i.e. low-level behaviour of clot is hidden in the fit parameters. There are however models, which contain the much more complete biochemistry of both primary and secondary hemostasis, e.g. [57]. One of the main outputs of the model [57] is the concentration of fibrin, which is the key component of the blood clot.

The next step in the modelling of development of the blood clot could be then dependence of the parameters of the constitutive equations of clot on the concentration of the relevant chemical species, which could either circulate in the blood flow or can be present or perfuse in the clot, e.g. fibrin.

The nonhomogeneous model of Owens is able to describe Fahraeus effect in a narrow blood vessel. The zone of the blood vessel, which is depleted of red blood cells, should, according to Aarts [19], be populated in elevated measures with blood platelets.

There are already some studies, which take into account margination of platelets by red blood cells, see [91], [92], [93], [94] or [95]. Future model could however achieve the required distribution of platelets, if it has the correct profile of red blood cells distribution, hematocrit, in the blood vessel. The model presented in this work seems to us as promising first step in this direction.

Bibliography

[1] F. Storti. "A continuum model for platelet plug formation, growth, and deformation". English. Proefschrift. PhD thesis. Department of Biomedical Engineering, 2014. DOI: 10.6100/IR782334.

[2] T. H. S. van Kempen et al. "A constitutive model for developing blood clots with various compositions and their nonlinear viscoelastic behavior". In: *Biomechanics and Modeling in Mechanobiology* 15.2 (2015), pp. 279–291. DOI: 10.1007/s10237-015-0686-9.

[3] F. F. Weller. "Modeling, Analysis, and Simulation of Thrombosis and Hemostasis". PhD thesis. Ruprecht-Karls-Universität Heidelberg, 2008.

[4] G. Alzetta et al. "The deal.II Library, Version 9.0". In: *Journal of Numerical Mathematics* 26.4 (2018), pp. 173–183. DOI: 10.1515/jnma-2018-0054.

[5] S. Falati et al. "Real-time in vivo imaging of platelets, tissue factor and fibrin during arterial thrombus formation in the mouse". In: *Nature Medicine* 8.10 (2002), pp. 1175–1180. DOI: 10.1038/nm782.

[6] F. F. Weller. "A free boundary problem modeling thrombus growth". In: *Journal of Mathematical Biology* 61.6 (2010), pp. 805–818. DOI: 10.1007/s00285-009-0324-1.

[7] R. G. Owens. "A new microstructure-based constitutive model for human blood". In: *Journal of Non-Newtonian Fluid Mechanics* 140.1-3 (2006), pp. 57–70. DOI: 10.1016/j.jnnfm.2006.01.015.

[8] F. Storti et al. "A continuum model for platelet plug formation and growth". In: *International Journal for Numerical Methods in Biomedical Engineering* 30.6 (2014), pp. 634–658. DOI: 10.1002/cnm.2623.

[9] H. M. Lazarus and A. H. Schmaier, eds. *Concise Guide to Hematology*. Springer International Publishing, 2019. DOI: 10.1007/978-3-319-97873-4.

[10] A. Fasano and A. Sequeira. "Hemorheology and Hemodynamics". In: *Hemomath*. Springer International Publishing, 2017, pp. 1–77. DOI: 10.1007/978-3-319-60513-5_1.

[11] J. M. Tarbell. "Mass Transport in Arteries and the Localization of Atherosclerosis". In: *Annual Review of Biomedical Engineering* 5.1 (2003), pp. 79–118. DOI: 10.1146/annurev.bioeng.5.040202.121529.

[12] N. S. Key et al., eds. *Practical Hemostasis and Thrombosis*. John Wiley & Sons, Ltd, 2017. DOI: 10.1002/9781118344729.

[13] L. D. Casa et al. "Role of high shear rate in thrombosis". In: *Journal of Vascular Surgery* 61.4 (2015), pp. 1068–1080. DOI: 10.1016/j.jvs.2014.12.050.

[14] K. S. Sakariassen et al. "The impact of blood shear rate on arterial thrombus formation". In: *Future Science OA* 1.4 (2015). DOI: 10.4155/fso.15.28.

[15] A. V. Hoffbrand et al., eds. *Color Atlas of Clinical Hematology: Molecular and Cellular Basis of Disease*. Wiley-Blackwell, 2019.

[16] G. A. Nuttall. “Hemostasis and Thrombosis: Basic Principles and Clinical Practice, 5th ed.” In: *Anesthesia & Analgesia* 104.5 (2007), p. 1317. DOI: 10.1213/01.ane.0000263681.99710.0b.

[17] AnaesthesiaUK. *Coagulation- classical model*. 2005. URL: http://www.frca.co.uk/article.aspx?articleid=100096.

[18] M. Tamagawa. “Observation of Thrombus Formation Process by High Shear Rate on Various Flows and CFD Based Prediction Method for Thrombus Formation Rate”. In: *Volume 3: Biomedical and Biotechnology Engineering*. ASME, 2014. DOI: 10.1115/imece2014-38002.

[19] P. A. Aarts et al. “Blood platelets are concentrated near the wall and red blood cells, in the center in flowing blood.” In: *Arteriosclerosis: An Official Journal of the American Heart Association, Inc.* 8.6 (1988), pp. 819–824. DOI: 10.1161/01.atv.8.6.819.

[20] K. Zlobina and G. T. Guria. “Platelet activation risk index as a prognostic thrombosis indicator”. In: *Scientific reports* 6 (2016), p. 30508. DOI: 10.1038/srep30508.

[21] L. D. Casa and D. N. Ku. “Thrombus Formation at High Shear Rates”. In: *Annual Review of Biomedical Engineering* 19.1 (2017). PMID: 28441034, pp. 415–433. DOI: 10.1146/annurev-bioeng-071516-044539.

[22] Huck. 2008. URL: http://www.shenc.de/A2-Huck-res.htm.

[23] R. G. Owens and T. N. Phillips. *Computational Rheology*. World Scientific Publishing Company, 2002. DOI: 10.1142/9781860949425.

[24] H. A. Barnes. “The yield stress—a review or ‘παντα ρει’—everything flows?” In: *Journal of Non-Newtonian Fluid Mechanics* 81.1 (1999), pp. 133–178. DOI: 10.1016/S0377-0257(98)00094-9.

[25] P. Moller et al. “Yield stress and thixotropy: on the difficulty of measuring yield stresses in practice”. eng. In: *Soft matter* 2.4 (2006), pp. 274–283.

[26] C. N. “A Flow Equation for Pigment-Oil Suspensions of the Printing Ink Type”. In: *Rheology of Disperse Systems* (1959), pp. 84–104.

[27] J. R. A. Pearson. “The Non-linear Field Theories of Mechanics (Vol. III, part 3, of Encyclopaedia of Physics). By C. TRUESDELL and W. NOLL. Springer, 1965. 602 pp. DM. 198.” In: *Journal of Fluid Mechanics* 25.3 (1966), pp. 638–640. DOI: 10.1017/S0022112066210302.

[28] W. Noll. “A Mathematical Theory of the Mechanical Behavior of Continuous Media”. In: *Archive for Rational Mechanics and Analysis* 2 (1958), pp. 197–226. DOI: 10.1007/BF00277929.

[29] B. D. Coleman and W. Noll. “An approximation theorem for functionals, with applications in continuum mechanics”. In: *Archive for Rational Mechanics and Analysis* 6.1 (1960), pp. 355–370. DOI: 10.1007/BF00276168.

[30] B. T. y. s. Coleman and W. Noll. “Foundations of Linear Viscoelasticity”. In: *Rev. Mod. Phys.* 33 (2 1961), pp. 239–249. DOI: 10.1103/RevModPhys.33.239.

[31] K. R. Rajagopal and A. R. Srinivasa. “On thermomechanical restrictions of continua”. In: *Proceedings of the Royal Society A: Mathematical, Physical and Engineering Sciences* 460.2042 (2004), pp. 631–651. DOI: 10.1098/rspa.2002.1111.

[32] K. R. Rajagopal and A. R. Srinivasa. “On the thermomechanics of materials that have multiple natural configurations Part I: Viscoelasticity and classical plasticity”. In: *Zeitschrift für angewandte Mathematik und Physik ZAMP* 55.5 (2004), pp. 861–893. DOI: 10.1007/s00033-004-4019-6.

[33] J. R. A. Pearson. “Fluid Dynamics of Viscoelastic Liquids”. In: *Journal of Fluid Mechanics* 266 (1994), pp. 373–376. DOI: 10.1017/S0022112094221055.

[34] M. Johnson and D. Segalman. “A model for viscoelastic fluid behavior which allows non-affine deformation”. In: *Journal of Non-Newtonian Fluid Mechanics* 2.3 (1977), pp. 255–270. DOI: 10.1016/0377-0257(77)80003-7.

[35] S. Claus. “Numerische Simulation von instationären dreidimensionalen viskoelastischen Oldroyd-B- und Phan-Thien Tanner-Strömungen”. MA thesis. Germany: Mathematisch-Naturwissenschaftlichen Fakultät der Rheinischen Friedrich-Wilhelms-Universität Bonn, 2008.

[36] W. H. Bauer and E. A. Collins. “THIXOTROPY AND DILATANCY”. In: *Rheology*. Elsevier, 1967, pp. 423–459. DOI: 10.1016/b978-1-4832-2941-6.50014-3.

[37] H. A. Barnes. “Thixotropy—a review”. In: *Journal of Non-Newtonian Fluid Mechanics* 70.1 (1997), pp. 1–33. DOI: 10.1016/S0377-0257(97)00004-9.

[38] H. Schmid-Schönbein and R. Wells. “Rheological properties of human erythrocytes and their influence upon the "anomalous" viscosity of blood”. In: *Ergebnisse der Physiologie, biologischen Chemie und experimentellen Pharmakologie* 63 (1971), pp. 146–219.

[39] R. E. Wells et al. “Influence of fibrinogen on flow properties of erythrocyte suspensions”. In: *American Journal of Physiology-Legacy Content* 207.5 (1964). PMID: 14237445, pp. 1035–1040. DOI: 10.1152/ajplegacy.1964.207.5.1035.

[40] E. W. Merrill et al. “Non-newtonian Rheology of Human Blood–effect of Fibrinogen Deduced by "subtraction".” In: *Circulation research* 13 (1963), pp. 48–55.

[41] S. Chien. “Shear dependence of effective cell volume as a determinant of blood viscosity.” In: *Science* 168 3934 (1970), pp. 977–9.

[42] J. J. Bishop et al. “Rheological effects of red blood cell aggregation in the venous network: A review of recent studies”. In: *Biorheology* 38 (2001), pp. 263–274.

[43] J. Goldstone et al. “The rheology of red blood cell aggregates”. In: *Microvascular Research* 2.3 (1970), pp. 273–286. DOI: 10.1016/0026-2862(70)90018-X.

[44] A. S. Popel and P. C. Johnson. “Microcirculation and hemorheology”. In: *Annual Review of Fluid Mechanics* 37.1 (2005), pp. 43–69. DOI: 10.1146/annurev.fluid.37.042604.133933.

[45] J.-F. Stoltz et al. *Hemorheology in Practice*. IOS Press, 1999.

[46] E. Merrill et al. “Rheology of Human Blood, near and at Zero Flow: Effects of Temperature and Hematocrit Level”. In: *Biophysical Journal* 3.3 (1963), pp. 199–213. DOI: 10.1016/S0006-3495(63)86816-2.

[47] D. M. Eckmann et al. “Hematocrit, Volume Expander, Temperature, and Shear Rate Effects on Blood Viscosity”. In: *Anesthesia & Analgesia* 91.3 (2000), pp. 539–545. DOI: 10.1213/00000539-200009000-00007.

[48] P. W. Rand et al. “Viscosity of normal human blood under normothermic and hypothermic conditions”. In: *Journal of Applied Physiology* 19.1 (1964). PMID: 14104265, pp. 117–122. DOI: 10.1152/jappl.1964.19.1.117.

[49] G. Thurston. “Viscoelasticity of Human Blood”. In: *Biophysical Journal* 12.9 (1972), pp. 1205–1217. DOI: 10.1016/S0006-3495(72)86156-3.

[50] S. Chien et al. “Viscoelastic Properties of Human Blood and Red Cell Suspensions”. In: *Biorheology* 12 (1975), pp. 341–6. DOI: 10.3233/BIR-1975-12603.

[51] H. Chmiel et al. “The determination of blood viscoelasticity in clinical hemorheology”. In: *Biorheology* 27 (1990), pp. 883–94.

[52] H. A. Barnes and K. Walters. “The yield stress myth?” In: *Rheologica Acta* 24.4 (1985), pp. 323–326. DOI: 10.1007/BF01333960.

[53] L. Dintenfass. *Blood Microrheology: Viscosity Factors in Blood Flow, Ischaemia and Thrombosis*. Butterworth & Co Publishers Ltd., 1971.

[54] C. Picart et al. “Human blood shear yield stress and its hematocrit dependence”. In: *Journal of Rheology* 42.1 (1998), pp. 1–12. DOI: 10.1122/1.550883.

[55] R. B. Bird et al. *Dynamics of polymeric liquids, second edition, volume 1: Fluid mechanics, , Wiley-Interscience, New York, 1987, 649 pp. Price: $69.95*. Wiley-Interscience, 1987.

[56] K. Yeleswarapu et al. “The flow of blood in tubes: theory and experiment”. In: *Mechanics Research Communications* 25.3 (1998), pp. 257–262. DOI: 10.1016/S0093-6413(98)00036-6.

[57] A. Mohan. “Modeling the growth and dissolution of clots in flowing blood”. PhD thesis. Texas A&M University, 2005.

[58] K. Rajagopal and A. Srinivasa. “A thermodynamic frame work for rate type fluid models”. In: *Journal of Non-Newtonian Fluid Mechanics* 88.3 (2000), pp. 207–227. DOI: 10.1016/s0377-0257(99)00023-3.

[59] D. Quemada. “A non-linear Maxwell model of biofluids: Application to normal blood”. In: *Biorheology* 30.3-4 (1993), pp. 253–265. DOI: 10.3233/BIR-1993-303-410.

[60] D. Quemada. “Rheological modelling of complex fluids. I. The concept of effective volume fraction revisited”. In: *The European Physical Journal Applied Physics* 1.1 (1998), pp. 119–127. DOI: 10.1051/epjap:1998125.

[61] D. Quemada. “Rheological modelling of complex fluids: IV: Thixotropic and "thixoelastic? behaviour. Start-up and stress relaxation, creep tests and hysteresis cycles”. In: *The European Physical Journal Applied Physics* 5.2 (1999), pp. 191–207. DOI: 10.1051/epjap:1999128.

[62] M. C. Williams et al. “Theory of Blood Rheology Based on a Statistical Mechanics Treatment of Rouleaux, and Comparisons with Data”. In: *International Journal of Polymeric Materials and Polymeric Biomaterials* 21.1-2 (1993), pp. 57–63. DOI: 10.1080/00914039308048512.

[63] N. S. And and D. De Kee. “Simple shear, hysteresis and yield stress in biofluids”. In: *The Canadian Journal of Chemical Engineering* 79.1 (2009), pp. 36–41. DOI: 10.1002/cjce.5450790107.

[64] D. De Kee and C. F. Chan Man Fong. “Rheological properties of structured fluids”. In: *Polymer Engineering & Science* 34.5 (1994), pp. 438–445. DOI: 10.1002/pen.760340510.

[65] M. Moyers-Gonzalez et al. “A non-homogeneous constitutive model for human blood. Part 1. Model derivation and steady flow”. In: *Journal of Fluid Mechanics* 617 (2008), pp. 327–354. DOI: 10.1017/S002211200800428X.

[66] M. A. Moyers-Gonzalez et al. “A non-homogeneous constitutive model for human blood: Part III. Oscillatory flow”. In: *Journal of Non-Newtonian Fluid Mechanics* 155.3 (2008), pp. 161–173. DOI: 10.1016/j.jnnfm.2008.04.001.

[67] A. Iolov et al. “A finite element method for a microstructure-based model of blood”. In: *International Journal for Numerical Methods in Biomedical Engineering* 27.9 (2011), pp. 1321–1349. DOI: 10.1002/cnm.1427.

[68] R. B. Bird et al. *Dynamics of polymeric liquids, volume 2: Kinetic theory*. Wiley-Interscience, 1987.

[69] Y. Dimakopoulos et al. “Hemodynamics in stenotic vessels of small diameter under steady state conditions: Effect of viscoelasticity and migration of red blood cells”. In: *Biorheology* 52.3 (2015), pp. 183–210. DOI: 10.3233/BIR-14033.

[70] T. H. S. van Kempen et al. “A constitutive model for the time-dependent, nonlinear stress response of fibrin networks”. In: *Biomechanics and Modeling in Mechanobiology* 14.5 (2015), pp. 995–1006. DOI: 10.1007/s10237-015-0649-1.

[71] T. Bodnár et al. “Mathematical Models for Blood Coagulation”. In: *Fluid-Structure Interaction and Biomedical Applications*. Ed. by T. Bodnár et al. Birkhäuser, Basel, 2014, pp. 483–569.

[72] M. Anand et al. “A model incorporating some of the mechanical and biochemical factors underlying clot formation and dissolution in flowing blood”. English. In: *Computational and Mathematical Methods in Medicine* 5.3-4 (2003), pp. 183–218. DOI: 10.1080/10273660412331317415.

[73] A. Fasano and A. Sequeira. “Blood Coagulation”. In: *Hemomath*. Springer International Publishing, 2017, pp. 79–158. DOI: 10.1007/978-3-319-60513-5_2.

[74] F. F. Weller. “Platelet deposition in non-parallel flow. Influence of shear stress and changes in surface reactivity”. In: *Journal of Mathematical Biology* 57.3 (2008), pp. 333–359. DOI: 10.1007/s00285-008-0163-5.

[75] J. A. Sethian. *Level Set Methods and Fast Marching Methods*. Second Edition. Cambridge University Press, 1999.

[76] S. Osher and R. Fedkiw. *Level Set Methods and Dynamic Implicit Surfaces*. Springer Verlag, 2003.

[77] E. N. Sorensen et al. “Computational Simulation of Platelet Deposition and Activation: I. Model Development and Properties”. In: *Annals of Biomedical Engineering* 27.4 (1999), pp. 436–448. DOI: 10.1114/1.200.

[78] E. N. Sorensen et al. “Computational Simulation of Platelet Deposition and Activation: II. Results for Poiseuille Flow over Collagen”. In: *Annals of Biomedical Engineering* 27.4 (1999), pp. 449–458. DOI: 10.1114/1.201.

[79] F. Storti and F. N. Vosse. “A continuum model for platelet plug formation, growth and deformation”. In: *International Journal for Numerical Methods in Biomedical Engineering* 30.12 (2014), pp. 1541–1557. DOI: 10.1002/cnm.2688.

[80] X. Li et al. “Solving pdes in complex geometries: A diffuse domain approach”. In: *Commun. Math. Sci.* 7 (2009), pp. 81–107.

[81] K. E. Teigen et al. “A Diffuse-interface Approach for Modeling Transport, Diffusion and Adsorption/desorption of Material Quantities on a Deformable Interface.” In: *Communications in mathematical sciences* 4 7 (2009), pp. 1009–1037.

[82] J. Guermond et al. “An overview of projection methods for incompressible flows”. In: *Computer Methods in Applied Mechanics and Engineering* 195.44 (2006), pp. 6011–6045. DOI: 10.1016/j.cma.2005.10.010.

[83] S. Turek. *Efficient Solvers for Incompressible Flow Problems: An Algorithmic Approach and Computational Approach*. 1998.

[84] D. Kuzmin. 2000. URL: http://www.mathematik.uni-dortmund.de/~kuzmin/cfdintro/lecture8.pdf.

[85] D. Brands. “Predicting brain mechanics during closed head impact : numerical and constitutive aspects”. English. PhD thesis. Department of Mechanical Engineering, 2002. DOI: 10.6100/IR552152.

[86] K. Affeld et al. “Fluid Mechanics of the Stagnation Point Flow Chamber and Its Platelet Deposition”. In: *Artificial Organs* 19.7 (1995), pp. 597–602. DOI: 10.1111/j.1525-1594.1995.tb02387.x.

[87] K. L. Gregg. “A mathematical model of blood coagulation and platelet deposition under flow”. PhD thesis. The University of Utah, 2010.

[88] S. Aland and A. Voigt. “Benchmark computations of diffuse interface models for two-dimensional bubble dynamics”. In: *International Journal for Numerical Methods in Fluids* 69.3 (2011), pp. 747–761. DOI: 10.1002/fld.2611.

[89] M. Heroux et al. *An Overview of Trilinos*. Tech. rep. SAND2003-2927. Sandia National Laboratories, 2003.

[90] W. Bangerth et al. “deal.II – a General Purpose Object Oriented Finite Element Library”. In: *ACM Trans. Math. Softw.* 33.4 (2007), pp. 24/1–24/27.

[91] A. Tokarev et al. “Continuous mathematical model of platelet thrombus formation in blood flow”. In: *Russian Journal of Numerical Analysis and Mathematical Modelling* 27.2 (2012). DOI: 10.1515/rnam-2012-0011.

[92] A. Tokarev et al. “Segregation of Flowing Blood: Mathematical Description”. In: *Mathematical Modelling of Natural Phenomena* 6.5 (2011), pp. 281–319. DOI: 10.1051/mmnp/20116511.

[93] A. Tokarev et al. “Finite Platelet Size Could Be Responsible for Platelet Margination Effect”. In: *Biophysical Journal* 101.8 (2011), pp. 1835–1843. DOI: 10.1016/j.bpj.2011.08.031.

[94] S. J. Hund and J. F. Antaki. “An extended convection diffusion model for red blood cell-enhanced transport of thrombocytes and leukocytes”. In: *Physics in Medicine and Biology* 54.20 (2009), pp. 6415–6435. DOI: 10.1088/0031-9155/54/20/024.

[95] W.-T. Wu et al. “Transport of platelets induced by red blood cells based on mixture theory”. In: *International Journal of Engineering Science* 118 (2017), pp. 16–27. DOI: 10.1016/j.ijengsci.2017.05.002.

[96] M. Dubash. *Moore’s Law is dead, says Gordon Moore*. 2006.

[97] G. Barlas. *Multicore and GPU Programming: An Integrated Approach*. San Francisco, CA, USA: Morgan Kaufmann Publishers Inc., 2015.

[98] *The Message Passing Interface (MPI) standard*. 2018. URL: https://www.mcs.anl.gov/research/projects/mpi/.

[99] *MPI Implementations*. 2018. URL: https://www.mcs.anl.gov/research/projects/mpi/implementations.html.

[100] P. Pacheco. *An Introduction to Parallel Programming*. 1st. San Francisco, CA, USA: Morgan Kaufmann Publishers Inc., 2011.

[101] J. Reinders. *Intel threading building blocks - outfitting C++ for multi-core processor parallelism*. O’Reilly, 2007.

[102] S. Balay et al. *PETSc Web page*. 2018. URL: http://www.mcs.anl.gov/petsc.

[103] S. Balay et al. *PETSc Users Manual*. Tech. rep. ANL-95/11 - Revision 3.11. Argonne National Laboratory, 2019.

[104] G. Karypis and V. Kumar. *MeTis: Unstructured Graph Partitioning and Sparse Matrix Ordering System, Version 4.0*. http://www.cs.umn.edu/~metis. University of Minnesota, Minneapolis, MN, 2009.

[105] C. Burstedde et al. “p4est: Scalable Algorithms for Parallel Adaptive Mesh Refinement on Forests of Octrees”. In: *SIAM Journal on Scientific Computing* 33.3 (2011), pp. 1103–1133. DOI: 10.1137/100791634.

[106] The HDF Group. *Hierarchical data format version 5*. 2010-2019. URL: http://www.hdfgroup.org/HDF5.

[107] Y. Saad. *Iterative Methods for Sparse Linear Systems*. Society for Industrial and Applied Mathematics, 2003. DOI: 10.1137/1.9780898718003.

List of Figures

List of Tables

List of Publications

Marek Čapek, *Overview of Mathematical Models for Blood Flow and Coagulation Process*, Week of doctoral students 2011, Proceedings of contributed papers, Charles University, ISBN 978-80-7378-186-6

Marek Čapek, *A Phase-field method applied to interface tracking for blood clot formation*, Applications of Mathematics, submitted

Marek Čapek, **Jaroslav Hron**, *Thrombus development model capturing primary and secondary hemostasis in the flowing blood*, Biomechanics and Modeling in Mechanobiology, submitted

Marek Čapek, *A non-Newtonian Model of Blood Capturing Segregation of Erythrocytes– First Step to Proper Modelling of the Blood Coagulation Process*, Supercomputing in Science and Engineering, 2017, VŠB - Technical University of Ostrava, ISBN 978-80-248-4037-6

A. Used software and hardware

A.1 Introduction

A.1.1 Different programming paradigms in scientific computing

Current development of new hardware has shown, that it is not possible to scale-up, scale vertically, the performance of computational units for scientific computations. It is the well known fact, that the number of transistors on a chip is limited due to the spacial requirements and the requirements of cooling of processors with billions of transistors.
In 1965 Gordon Moore formulated the so called Moore's Law, which stated, that the quantitity of transistors on a chip would double every year. However the validity of this extrapolation is valid only until certain time in the future, as the smallest transistor can have dimensions of an atomic particle, not smaller, [96].
On the other hand the need for more computational power is emerging not only in different areas of science, but also in engineering and commercial areas, e.g. in current finance industry.
It was therefore necessary to tackle the problem of the limits of vertical scaling. The solution is now not to increase performance by adding more computational power to CPU or by adding more RAM to the computer. Current development in the high-performance computing steps forward either by putting more cores in one CPU or by connection of multiple computers into the network of computers working on one assigned task, [97].
We will refer to the first solution as parallel computing, whereas the second solution we will call distributed computing.
We meet parallel computers every day, as multicore processors appear in PCs, notebooks, smart devices etc. The fact typical for them is that cores communicate with one another using shared memory. The shared memory is accessible to all cores in the computer or in the node.
Distributed computers are now used in computational centers in industry, they are also known as clusters. Each computing node of the cluster owns its own memory and it communicates with other nodes by exchange of messages. It is apparent, that exchange of messages brings some overhead in comparison with exchange of information using shared memory in parallel computers. The speed of messaging is also limited by the speed of the network connecting the nodes.
The number of nodes fitting into one CPU is however also limited, whereas the number of computers connected by a network in a cluster is theoretically unlimited.
It must however be said, that an hybrid approach is possible as well: the threads of execution on each core communicate in a process running on a node containing the cores. The advantages and disadvantages of the hybrid approach are the following: On the one hand one gets the performance gain by using of shared memory for all cores of a node, on the other hand one can connect multiple such nodes together, which will communicate by messages. One drawback of such approach is however the complexity of development in comparison with development of purely parallel or distributed code.

In our outline we stick to the distributed model of high performance computing, as it is used for computations of problems outlined in this work. We will start by the description of MPI, an message passing standard for scientific computations.

A.1.2 Message Pasing Interface - MPI

MPI [98] is a message passing portable standard. There are several implementations of MPI in, even the open source ones, [99].
The key concept of MPI is the communicator. Communicators are objects which group together processes in the MPI session. Each process in a communicator obtains an independent identifier. Based on the type of computation we do not have to let every process communicate with every other process. Instead we can define a topology, which reflects the type of computation.
Should we have computation in 2D, e.g. Laplace equation discretized using finite elements or finite difference method, then is is natural to assume, that processes behave as if they were in two-dimensional grid and they communicate with top, bottom, left, right, neighbours.
MPI provides two types of communication [100], [97]. The first one is the *point-to-point* communication, which enables exchange of messages between two specific processes identified by their unique identifiers in the corresponding communicator. The second type of communication is the *collective* one. The communication occurs among all processes in the communicator. The basic types of collective communication are synchronization, data movement and collective computation (reduction).
On synchronization all processes wait until all members of communicator reach some synchronization point. Under data movement type belong *broadcast*, *all to all*, *scatter*, *gather* operations. The reduction is performing an operation on data obtained from the other members of communicator.

Finite element library deal.ii

The finite element library deal.ii, [4], [90] is an open source library developed in C++. It uses features of C++ to allow mathematicians rapid finite element code development. It features wrapping of general parts of finite element codes such as grid creation and refinement, processing of degrees of freedom, output of results into different graphics formats, output of meshes. For that purpose deal.ii leverages the object orientation of C++, which allows to write highly modular code. Writing of modular code is a must, when one starts to develop a large project.
Another feature of C++ used in deal.ii library design is the support of generic programming, i.e. template (meta-)programming. One great example of using templates in deal.ii, is so called dimension independent programming. It allows to change the spatial dimension of the solved problem from one to two or three spatial dimensional withour principially great effort.
Deal.ii library supports different kinds of refinement - h- , p-, hp-. The refinement criterion is based on the on local errror indicator or error estimator. In deal.ii refinement functions are implemented, which take the indicator or estimator object as an argument. The function then refines, either in h-, p-, hp-, manner, based on the current numerical solution and the object of indicator or estimator.

Deal.ii library allows to use the computational sources of multiple cores on one node or use multiple nodes in a network. The first case is implemented using the library Threading Building Blocks, [101], i.e. it uses a threading technology. The latter one is the communication among nodes in a network implemented using the commucation framework of MPI, which was mentioned above.
In deal.ii the backend for linear algebra operations is implemented. It contains support for sparse matrices, vectors, Krylov subspace methods, direct solvers, blocked matrices.
Deal.ii provides rich interface with well established numerical packages Petsc [102], [103] and Trilinos [89], which are to be used mainly in the cases of computations distributed across multiple nodes in the cluster.
Deal.ii library needs to solve the problem of partitioning of complicated large computational domains into small chunks, in the case of parallel or distributed computations. For that purpose it uses the libraries METIS [104] and p4est [105].
Above we said, that deal.ii library supports multiple graphics formats. For the distributed computations used in our case we output the solution into hdf5/xdmf format supporting persistence of large data. For that purpose deal.ii interfaces with HDF5 library [106].

Key concepts of distributed linear algebra

We used in our computations Krylov methods for solution of the following problem

$$\mathbf{A}\mathbf{x} = \mathbf{b}, \tag{A.1}$$

where $\mathbf{x} \in \mathbb{R}^n$ is the vector of unknowns, $\mathbf{A} \in \mathbb{R}^{n \times n}$ is square and regular matrix and $\mathbf{b} \in \mathbb{R}^n$ is the right hand side.
Krylov methods search for the solution in the subspace $\mathbf{x_0} + \mathbf{K_m}$ of the whole solution space $\mathbb{R}^n$, where we define the Krylov space $\mathbf{K_m}$ of order m for the vector $\mathbf{v}$ and the matrix $\mathbf{A}$ in the following way:

$$\mathbf{K_m}(A, v) = \text{span}\left\{\mathbf{v}, \mathbf{A}\mathbf{v}, \mathbf{A}^2\mathbf{v}, \ldots, \mathbf{A}^{m-1}\mathbf{v}\right\} \tag{A.2}$$

The Krylov methods work only with matrix-vector products, scalar products and linear combinations of vectors, there is no necessity of accessing the elements of matrix $\mathbf{A}$. We use the finite element method, which produces sparse matrices. As the matrix-vector product computational price is determined by the quantity of non-zero entries per row, the Krylov methods appear good for the finite element method codes [107].
We will now go through the all above mentioned key matrix and vector operations necessary for the Krylov subspace methods. The simplest one are the linear combinations of vector, as there is no necessity of internode communication.
The scalar product can be more expensive than the matrix vector product, as after quite fast local computations it is necessary to perform a global reduction operation.
The matrix vector product can be better scalable than the scalar product computation, as it contains a larger number of local computations. In this step it is necessary to get values of solution, which are not local. However due to sparsity of matrix, the number of imported values is relatively low. It is necessary to perform

MPI scatter operation on the values of solution. In the meantime it is however possible to compute the necessary local computation for the matrix vector product.

A.2 Distributed solvers

One of the main reasons for using the parallel solvers based on Krylov subspace methods is their scalability. This scalability is hardly to be reached with parallel direct solvers, which limits their field of application to problems of rather smaller dimension.
Deal.ii distributes the rows of linear system originating from the assemble row-wise, i.e. each machine, process, CPU has only specific number of rows from the whole linar system. The Krylov subspace methods can then be implemented in distributed manner using the above discussed key operations - linear combinations of vectors, scalar products of vectors and matrix vector products. In this way we can paralellize the solvers like GMRES, CG, BiCGStab.

A.3 Key parts of computations with deal.ii

In this section we will show the way deal.ii library is used to solve the finite element problems.
Firstly we show and comment on setting up of the computation, on assembling of linear system and on the solution procedure of the linear system. We limit ourselves in this sketch to Laplace equation, we show however the computation in the fully distributed setting. Secondly we present our way of approaching of solution of linear systems originating from the models formulated in this work. We call it *fallback* strategy.

A.3.1 Setup and assemble for Laplace problem

Deal.ii library relies on C++, therefore each simulation is represented by a C++ class, here it is class *LaplaceProblem*:

```
template <int dim>
class LaplaceProblem
{
public:
  LaplaceProblem ();
  ~LaplaceProblem ();
  void run ();
private:
  void setup_system ();
  void assemble_system ();
  void solve ();

  MPI_Comm                                  mpi_communicator;
  parallel::distributed::Triangulation<dim> triangulation;
  DoFHandler<dim>                           dof_handler;
```

```
  FE_Q<dim>                                fe;
  IndexSet                                 locally_owned_dofs;
  IndexSet                                 locally_relevant_dofs;
  ConstraintMatrix                         constraints;
  LA::MPI::SparseMatrix                    system_matrix;
  LA::MPI::Vector                          locally_relevant_solution;
  LA::MPI::Vector                          system_rhs;
```

In constructor of *LaplaceProblem* MPI communicator, distribute triangulation, degree of freedom handler and used finite element (here quadratic) are initialized:

```
        template <int dim>
LaplaceProblem<dim>::LaplaceProblem ()
  :
  mpi_communicator (MPI_COMM_WORLD),
  triangulation (mpi_communicator),
  dof_handler (triangulation),
  fe (2)
{}
```

The code is run on each node. In setup method the fundamental data structures are initialized locally relevant degrees of freedom, locally owned degrees of freedom, constraint matrix (takes care of hanging nodes and boundary conditions), sparsity pattern of the global matrix and the global matrix.

```
template <int dim>
void LaplaceProblem<dim>::setup_system ()
 {
  dof_handler.distribute_dofs (fe);
  locally_owned_dofs = dof_handler.locally_owned_dofs ();
  DoFTools::extract_locally_relevant_dofs (dof_handler,
                                locally_relevant_dofs);
  locally_relevant_solution.reinit (locally_owned_dofs,
                locally_relevant_dofs, mpi_communicator);
    system_rhs.reinit (locally_owned_dofs, mpi_communicator);
    constraints.clear ();
    constraints.reinit (locally_relevant_dofs);
    DoFTools::make_hanging_node_constraints (dof_handler, constraints);
    VectorTools::interpolate_boundary_values (dof_handler,
            0,Functions::ZeroFunction<dim>(), constraints);
    constraints.close ();
    DynamicSparsityPattern dsp (locally_relevant_dofs);
    DoFTools::make_sparsity_pattern (dof_handler, dsp,
                                     constraints, false);
    SparsityTools::distribute_sparsity_pattern (dsp,
                dof_handler.n_locally_owned_dofs_per_processor(),
                mpi_communicator,
                locally_relevant_dofs);
    system_matrix.reinit (locally_owned_dofs,
                          locally_owned_dofs,
                          dsp,
```

```
                        mpi_communicator);
  }
```

In the code for the assembling of linear system we iterate over all cells of the mesh, which the current node owns. On each of these cells we assemble contributions to local full matrix and to local right hand side vector.

```
template <int dim>
  void LaplaceProblem<dim>::assemble_system ()
  {
  const QGauss<dim>  quadrature_formula(3);
  FEValues<dim> fe_values (fe, quadrature_formula,
                   update_values    |  update_gradients |
                   update_quadrature_points |
                   update_JxW_values);
  const unsigned int   dofs_per_cell = fe.dofs_per_cell;
  const unsigned int   n_q_points    = quadrature_formula.size();
  FullMatrix<double>   cell_matrix (dofs_per_cell, dofs_per_cell);
  Vector<double>       cell_rhs (dofs_per_cell);
  std::vector<types::global_dof_index> local_dof_indices (dofs_per_cell);
  typename DoFHandler<dim>::active_cell_iterator
  cell = dof_handler.begin_active(),
  endc = dof_handler.end();
  for (; cell!=endc; ++cell)
    if (cell->is_locally_owned())
      {
        cell_matrix = 0;
        cell_rhs = 0;
        fe_values.reinit (cell);
        for (unsigned int q_point=0; q_point<n_q_points; ++q_point)
          {
            const double rhs_value= 1.;
            for (unsigned int i=0; i<dofs_per_cell; ++i)
              {
                for (unsigned int j=0; j<dofs_per_cell; ++j)
                  cell_matrix(i,j) += (fe_values.shape_grad(i,q_point) *
                                       fe_values.shape_grad(j,q_point) *
                                       fe_values.JxW(q_point));
                cell_rhs(i) += (rhs_value *
                                fe_values.shape_value(i,q_point) *
                                fe_values.JxW(q_point));
              }
          }
        cell->get_dof_indices (local_dof_indices);
        constraints.distribute_local_to_global (cell_matrix,
                                                cell_rhs,
                                                local_dof_indices,
                                                system_matrix,
                                                system_rhs);
      }
  system_matrix.compress (VectorOperation::add);
```

```
  system_rhs.compress (VectorOperation::add);
  }
```

In the solve method we can choose among different distribute solvers from the stack of Trilinos or PETSC:

```
template <int dim>
  void LaplaceProblem<dim>::solve ()
  {
  LA::MPI::Vector
  completely_distributed_solution (locally_owned_dofs, mpi_communicator);
  SolverControl solver_control (dof_handler.n_dofs(), 1e-12);
#ifdef USE_PETSC_LA
  LA::SolverCG solver(solver_control, mpi_communicator);
#else
  LA::SolverCG solver(solver_control);
#endif
  LA::MPI::PreconditionAMG preconditioner;
  LA::MPI::PreconditionAMG::AdditionalData data;
#ifdef USE_PETSC_LA
  data.symmetric_operator = true;
#else
#endif
  preconditioner.initialize(system_matrix, data);
  solver.solve (system_matrix, completely_distributed_solution, system_rhs,
                preconditioner);
  constraints.distribute (completely_distributed_solution);
  locally_relevant_solution = completely_distributed_solution;
  }
```

In the run method we call the above defined methods consecutively.

```
template <int dim>
  void LaplaceProblem<dim>::run ()
  {

  const unsigned int n_cycles = 8;

 GridGenerator::hyper_cube (triangulation);
 triangulation.refine_global (5);
 setup_system ();
 assemble_system ();
 solve ();
 }
```

A.3.2 Fallback strategy use of linear solvers in deal.ii

Frequently we use in our code the *fallback* strategy. We use the mechanics of exceptions in C++ to capture the case, when one not so robust but effective solver is not successful. Then other not so effective, but more robust solver, has a try. We will show this workaround on the example of the solution of the tentative

velocity step from the splitting method.
Firstly we try GMRES solver with SOR preconditioner. If we are not successfull, than we resort to GMRES solver with ILU preconditioner. Should we again be unsuccessful we end with GMRES with algebraic multigrid preconditioner. The computation will only crash, if all solvers are unsuccessful.

```
LA::MPI::Vector completely_distributed_solution(locally_owned_dofs_vel,
               MPI_COMM_WORLD);
LA::SolverGMRES::AdditionalData add_data_solver(true);

try {
 SolverControl solver_control(500, 1e-8);

 LA::SolverGMRES solver(solver_control, add_data_solver);

 TrilinosWrappers::PreconditionSOR::AdditionalData add_data_prec_sor;
 TrilinosWrappers::PreconditionSOR prec_sor;
 prec_sor.initialize(system_matrix_vel, add_data_prec_sor);

 solver.solve(system_matrix_vel, completely_distributed_solution,
 system_rhs_vel, prec_sor);

this->pcout << "         Error: " << solver_control.initial_value()
 << " -> " << solver_control.last_value() << " in "
 << solver_control.last_step() << " SOR+ Gmres iterations."
 << std::endl;

} catch (...) \{
  this->pcout
   << "Catching in solve_tentative_velocity_step-trying ILU + GMRES solver"
   << std::endl;
 try {
  SolverControl solver_control(500, 1e-7);
  LA::SolverGMRES solver(solver_control, add_data_solver);
  TrilinosWrappers::PreconditionILU::AdditionalData add_data_prec_ilu;
  TrilinosWrappers::PreconditionILU prec_ilu;
  prec_ilu.initialize(system_matrix_vel, add_data_prec_ilu);
  solver.solve(system_matrix_vel, completely_distributed_solution,
               system_rhs_vel, prec_ilu);
  this->pcout << "         Error: " << solver_control.initial_value()
               << " -> " << solver_control.last_value() << " in "
               << solver_control.last_step() << " ILU + Gmres iterations."
               << std::endl;

         } catch (...) {
  this->pcout
       << "Catching in solve_tentative_velocity_step-trying AMG + GMRES solver"
       << std::endl;

    try {
         TrilinosWrappers::PreconditionAMG::AdditionalData add_data_prec_amg(
                              false, true, 2, true);
```

```
        TrilinosWrappers::PreconditionAMG prec_amg;
        {
                std::vector<std::vector<bool> > constant_modes;
                DoFTools::extract_constant_modes(dof_handler_vel,
                                                 ComponentMask(), constant_modes);
                TrilinosWrappers::PreconditionAMG::AdditionalData add_data_prec_amg;
                add_data_prec_amg.constant_modes = constant_modes;
                add_data_prec_amg.higher_order_elements = true;
                add_data_prec_amg.elliptic = false;
                add_data_prec_amg.n_cycles = 2;
                add_data_prec_amg.w_cycle = true;
                add_data_prec_amg.output_details = false;
                add_data_prec_amg.smoother_sweeps = 2;
                add_data_prec_amg.aggregation_threshold = 1e-6;
                prec_amg.initialize(system_matrix_vel, add_data_prec_amg);
        }

        SolverControl solver_control(500, 1e-7);
        LA::SolverGMRES solver(solver_control, add_data_solver);

        solver.solve(system_matrix_vel, completely_distributed_solution,
                        system_rhs_vel, prec_amg);
        this->pcout        << "         Error: "
                                << solver_control.initial_value() << " -> "
                                << solver_control.last_value() << " in "
                                << solver_control.last_step()
                                << " AMG + Gmres iterations." << std::endl;

        } catch (...) {
        this->pcout        << "Catching in solve_tentative_velocity_step
                        - failure of AMG +GMRES << std::endl;
        throw;
        }

}
constraint_matrix_vel_all.distribute(completely_distributed_solution);
```

A.4 Used harware

We have used hardware facilities on three clusters. Initial computations were performed on cluster Snehurka, Karlin computational cluster.
More complicated and demanding computations were performed on the clusters Anselm and Salomon under OPEN acces calls competion provided by IT4ICZ. The computational part of this work was supported by The Ministry of Education, Youth and Sports from the Large Infrastructures for Research, Experimental Development and Innovations project „IT4Innovations National Supercomputing Center – LM2015070“.

List of Notations

$f_{ss}(.)$ scalar function capturing increase of clot stiffness with strain 46

f_s saturation function of the reacting surface 39

f_{vi} scalar function capturing nonlinear viscous dissipation 46

$f_v(t)$ time dependent scalar function 46

G shear modulus 43

G_i fitting parameters 46

g_k fragmentation rate 29

H Heaviside function 49

h_k aggregation rate 29

I_D first principal invariant of the tensor $\mathbf{D}$ 19

II_D second principal invariant of the tensor $\mathbf{D}$ 19

III_D third principal invariant of the tensor $\mathbf{D}$ 19

J $\det(\mathbf{F})$ 43

j_{bp} flux of deposited bounded platelets 41

K spring constant 24

k_{1j} rate of inhibition of thromboxane 38

k_{2j} rate at which creation of thrombin is inhibited by antithrombin 39

k_2 fit parameter 46

k_{aa} adherence constant of activated platelets to each other 39

k_{as} adherence constant of activated platelets to the damaged wall 39

k_B Boltzmann constant 24

$K_{i,j}$ aggregation kernel 30

k_{pa} reaction rate for activation of platelets 38

k_{rs} reaction constant capturing adherence of unactivated platelets to the reactive surface 39

$L_\phi(\mathbf{u})$ viscous term in IPCS with variable viscosity 64

L_{DEVSS} augmented viscous term from DEVSS 68

M scaled number density of rouleaux 29

M_∞ total capacity of the surface for platelets 39

x_0 fit parameter 46

x_i time dependent state parameters 46

x_i^k value of x_i at timestep k 79